Study and implementation of widely linear (WL) receiver for filter bank based multicarrier (FBMC-OQAM) modulations over frequency selective channels

Hayfa Fhima

École Doctorale d'Informatique, Télécommunication et Électronique

Centre d'Études et de Recherche en Informatique et Communications

&

École Supérieure des Communications de Tunis

Innovation of Communicant and cooperative mobiles

THÈSE DE DOCTORAT

présenté par : **Hayfa FHIMA**

***soutenu le :* 12 Décembre 2019**

pour obtenir le grade de :

Docteur du Conservatoire National des Arts et Métiers et de l'École Supérieure des Communications de Tunis

Discipline/Spécialité : Informatique

Study and implementation of Widely Linear (WL) Receiver for Filter Bank based Multicarrier (FBMC-OQAM) modulations over Frequency Selective Channels.

THÈSE dirigée par

M. Daniel ROVIRAS, CNAM (France)

M. Ridha BOUALLEGUE, SUP'COM (Tunisie)

Et co-encadrée par

M. Rafik ZAYANI, ISI (Tunisie)

M. Hmaied SHAIEK, CNAM (France)

RAPPORTEURS

M. Kosai RAOOF, Université de MANS (France)

M. Taher EZZEDINE, ENIT (Tunisie)

EXAMINATEURS

Mme. Genevieve BAUDOIN, ESIEE (France)

M. Jamel BELHADJ TAHER, ENISO (Tunisie)

Acknowledgements

First and foremost, I would like to express my deepest gratitude to my supervisors Prof. Daniel ROVIRAS, Prof. Ridha BOUALLEGUE, Dr. Rafik ZAYANI and Dr.Hmaied SHAIEK for their guidance, encouragement and outstanding expertise and knowledge. I am very thankful for their invaluable support and the wholehearted confidence they have shown in me. I am very grateful to Dr. Bruno SENS CHANG for his patience and help during my thesis. Furthermore, I would like to thank the financial support provided by the WONG5 project. Besides, I would also like to thank all my Friends and colleagues belonging to Innov'COM Lab and LAETTITIA members. Finally, I dedicate this dissertation to my parents, my sister, my husband and my son and daughter.

Paris, December 2019
Hayfa FHIMA

Abstract

The increasing demand of user's requirements is one of the main reasons in technical progress and development of modern wireless communication systems. Thus, since 2G and beyond, there have been many changes, especially, the switch from the mono carrier to the multi-carrier (MC), introduced for the Down-Link (DL) 4G transmission. Indeed, the predominant idea behind introducing MC waveforms (WF) is to get rid of the propagation channel effects, by relaxing the equalization process through the transmission of the data symbols over flat fading sub-channels or sub-carriers. Furthermore, the widely adopted MC WF is the orthogonal frequency division multiplexing (OFDM), which became very popular and widely used in many wireless standards like long term evolution (LTE)- Advanced (LTE-A) and Wi-Fi. The standardization of OFDM, for these applications and also for some others, is related to the advantages shown by this MC WF. One of these advantages is its simple implementation through the use of the inverse fast Fourier transform (IFFT) at the transmitter side, and a FFT at the receiver side. Also, OFDM introduces a cyclic prefix (CP), making the transmission free from inter-symbol-interference (ISI).

Despite the large success of the OFDM WF, this technique suffers from the loss of spectral efficiency due to the use of the CP. Besides, it suffers from bad frequency localization due the use of a rectangular prototype filter. These OFDM drawbacks, have motivated researchers to design new MC WF, with better frequency domain localization, better robustness to user's synchronism, while keeping moderate implementation complexity. In this context, high number of post-OFDM MC WF have been proposed and implemented to meet 5G scenarios and requirements in a flexible manner.

Therefore, the offset-quadrature amplitude modulation-based filter-bank multi-carrier (FBMC-OQAM) has been proposed as an alternative to overcome some drawbacks of the OFDM WF. Indeed, FBMC-OQAM is characterized by owning one of the best frequency localization among all the post-OFDM WFs, thanks to its prototype filter (Phydyas), providing then the best performance in supporting asynchronous and mixed numerologies transmissions. Besides, it offers high spectrum efficiency since it avoids the use of CP and large guard bands. Furthermore, the orthogonality in real domain is guaranteed thanks to the use of the OQAM modulation. However, this orthogonality is lost under frequency selective channels which requires advanced equalization techniques.

In this context, the main objective of this thesis is to study different types of equalization applied on FBMC-OQAM system. Since the modulation used in the FBMC-OQAM system can be seen as the transmission of two $M-$PAM modulations over one single carrier and since the widely linear processing outperforms the classical one for $M-$PAM modulation, we will focus on the advantages of using the widely linear processing over FBMC-OQAM

system. Additionally, and based on the cyclo-stationarity of the FBMC-OQAM signal, we have proposed an advanced equalization structure based on FRESH processing that have been applied in to a FBMC-OQAM system using different numerologies.

Keywords : OFDM, FBMC-OQAM, PAM, ISI, ICI, equalization, widely linear processing, numerology, frequency selective channel

Résumé

La forte demande des besoins, des services et des exigences des utilisateurs est le moteur du développement des systèmes de communication sans fils modernes. Ainsi, depuis les systèmes de deuxième génération (2G), de nombreux changements ont eu lieu, principalement, le passage des modulations mono-porteuses aux modulations multi-porteuses (MC) introduites pour la transmission de la 4G en sens descendant. En effet, l'idée d'introduire les formes d'ondes (WF) MC est de combattre les effets du canal de propagation, en relâchant le processus d'égalisation par la transmission des symboles de données sur des sous-canaux ou des sous-porteuses à évanouissements plats. En outre, la modulation MC la plus répandue est l'orthogonal frequency division multiplexing (OFDM), qui est devenue très dominante et largement utilisée dans de nombreuses normes sans fil, telles que long term evolution (LTE)-Advanced (LTE-A) et le Wi-Fi. Le succès de l'OFDM est principalement du à ses avantages présentés dans la simple implémentation par le biais de l'utilisation d'une transformée de Fourrier rapide inverse (IFFT) à la transmission et d'une FFT à la réception. De plus, avec l'utilisation du préfixe cyclique (CP), la transmission est sans interférences inter-symboles (ISI) avec une égalisation simple.

Malgré la dominante utilisation de l'OFDM, cette modulation présente des inconvénients. En effet, cette technique souffre de la perte de l'efficacité spectrale à cause de l'utilisation du CP, sans oublier la mauvaise localisation fréquentielle à cause de la mise en forme rectangulaire du filtre prototype utilisé dans OFDM. Ces inconvénients ont été une source de motivation pour les chercheurs pour la conception de nouvelles MC WF, ayant une meilleure localisation fréquentielle, une meilleure robustesse au synchronisme des utilisateurs, tout en conservant une complexité de mise en oeuvre modérée. Dans ce contexte, un nombre élevé de MC WF post-OFDM ont été proposés et mises en oeuvre pour répondre aux scénarios et aux exigences de la 5G d'une manière flexible.

Ainsi, la modulation multi-porteuse à base des bancs de filtres (FBMC-OQAM) a été proposée en tant que solution alternative à la WF OFDM et ce pour surmonter ses inconvénients. En effet, la modulation FBMC-OQAM utilise un filtre prototype (Phydyas) qui lui permet d'avoir une excellente localisation fréquentielle ce que lui permet de fournir une meilleure performance en supportant les phénomènes d'asynchronisme entre les utilisateurs ainsi que la transmission avec différentes numérologies. En outre, l'efficacité spectrale est améliorée grâce à la suppression du CP et de large bandes de garde. De plus, l'orthogonalité dans le domaine réel est garantie grâce à l'utilisation de la modulation OQAM. Cependant, cette orthogonalité est perdue dans les canaux sélectifs en fréquence, ce qui nécessite des techniques d'égalisation avancées.

Dans ce contexte, l'objectif de cette thèse est d'étudier plusieurs types d'égalisation ap-

pliqués aux systèmes FBMC-OQAM. Vu que la modulation utilisée en FBMC-OQAM peut être considérée comme la transmission de deux flux de modulation $M-$PAM sur la même sous porteuse et comme le traitement largement linéaire (widely linéaire) est plus performant par rapport au traitement classique pour la modulatyion $M-$PAM, on va se concentrer sur les avantages de ce traitement largement linéaire utilisé pour le système FBMC-OQAM. En outre, en se basant sur le caractère cyclo-stationnaire du signal FBMC-OQAM, nous avons proposés une structure d'égalisation avancée basée sur le traitement FRESH (FREquency SHift) qui a été appliqué sur un système FBMC-OQAM utilisant différentes numérologies.

Mots clés : OFDM, FBMC-OQAM, PAM, ISI, ICI, égalisation, traitement widely linear, numérologie, canal sélectif en fréquence.

Résumé des travaux de thèse

Introduction

De nos jours, les systèmes radio-mobiles ne cessent de se développer afin de répondre aux énormes besoins des différents utilisateurs. En effet, depuis la deuxième génération (2G), les systèmes radio-mobiles ont beaucoup évolué tant sur le plan des débits, des services et du nombre d'utilisateurs et de terminaux. Ainsi le nombre d'utilisateurs possédant des appareils mobiles est passé de 62.6 millions d'utilisateurs en 2010 à 171 millions en 2014 et les estimations sont de 285.6 millions d'utilisateurs en 2023 [1]. Pour répondre aux différents besoins et exigences en termes de service des utilisateurs, les services fournis doivent être améliorés et diversifiés. Ainsi, les services fournis doivent prendre en considération la réduction du temps de latence, l'amélioration de l'efficacité énergétique (EE) ainsi que l'efficacité spectrale (SE). En outre, les principaux enjeux, pour chaque génération de systèmes de communication sans fil, se présentent principalement dans la prise en considération de la mobilité, l'augmentation du débit dans les deux sens de transmission (descendant et montant), la réduction de la consommation, l'amélioration de la sécurité ainsi que la fiabilité, la réduction des coûts, l'amélioration des formes d'ondes utilisées [2], etc,... et, ce, pour s'adapter aux exigences de chaque nouveau système de communication.

Pour faire face à ces exigences, la forme d'onde (WF) utilisée a subi plusieurs évolutions d'une génération à une autre. Cette évolution se présente principalement par le passage de la WF mono-porteuse (systèmes 2G/3G) vers la WF multi-porteuses (MWFs) pour les systèmes 4G et 5G. La forme d'onde la plus répandue qui est utilisée dans le système radio-mobile de 4ème génération est l'orthogonal frequency division multiplexing (OFDM) [3]. L'OFDM est utilisée dans plusieurs standards de radiocommunication tels que, par exemple, le long term evolution (LTE)- Advanced (LTE-A), la TNT et le Wi-Fi. Le succès de cette forme d'onde est principalement lié à la simplicité d'implémentation par le biais d'une transformée de Fourier inverse rapide (IFFT) à l'émission et d'une transformée de Fourier rapide (FFT) à la réception. De plus, l'insertion d'un préfixe cyclique (CP), garantit une émission sans interférences entre symboles (ISI) et une égalisation très simple utilisant un égaliseur avec un seul coefficient pour chaque sous-porteuse [4].

Malgré le succès et l'utilisation généralisée de l'OFDM, cette forme d'onde possède, néanmoins, des inconvénients qui l'empêchent de répondre à certains défis envisagés par les systèmes de la 5G et plus [5–7]. En effet, l'OFDM souffre d'une mauvaise localisation fréquentielle à cause de la mise en forme rectangulaire du filtre et, de plus, elle souffre de la perte de l'efficacité spectrale à cause de l'insertion du préfixe cyclique. Pour ce qui concerne les services envisagés pour la 5G, on peut les classer dans 3 catégories : massive machine type

machine (mMTC) ou encore internet des objets (IoT), enhanced mobile broadband (eMBB) et ultra reliable and low latency communications (URLLC) [2–8]. Ces trois classes de services ont des exigences différentes. En effet, les services appartenant à la classe eMBB nécessitent une efficacité spectrale et des débits élevés. Ils nécessitent une bande passante plus large ainsi qu'un temps de latence réduit [5]. Par contre, les applications de mMTC nécessitent un espacement étroit entre les sous-porteuses afin de supporter un maximum d'équipements connectés allant jusqu'au 10^6 appareils/km^{2}et celles du service URLLC nécessitent une grande fiabilité et de faible temps de latence.

Vis-à-vis de cette multitude d'exigences, l'OFDM est incapable de les fournir de manière flexible, d'où la standardisation de la release 15 (NR) par le projet partenariat de la troisième génération (3GPP) dans le but de supporter les classes de services avec leurs différentes exigences. En effet, le système de communication sans fil de la 5G est dimensionné pour pouvoir supporter une grande variété de services avec différentes exigences. En outre, il devrait supporter des transmissions asynchrones [4] ainsi que des transmissions avec plusieurs numérologies sous la même NR [3, 9].

C'est dans ce contexte que plusieurs formes d'ondes (appelées aussi post-OFDM MWFs) ont été proposées comme des candidates pour les systèmes 5G. Parmi ces MWFs, la modulation multi-porteuses à base des bancs de filtres (FBMC-OQAM) a été proposée comme étant une alternative pour faire face aux inconvénients de l'OFDM principalement la mauvaise localisation fréquentielle et l'émission hors bande (OOB) élevée [10, 11]. En effet, la modulation FBMC-OQAM possède une des meilleures localisations fréquentielles grâce à l'utilisation d'un filtre prototype très bien localisé en fréquence (filtre Phydyas) [11], ce qui permet d'obtenir de bonnes performances avec les scénarios d'asynchronisme temporel ainsi qu'en présence de différents numérologies. De plus, avec FBMC-OQAM, on n'a pas besoin d'insérer de CP ni de larges bandes de garde, ce qui permet d'avoir une efficacité spectrale améliorée vis-à-vis de l'OFDM. La modulation OQAM garantit l'orthogonalité dans le domaine réel sur des canaux plats non sélectifs en fréquence. Malheureusement, sur des canaux fortement sélectifs en fréquence, cette condition n'est plus garantie ce qui nécessite des traitements avancés d'égalisation.

Pour le traitement optimal de l'égalisation, on doit étudier les propriétés, à l'ordre 2, du signal transmis afin d'adopter un meilleur traitement et de concevoir un meilleur égaliseur. En se basant sur les propriétés à l'ordre 2, selon que le signal soit circulaire à l'ordre 2 (SOC) ou non (NSOC), ou bien qu'il soit stationnaire ou cyclo-stationnaire, le traitement dans l'égaliseur est différent. Quand le signal transmis est caractérisé comme étant circulaire à l'ordre 2 (SOC), le traitement linéaire est suffisant. Néanmoins, quand il est caractérisé comme étant NSOC, l'égalisation largement linéaire est requise. Dans la suite, nous utiliserons le terme anglais de « widely linear » pour ce type d'égaliseur.

Le principal objectif de cette thèse est d'étudier plusieurs formes d'égalisation adaptées au système multi-porteuses FBMC-OQAM. La modulation FBMC-OQAM utilise une technique OQAM qui peut être considérée comme la transmission de deux flux de modulation $M-$PAM sur la même sous-porteuse. Les modulations $M-$PAM étant NSOC, il apparait que le traitement de type widely linear pourra fournir de meilleures performances par rapport au traitement linéaire classique. C'est la raison pour laquelle on s'intéresse à l'étude de l'apport de l'égalisation widely linear appliquée au système FBMC-OQAM.

Le plan de la thèse est le suivant :

Chapitre 2 : ce chapitre introduit les notions de circularité et de non circularité avec une classification des modulations classiques selon le critère de circularité au second ordre (SOC) ou de non circularité au second ordre (NSOC). Le principe de la modulation FBMC-OQAM (Filter Bank based Multi-Carrier- modulation Offset QAM) est également présenté ainsi que les canaux de propagation de radiocommunication sélectifs en fréquence.

Chapitre 3 : dans ce chapitre, les notions de stationnarité et de cyclo-stationnarité sont introduites. Un état de l'art sur les techniques d'égalisation est réalisé avec les adaptations de l'égaliseur aux signaux selon leur circularité et leur stationnarité.

Chapitre 4 : ce chapitre porte sur l'application de l'égalisation widely linear (WL) à des modulations de type rectiligne (modulation NSOC de type $M-$PAM) dans des canaux plats ou sélectifs en fréquence et en présence de plusieurs utilisateurs. Les égaliseurs mis en oeuvre et comparés sont : un égaliseur linéaire classique, un égaliseur widely linear (WL), et un égaliseur de type Fresh (FREquency SHift). L'apport des traitements WL et Fresh sont clairement mis en évidence.

Chapitre 5 : ce chapitre traite de l'étude et de l'application des techniques développées dans le chapitre précédent aux modulations de type quasi-rectilignes de type FBMC-OQAM. La modulation de type Offset QAM peut être considérée comme la transmission de deux flux modulés en $M-$PAM sur la même sous porteuse. Les structures d'égalisation précédemment développées sont ainsi adaptées et mises en oeuvre sur la modulation FBMC-OQAM. Les résultats de simulation comparent les performances des différents égaliseurs et montrent le gain du traitement WL dans sa version classique ainsi que dans sa version Fresh.

Conclusion et perspectives : Conclusion générale sur le travail et perspectives futures de travail.

Chapitre 2 : Généralités : Circularité et sélectivité de canal

Dans ce chapitre, nous introduisons plusieurs notions importantes qui serviront à l'élaboration de ce travail et seront utilisées dans les chapitres suivants. Nous allons tout d'abord présenter le concept de la circularité élaborée à l'ordre 2. Par la suite nous décrivons le système FBMC-OQAM et proposons une description des canaux de propagation radio-mobile.

Circularité

La notion de circularité d'un signal est déduite à partir de l'étude des propriétés statistiques à l'ordre 2. Ces dernières se présentent sous la forme de la matrice de covariance ainsi que de la matrice de pseudo-covariance de ce signal. Pour un vecteur $\boldsymbol{z}$, les matrices de covariance et pseudo-covariance sont, respectivement, exprimées par

$$\boldsymbol{R} = \mathbb{E}\left[\boldsymbol{z}\boldsymbol{z}^H\right] \tag{0.1}$$

$$\boldsymbol{C} = \mathbb{E}\left[\boldsymbol{z}\boldsymbol{z}^T\right] \tag{0.2}$$

Un vecteur $\boldsymbol{z}$ est dit circulaire au second ordre (SOC), si sa matrice de pseudo-covariance est nulle, c'est à dire, elle vérifie l'équation suivante

$$\mathbb{E}\left[\boldsymbol{z}\boldsymbol{z}^T\right] = 0. \tag{0.3}$$

En se basant sur l'équation (0.3), si la condition de matrice de pseudo-covariance nulle est vérifiée, le signal est caractérisé comme SOC, autrement, le signal est défini comme non circulaire au second ordre (NSOC). D'une manière générale, l'information portée par les propriétés statistiques sont contenues dans les matrices de covariance et de pseudo-covariance. Ainsi, pour un signal SOC dont la matrice pseudo-covariance est nulle, toute l'information est contenue dans la matrice de covariance. Nous définissons le coefficient de non circularité [12] du signal z comme suit

$$\delta \triangleq \frac{\mathbb{E}[z^2]}{\mathbb{E}[|z|^2]} \triangleq |\delta| e^{j\phi}, \tag{0.4}$$

où $\phi \in [0, 2\pi)$ est la phase de non circularité du signal z. Selon les valeurs du coefficient de non circularité $|\delta|$ (valeurs qui sont comprises entre 0 et 1) [13], nous pouvons classer les signaux comme suit :

— Si $|\delta| = 0$, le signal est caractérisé comme étant SOC ou encore qualifié de «propre»,
— Si $|\delta| \neq 0$, le signal est dit NSOC ou encore qualifié d'«impropre»,
— Si $|\delta| = 1$, le signal NSOC est qualifié de rectiligne [14].

Exemples des modulations SOC et NSOC

Les modulations d'amplitudes en quadrature $M-$QAM appartiennent à la famille des modulations circulaires au second ordre (SOC), alors que les modulations $M-$PAM appartiennent à la famille des modulations non circulaires au second ordre (NSOC). Les modulations $M-$PAM sont, de plus, caractérisées comme rectilignes. Parmi les modulations NSOC, nous rencontrons aussi, les modulations quasi-rectilignes (QR) qui, après une dérotation, peuvent devenir des modulations rectilignes. Parmi ces modulations, nous trouvons quelques modulations CPM et les modulations de type Offset QAM (OQAM).
La description d'une modulation $M-$QAM et $M-$OQAM est illustrée par la Figure 0.1

D'après la Figure 0.1, nous constatons que les symboles complexes QAM sont transmis à chaque durée période T pour la modulation $M-$QAM, alors que pour la modulation $M-$OQAM, les parties réelles et imaginaires des symboles QAM sont transmises alternativement à la cadence d'une demi-période QAM, c-à-d $\frac{T}{2}$. De ce fait, la modulation $M-$OQAM peut être considérée comme la transmission de deux flux de modulations $M-$PAM (les parties réelles et imaginaires des symboles QAM) d'une durée de période de $\frac{T}{2}$.

FBMC-OQAM

La modulation FBMC-OQAM représente une alternative pour corriger les inconvénients de la modulation CP-OFDM [15], [16], modulation adoptée pour les systèmes de la 4G. En effet, la modulation CP-OFDM souffre de la mauvaise localisation fréquentielle à cause de l'utilisation du filtre de mise en forme rectangulaire. De plus, le fait d'insérer le préfixe cyclique (CP) aboutit à une perte de l'efficacité spectrale à cause de la redondance introduite.

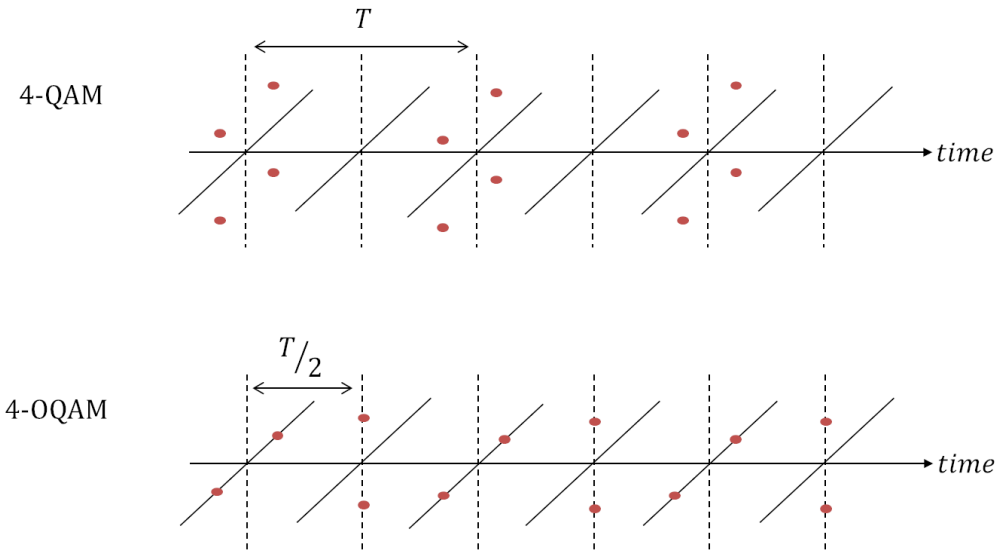

FIGURE 0.1: Les modulations 4-QAM et 4-OQAM.

Le système FBMC-OQAM, de par ses qualités, peut répondre aux besoins du système 5G. En effet, ce système possède une très bonne localisation fréquentielle grâce à l'utilisation du filtre Phydyas [17–19]. De plus, ce système a une meilleure efficacité spectrale puisqu'il n'utilise pas de CP et ne nécessite pas de larges bandes de garde entre deux systèmes. Il est aussi moins sensible à l'effet Doppler.
Les réponses impulsionnelles et fréquentielles des deux filtres, rectangulaire et Phydyas, utilisés respectivement dans les systèmes, OFDM et FBMC, sont données par les Figures 0.2 et 0.3. Le filtre Phydyas de la Figure 0.2 est calculé avec un facteur de recouvrement (overlapping factor) $K = 4$.

En regardant la Figure 0.3, il est clair que le filtre Phydyas possède bien une meilleure localisation fréquentielle que le filtre rectangulaire qui engendre des lobes secondaires importants avec une faible décroissance. Avec tous les avantages précédemment mentionnés, le système FBMC-OQAM est capable de répondre aux exigences des systèmes de communications modernes tout en assurant la possibilité de transmissions asynchrones ainsi que l'existence de plusieurs numérologies.

Le système FBMC-OQAM adopté dans notre étude est présenté sur les Figures 0.4 et 0.5 qui représentent, respectivement, l'émetteur et le récepteur du système. Le système FBMC-OQAM avec N sous-porteuses possède 4 blocs principaux qui sont : le modulateur OQAM, le banc de filtre de synthèse (SFB), comme illustrés par la Figure 0.4, le banc de filtre d'analyse (AFB) et finalement le démodulateur OQAM comme présentés par la Figure 0.5.

Nous commençons par la description du système FBMC coté transmetteur, où les symboles QAM complexes $c_k(i)$ transmis sur la k^{eme} sous-porteuse sont convertis en des symboles réels $x_k(n)$ via l'opération $\mathbb{C}2\mathbb{R}$ (Complex to Real) résultant un flux doublé. Les parties réelles et imaginaires du symbole $c_k(i)$ sont transmises à chaque demi période. Ensuite, ce flux est multiplié par le facteur $\theta_k(n)$ qui convertit les symboles réels $x_k(n)$ en des symboles qui sont soit purement réels soit purement imaginaires $v_k(n)$. Le facteur multiplicatif $\theta_k(n)$

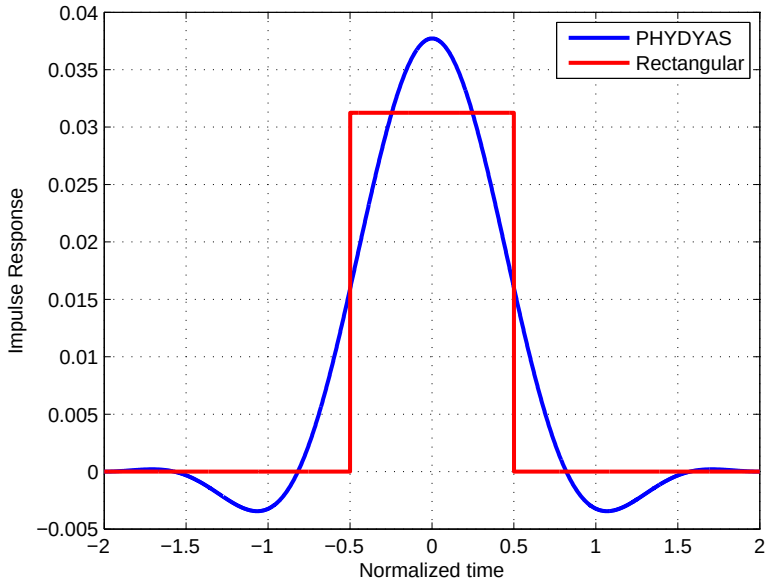

FIGURE 0.2: Réponses impulsionnelles des filtres PHYDYAS et rectangulaire.

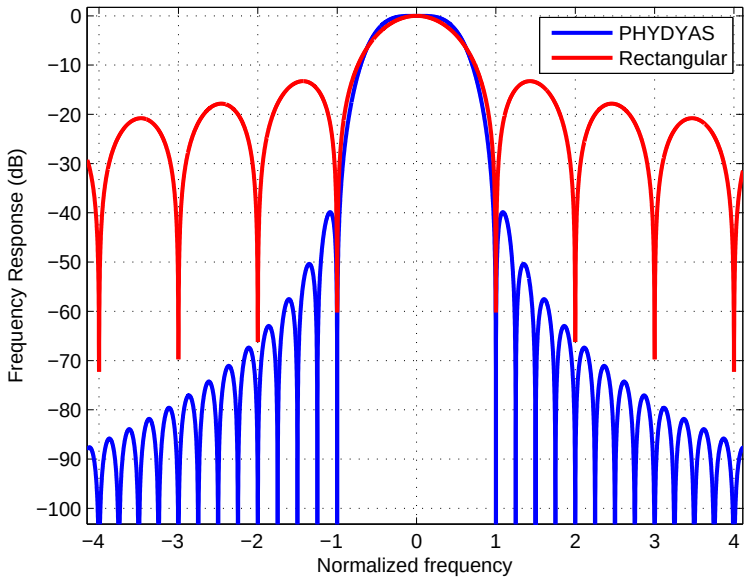

FIGURE 0.3: Réponses fréquentielle des filtres PHYDYAS et rectangulaire.

de la k^{eme} sous-porteuse est donné par l'équation (0.5)

$$\theta_k(n) = j^{k+n}. \tag{0.5}$$

Dans le bloc SFB, la première opération consiste à sur-échantillonner le signal $v_k(n)$ sur chaque sous-porteuse par le facteur $\frac{N}{2}$ suivi du filtrage par le filtre prototype de Phydyas de réponse impulsionnelle $p(m)$ de longueur L. Ensuite, le signal sur la k^{eme} sous-porteuse

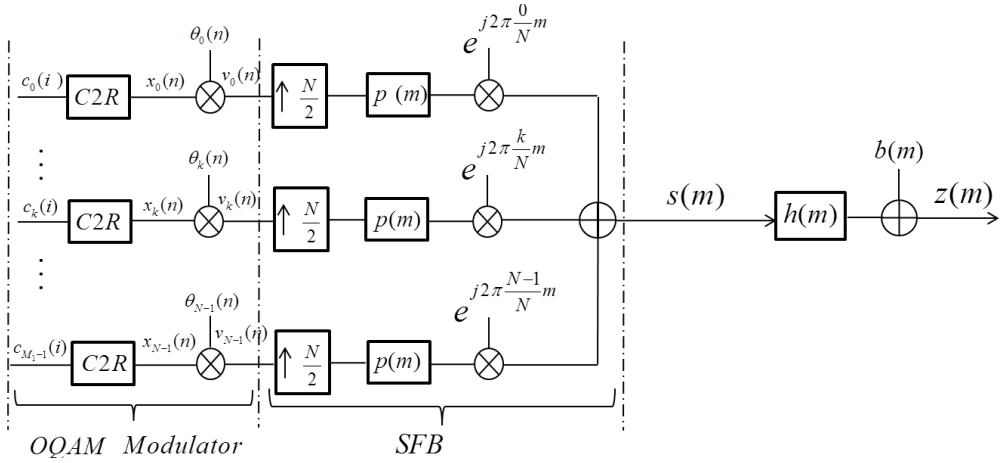

FIGURE 0.4: Le transmetteur FBMC-OQAM.

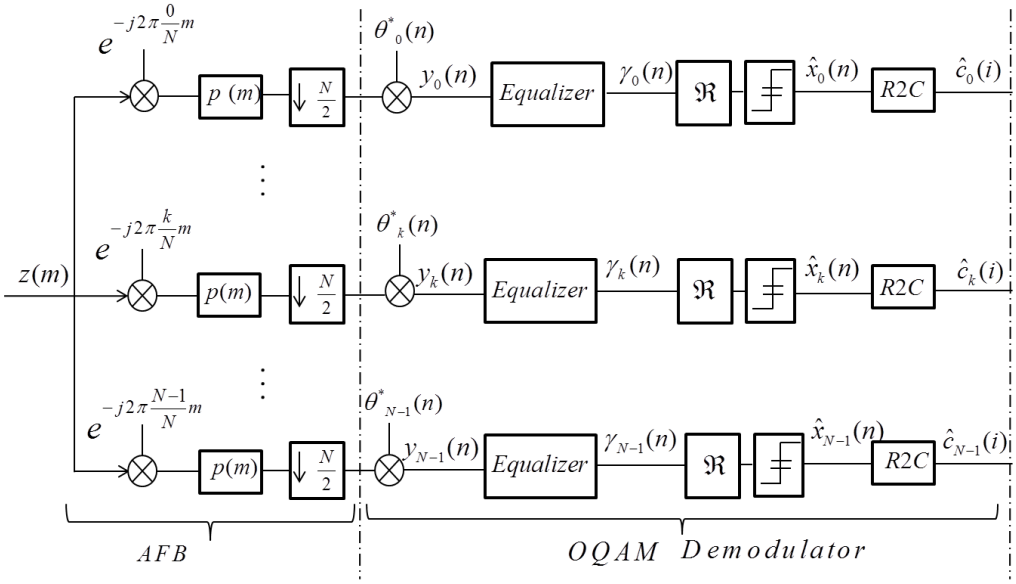

FIGURE 0.5: Le récepteur FBMC-OQAM.

est multiplié par $e^{j2\pi\frac{k}{N}m}$. Finalement, les signaux issus de toutes les sous-porteuses sont sommés pour former le signal transmis $s(m)$. Ce signal s'écrit ainsi

$$s(m) = \sum_{k=0}^{N-1} \sum_{n=-\infty}^{\infty} \left([x_k(n)\theta_k(n)]_{\uparrow \frac{N}{2}} \star p(m) \right) e^{j2\pi\frac{k}{N}m}. \tag{0.6}$$

Sur la Figure 0.4, le signal émis par le transmetteur, $s(m)$, est filtré par le canal $h(m)$ et perturbé par le bruit additif blanc Gaussien (AWGN) $b(m)$ pour former le signal reçu $z(m)$.

A la réception, (voir la Figure 0.5), le signal $z(m)$ est multiplié, à la k^{eme} sous-porteuse, par le facteur $e^{-j2\pi\frac{k}{N}m}$ puis filtré par le filtre $p(m)$ et sous échantillonné d'un facteur $\frac{N}{2}$. Les signaux en sortie de l'AFB sont multiplié par $\theta_k^*(n)$. Cette opération n'est que la dérotation du signal et résulte en le signal $y_k(n)$ qui correspond au signal d'entrée de l'égaliseur. Les signaux γ_k et $\hat{x}_k$ représentent respectivement le signal égalisé avant et après la prise de décision. La dernière opération du bloc récepteur consiste à convertir les symboles réels en des symboles complexes via l'opération $\mathbb{R}2\mathbb{C}$ (Real to Complex).

Canal de transmission

Lors du passage du signal transmis à travers le canal de transmission, les phénomènes qui peuvent intervenir sont principalement : la réflexion, la diffraction et la diffusion [20], [21]. Ces phénomènes causent la réception d'une multitude de versions du signal transmis avec des amplitudes, des phases et des retards différents, générés par les différents trajets. Ainsi, le canal de propagation à trajets multiples peut être modélisé comme étant un filtre linéaire dont la réponse impulsionnelle $h(t,\tau)$ [21] est donnée par l'équation suivante

$$h(t,\tau) = \sum_{k=0}^{L_h-1} a_k(t,\tau) e^{j\{2\pi f_h \tau_k(t) + \phi_k(t,\tau)\}} \delta(\tau - \tau_k(t)), \tag{0.7}$$

avec L_h représente le nombre de trajets, a_k et τ_k désignent, respectivement, l'amplitude et le retard du k^{eme} trajet.

Chapitre 3 : Les techniques d'égalisation

Dans ce chapitre nous introduisons, tout d'abord, la notion supplémentaire de stationnarité et de cyclo-stationnarité d'un signal. Les notions de cyclo-stationnarité conjointement au caractère NSOC seront utilisés dans les architectures des égaliseurs. Dans une deuxième partie du chapitre, toutes les architectures d'égaliseur qui seront utilisées dans la suite de la thèse seront présentées : Égaliseur linéaire, Égaliseur widely linear, Égaliseur linéaire et widely linear Fresh.

Cyclo-stationnarité

En plus des statistiques d'ordre deux vues dans le chapitre précédent, un signal peut être classé selon le critère de la stationnarité. En effet, il peut être soit stationnaire soit non stationnaire. La stationnarité est étudiée en observant les propriétés statistiques du premier (la moyenne) et du deuxième ordre (matrice de covariance et de pseudo-covariance). Si les

propriétés statistiques ne varient pas au cours du temps (elles sont indépendantes du temps), nous qualifions le signal de stationnaire. Par contre, si ces propriétés statistiques varient avec le temps, nous sommes alors dans le cas d'un signal non-stationnaire. De plus, si la moyenne, les matrices de covariance et de pseudo-covariance connaissent un rythme répétitif dans le temps, nous parlons d'un signal cyclo-stationnaire avec des propriétés statistiques qui se répètent périodiquement.

Ainsi, un signal stationnaire $x(t)$ et un signal cyclo-stationnaire $y(t)$ de période T vérifient les équations suivantes

— Pour le signal $x(t)$:

$$\mathbb{E}[x(t)] = m_x(t) = m_x \tag{0.8}$$

$$\mathbb{E}[x(t)x^*(t+\tau)] = R_x(t,\tau) = R_x(\tau), \quad \forall t \tag{0.9}$$

$$\mathbb{E}[x(t)x(t+\tau)] = C_x(t,\tau) = C_x(\tau), \quad \forall t \tag{0.10}$$

— Pour le signal $y(t)$:

$$\mathbb{E}[y(t)] = m_y(t) = m_y(t+T) = \mathbb{E}[y(t+T)] \tag{0.11}$$

$$\mathbb{E}[y(t)y^*(t+\tau)] = R_y(t,\tau) = R_y(t+T,\tau), \quad \forall t \tag{0.12}$$

$$\mathbb{E}[y(t)y(t+\tau)] = C_y(t,\tau) = C_y(t+T,\tau), \quad \forall t \tag{0.13}$$

Pour un signal cyclo-stationnaire $y(t)$ de période T, les propriétés statistiques d'ordre 2 sont périodiques et possèdent donc un développement en série de Fourier

$$R_y(t,\tau) = \sum_{\alpha_i \in \mathcal{A}_\alpha} R_y^{\alpha_i}(\tau) e^{j2\pi\alpha_i t} \tag{0.14}$$

$$C_y(t,\tau) = \sum_{\beta_i \in \mathcal{B}_\beta} C_y^{\beta_i}(\tau) e^{j2\pi\beta_i t} \tag{0.15}$$

Où les termes

— α_i désignent les fréquences cycliques du second ordre (SO) non conjuguées qui sont égales à : $\alpha_i = \dfrac{i}{T}, i \in \mathbb{Z}$,

— β_i sont les fréquences cycliques du SO conjuguées et sont égales à : $\beta_i = 2\Delta_f + \dfrac{i}{T}, i \in \mathbb{Z}$ [22], où Δ_f désigne la fréquence porteuse,

— $\mathcal{A}_\alpha$ et $\mathcal{B}_\beta$ représentent les ensembles de toutes les fréquences cycliques non conjuguées α_i et conjuguées β_i, respectivement,

— $R_y^{\alpha_i}(\tau)$ et $C_y^{\beta_i}(\tau)$ sont appelées, respectivement, les fonctions d'auto-corrélation cycliques non conjuguées et les fonctions pseudo-auto-corrélations conjuguées de période T.

Égalisation

Le traitement d'égalisation est requis quand le signal transmis est perturbé par des interférences avec d'autres utilisateurs et/ou par des interférences entre symboles causées par le canal de transmission. Afin de pouvoir récupérer avec un faible taux d'erreur les symboles transmis, un traitement d'égalisation doit être mis en place. Après l'adoption d'un

critère d'égalisation pour que le traitement d'égalisation soit fiable et performant, nous devons étudier les caractéristiques du signal transmis. Nous devons étudier s'il est SOC ou bien NSOC, stationnaire ou cyclo-stationnaire.
Afin de classifier les différents égaliseurs, nous allons nous baser sur le schéma de principe de la Figure 0.6.

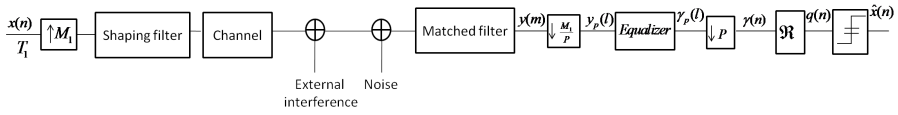

FIGURE 0.6: Système modèle.

Dans la Figure 0.6, les symboles $x(n)$ sont transmis avec une durée symbole égale à T_1 avec $T_1 = M_1 T_e$ où T_e désigne le temps d'échantillonnage. Ce signal est filtré par un filtre de mise en forme puis par le canal de transmission. Le signal émis est perturbé par des interférences extérieures venant d'autres utilisateurs ainsi que par un bruit additif. A la réception, le signal est filtré par un filtre adapté au filtre de mise en forme et le signal à la sortie de ce filtre, $y(m)$, est sous-échantillonné en prenant P échantillons par symbole avant d'être présenté à l'entrée de l'égaliseur. Si $P = 1$, nous parlerons d'égaliseur avec un seul échantillon par symbole. Si $P > 1$, nous parlerons alors d'égaliseur fractionnaire. Par la suite, les symboles $\gamma(n)$ et $q(n)$ représentent les symboles égalisés avant et après la prise de la partie réelle. Finalement, le signal $\hat{x}(n)$ représente les symboles estimés.

Nous choisirons comme critère de calcul des coefficients de l'égaliseur le critère de minimisation de l'erreur quadratique moyenne (MSE) entre les symboles émis et les symboles reçus. Nous allons introduire deux expressions de la MSE. La première exprimée par l'équation (0.16) sert à calculer les expressions des différents égaliseurs et l'autre donnée par l'équation 0.17 permet d'évaluer la performance globale du système.

$$MSE_\gamma = \mathbb{E}[|\gamma(n) - x(n-\Delta)|^2], \tag{0.16}$$

$$\begin{aligned} MSE_q &= \mathbb{E}[|\mathrm{Re}(\gamma(n)) - x(n-\Delta)|^2] \\ &= \mathbb{E}[|q(n) - x(n-\Delta)|^2], \end{aligned} \tag{0.17}$$

avec Δ qui désigne le retard de décision.

Égaliseurs à espacement de symboles et égaliseurs fractionnaires

Ce type d'égalisation est classifié en fonction du nombre d'échantillons par symbole pris P (voir la Figure 0.6). Ainsi, si P vaut 1, nous parlerons d'une égalisation dite à espacement de symbole (SSE). Si, $P > 1$, c'est à dire, plus d'un échantillon par symbole est utilisé dans le traitement d'égalisation, nous serons dans le cas d'une égalisation fractionnaire (FSE).

Égaliseur linéaire

Nous considérons le vecteur $\boldsymbol{y_p}(l)$ de longueur L_e tel que : $\boldsymbol{y_p}(l) = [y_p(lT_1), y_p(lT_1 - T_e), ..., y_p(lT_1 - (L_e - 1)T_e)]^T$.

Cet égaliseur utilise seulement les informations contenues dans la matrice de covariance du signal. Ainsi, l'égaliseur linéaire MMSE-LE est un vecteur de longueur L_e dont l'expression est donnée par

$$\boldsymbol{w_{LE}} = \boldsymbol{r}_{x\boldsymbol{y_p}} \boldsymbol{R}_{\boldsymbol{y_p}}^{-\mathbf{1}}, \tag{0.18}$$

où le vecteur $\boldsymbol{r}_{x\boldsymbol{y_p}} = \mathbb{E}[x(n)\boldsymbol{y_p^H}(l)] \in \mathbb{C}^{1\times L_e}$ représente le vecteur d'inter-corrélation entre les symboles émis et l'entrée de l'égaliseur. La matrice $\boldsymbol{R}_{\boldsymbol{y_p}} = \mathbb{E}[\boldsymbol{y_p}(l)\boldsymbol{y_p^H}(l)] \in \mathbb{C}^{L_e\times L_e}$ désigne la matrice de covariance du signal à l'entrée de l'égaliseur.

Égaliseur widely linear

Dans le cas où le signal transmis est NSOC, l'égaliseur linéaire n'est pas la solution optimale et peut être remplacé par le traitement widely linear. En effet, l'égaliseur widely linear, à l'opposé du traitement linéaire classique, exploite l'information contenue dans les deux matrices de covariance et de pseudo-covariance. Le schéma du traitement widely linear est illustré par la Figure 0.7.

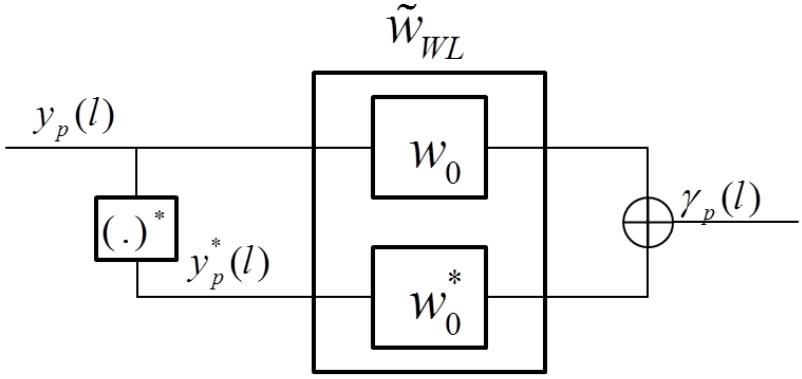

FIGURE 0.7: schéma de l'égalisation widely linear.

Nous considérons le vecteur $\tilde{\boldsymbol{y}}_{\boldsymbol{p}}(l) = [\boldsymbol{y_p^T}(l), \boldsymbol{y_p^*}(l)]^T$ de longueur $2L_e$ qui représente l'entrée de l'égaliseur widely linear. L'expression de l'égaliseur widely linear est exprimée par [14]

$$\tilde{\boldsymbol{w}}_{\boldsymbol{WL}} = \boldsymbol{r}_{x\tilde{\boldsymbol{y}}_{\boldsymbol{p}}} \boldsymbol{R}_{\tilde{\boldsymbol{y}}_{\boldsymbol{p}}}^{-\mathbf{1}}, \tag{0.19}$$

Le vecteur $\boldsymbol{r}_{x\tilde{\boldsymbol{y}}_{\boldsymbol{p}}} \in \mathbb{C}^{1\times 2L_e}$ désigne le vecteur d'inter-corrélation entre les symboles émis et le signal à l'entrée de l'égaliseur widely linear. La matrice $\boldsymbol{R}_{\tilde{\boldsymbol{y}}_{\boldsymbol{p}}} \in \mathbb{C}^{2L_e\times 2L_e}$ représente la matrice de covariance du signal $\tilde{\boldsymbol{y}}_{\boldsymbol{p}}(l)$.

Égaliseur linéaire et widely linear Fresh

Lorsqu'un signal est caractérisé comme cyclo-stationnaire, le traitement dit Fresh peut être mis en place avec profit. Ce traitement exploite en plus la corrélation existante entre les composantes spectrales du signal. Si nous considérons le cas où on a de l'énergie pour une fréquence cyclique non conjuguée α_1 et une fréquence cyclique conjuguée β_1, les schémas de

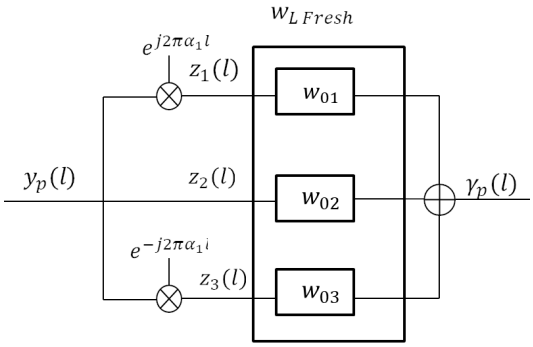

FIGURE 0.8: Schéma de l'égalisation linéaire Fresh.

l'égalisation Fresh dans leur version linéaire et widely linear sont donnés, respectivement, par les Figures 0.8 et 0.9.

Soient les vecteurs $\boldsymbol{z_p}(l) = [\boldsymbol{z_1^T}(l), \boldsymbol{z_2^T}(l), \boldsymbol{z_3^T}(l)]^T$ et $\tilde{\boldsymbol{z}}_{\boldsymbol{p}}(l) = [\boldsymbol{z_1^T}(l), \boldsymbol{z_2^T}(l), \boldsymbol{z_3^T}(l), \boldsymbol{z_4^T}(l), \boldsymbol{z_5^T}(l), \boldsymbol{z_6^T}(l)]^T$, où $\boldsymbol{z_i}(l) = [z_i(lT_1), z_i(lT_1 - T_e), ..., z_i(lT_1 - (L_e - 1)T_e)]^T$, pour $i = 1, .., 6$.
$z_i(l), i \in \{1, 3\}$ est le signal reçu décalé en fréquence en utilisant les fréquences cycliques $+\alpha_1, 0$ et $-\alpha_1$, respectivement. De même, $z_i(l), i \in \{4, 6\}$ représente la version décalée du signal $y_p^*(l)$ en utilisant les fréquences cycliques $+\beta_1, 0$ et $-\beta_1$, respectivement.
Les expressions des égaliseurs linéaire et widely linear Fresh sont données, respectivement, par

$$\boldsymbol{w_{LFresh}} = \boldsymbol{r}_{x\boldsymbol{z_p}} \boldsymbol{R}_{\boldsymbol{z_p}}^{-\mathbf{1}}, \tag{0.20}$$

$$\tilde{\boldsymbol{w}}_{\boldsymbol{WLFresh}} = \boldsymbol{r}_{x\tilde{\boldsymbol{z}}_{\boldsymbol{p}}} \boldsymbol{R}_{\tilde{\boldsymbol{z}}_{\boldsymbol{p}}}^{-\mathbf{1}}, \tag{0.21}$$

où les vecteurs $\boldsymbol{r}_{x\boldsymbol{z_p}} \in \mathbb{C}^{1\times 3L_e}$ et $\boldsymbol{r}_{x\tilde{\boldsymbol{z}}_{\boldsymbol{p}}} \in \mathbb{C}^{1\times 6L_e}$ représentent les vecteurs d'inter-corrélation entre les symboles transmis et le signal à l'entrée de l'égaliseur. $\boldsymbol{R}_{\boldsymbol{z_p}} = \mathbb{E}[\boldsymbol{z_p}(l)\boldsymbol{z_p^H}(l)] \in \mathbb{C}^{3L_e\times 3L_e}$ et $\boldsymbol{R}_{\tilde{\boldsymbol{z}}_{\boldsymbol{p}}} = \mathbb{E}[\tilde{\boldsymbol{z}}_{\boldsymbol{p}}(l)\tilde{\boldsymbol{z}}_{\boldsymbol{p}}^{\boldsymbol{H}}(l)] \in \mathbb{C}^{6L_e\times 6L_e}$, sont les matrices de covariance du signal à l'entrée de l'égaliseur linéaire Fresh et widely linear Fresh, respectivement.

Chapitre 4 : Analyse des performances des égaliseurs classiques et Fresh dans un système à modulation rectiligne

Dans ce chapitre, nous allons appliquer les différents traitements mentionnés dans le 3ième chapitre, sur un système utilisant une modulation rectiligne de type $M-$PAM, en présence de K interférences rectilignes. Une partie du chapitre concerne l'étude des performances de l'égalisation linéaire et widely linear appliquée en mode SSE. Dans une deuxième partie, nous allons tester l'apport du traitement Fresh ainsi que les gains apportés par des égaliseurs fractionnaires.

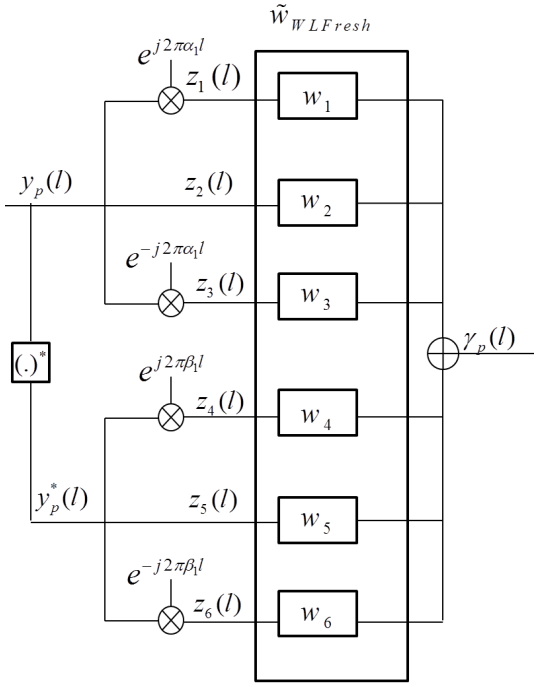

FIGURE 0.9: Schéma de l'égalisation widely linéaire Fresh.

Impact du nombre d'interférences sur les performances des égaliseurs

Pour étudier l'impact du nombre d'interférences sur les performances des égaliseurs linéaire et widely linear appliqués en mode SSE, nous considérons le système modèle donné par la Figure 0.10

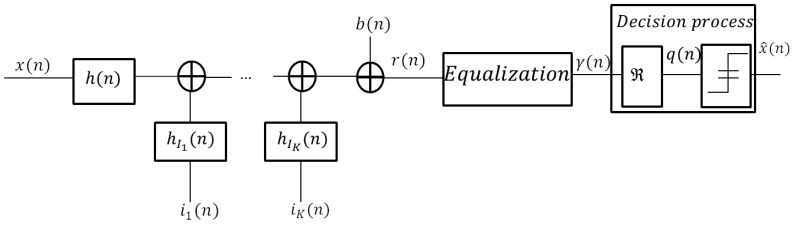

FIGURE 0.10: Le système modèle avec K interféreurs.

Dans ce système, nous transmettons des symboles $M-$PAM, $x(n)$, qui représente le signal d'intérêt. Le signal utile est perturbé par K interféreurs $M-$PAM, $i_1(n), .., i_K(n)$. $h(n), h_{I_1}, .., h_{I_K}$ désignent, respectivement, les réponses impulsionnelles du canal de transmission du signal d'intérêt et des K interféreurs. $b(n)$ est un bruit blanc additif Gaussien et $r(n)$ est le signal à égaliser.

Afin d'étudier l'impact de l'interférence entre utilisateurs (IUI), nous allons, dans un premier temps négliger l'effet du canal (nous prendrons des canaux plats). Les résultats de

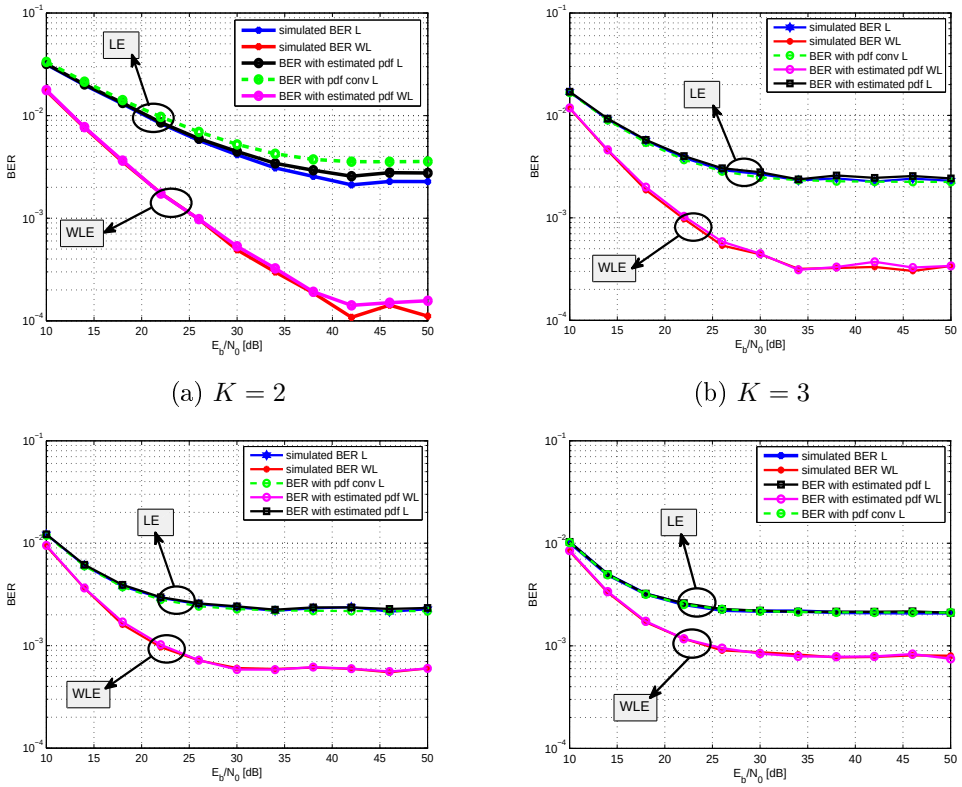

(a) $K = 2$ (b) $K = 3$

(c) $K = 4$ (d) $K = 5$

FIGURE 0.11: Performance des égaliseurs en terme de BER en fonction du nombre d'interféreurs K.

simulation sont présentés par la Figure 0.11.

D'après la Figure 0.11, il est clair que l'égaliseur widely linear donne de meilleures performances que l'égaliseur linéaire. Nous constatons toutefois une dégradation des performances du traitement widely linear, lorsque le nombre d'interférences K augmente. Néanmoins, celui-ci reste toujours plus performant que le traitement linéaire classique. Le gain de l'égaliseur WL vient du caractère NSOC du signal transmis.

Analyse des performances des égaliseurs LE, WLE et Fresh

Dans cette partie, nous allons étudier à la fois l'apport du traitement Fresh et de la technique fractionnaire pour les différents égaliseurs. Pour ce faire, nous considérons le système modèle donné par la Figure 0.12 avec des modulations rectilignes et deux utilisateurs.

Les deux utilisateurs de la Figure 0.12 sont, respectivement, l'utilisateur d'intérêt (UOI, $x(n)$) et un autre utilisateur (UNOI, $i(n')$). Ces deux utilisateurs sont supposés synchronisés en temps puisque le scénario considéré est la transmission dans le sens descendant de la station de base vers les terminaux mobiles. Même si ces deux utilisateurs sont synchrones dans le temps, ils ne le sont pas nécessairement en fréquence. Un écart fréquentiel existe entre eux et cela est modélisé par la bande de garde B_g entre les deux utilisateurs.

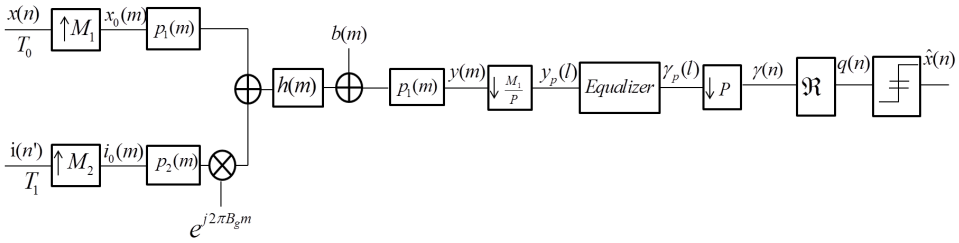

FIGURE 0.12: Système modèle à modulation rectiligne à deux utilisateurs.

En utilisant les différents égaliseurs décrits dans le chapitre 3, l'impact de la bande de garde entre les deux utilisateurs est étudié. Les performances en terme MSE sont données par la Figure 0.13.

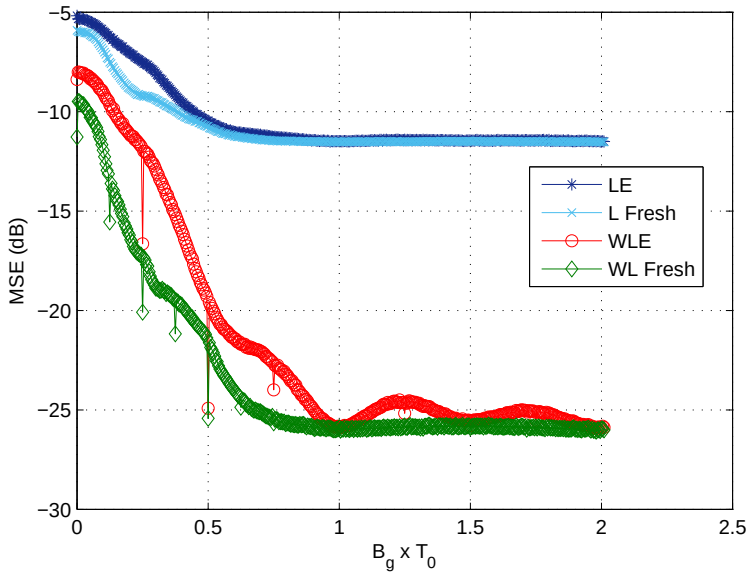

FIGURE 0.13: Performance des égaliseurs en terme de MSE en fonction du bande de garde pour $\frac{E_b}{N_0} = 20$ dB.

D'après la Figure 0.13, il est clair que le traitement widely linear dans sa version classique et Fresh donnent des performances bien meilleures que celles fournies par le traitement linéaire. De plus, à cause du caractère cyclo-stationnaire du signal étudié, le traitement WL Fresh est le plus performant. Nous pouvons constater un nouveau résultat (Figure 0.13) qui est l'existence de performance accrues du traitement widely linear pour certains valeurs bien précises de la bandes de garde. Pour ces valeurs particulières de la bande de garde ($B_g.T_0 = 0.125$, 0.25, 0.375, 0.5,...), la performance du traitement WL est nettement améliorée. Cela peut être expliqué par le fait qu'avec ces valeurs particulières de la bande de garde, la fréquence cyclique conjuguée exploitée par l'égaliseur widely linear est nulle.
Nous allons maintenant étudier l'influence du nombre d'échantillons par symboles, P. Pour

cela nous nous plaçons avec une bande de garde égale à : $B_g = \frac{0.65}{T_0}$ où T_0 est la durée des symboles de l'UOI. Les résultats de la Figure 0.14 montrent l'impact du nombre d'échantillons par symboles dans la procédure d'égalisation.

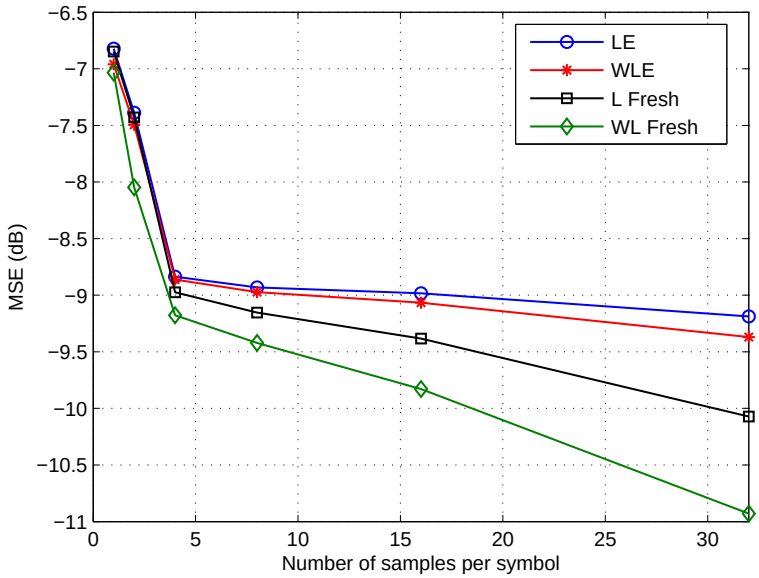

FIGURE 0.14: Impact de P sur la performance des égaliseurs pour $\frac{E_b}{N_0} = 20$ dB et $B_g = \frac{0.65}{T_0}$.

Nous constatons sur la Figure 0.14 que l'égalisation fractionnaire (FSE) est plus performante que l'égalisation SSE. Plus la valeur de P augmente, meilleure sera la performance des égaliseurs.

Chapitre 5 : Egalisation d'un signal quasi-rectiligne : Application au système FBMC-OQAM

Dans un premier temps, nous allons étudier l'apport du traitement widely linear sur un système FBMC-OQAM dans le cas d'une transmission mono-utilisateur. Tout d'abord, nous allons introduire le modèle $M-$PAM équivalent. Dans un deuxième temps, nous prendrons le cas du système FBMC-OQAM avec deux utilisateurs de numérologies différentes et nous allons étudier la performance des différentes structures d'égalisation dans le cas d'une transmission asynchrone.

Performance des égaliseurs LE et WLE pour une transmission mono-utilisateur

Le système modèle FBMC avec M_1 sous-porteuses utilisé pour l'étude de la performance des égaliseurs linéaire et widely linear en mode SSE est donné par les Figures 0.4 et 0.5 (en prenant $N = M_1$ et L_1 au lieu de L).

Soient les équations suivantes :

$$g_k(m) = p_1(m)e^{j\frac{2\pi k}{M_1}(m-\frac{L_1-1}{2})}, \tag{0.22}$$

$$f_k(m) = g_k^*(L_1 - 1 - m). \tag{0.23}$$

$g_k(m)$ et $f_k(m)$ représentent, respectivement, le SFB et l'AFB pour la k^{eme} sous-porteuse et L_1 est la longueur du filtre Phydyas.

Il est possible d'élaborer un modèle équivalent de la cascade formée par le SFB, le canal et l'AFB comme suit [23] :

$$q_{ji}(n) = (g_i \star h \star f_j)(m)_{\downarrow \frac{M_1}{2}}, \tag{0.24}$$

où $\star$ représente l'opération de convolution, $g_i(m)$ et $f_j(m)$ représentent, respectivement, le SFB et l'AFB sur la i^{eme} et la j^{eme} sous-porteuse.
Avec le système FBMC à M_1 sous-porteuses, le signal de la k^{eme} sous-porteuse est interféré par les signaux venant des sous-porteuses adjacentes ; c-à-d, les interférences viennent de la $k^{eme}-1$ et de la $k^{eme}+1$ sous-porteuse, respectivement. Le système modèle $M-$PAM équivalent au système FBMC-OQAM est donné par la Figure 0.15

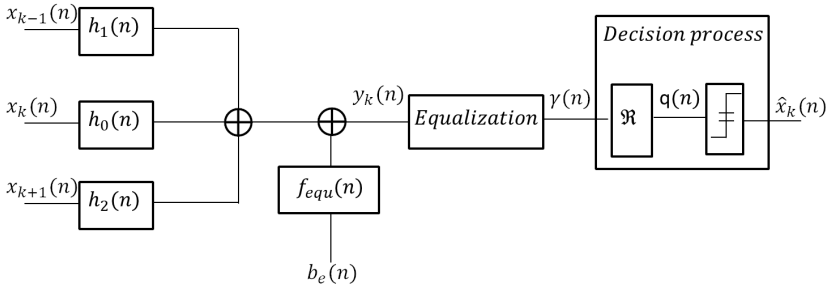

FIGURE 0.15: Le système équivalent à FBMC-OQAM utilisant la modulation $M-$PAM.

En se basant sur ce système modèle équivalent, les équations des égaliseurs linéaire et widely linear en mode SSE précédemment élaborés via les équations (0.18) et (0.19) restent toujours valables dans notre cas. Les performances en termes de BER de ces égaliseurs en fonctions du nombre de sous porteuses adjacentes actives, en canal plat et en canal sélectif sont présentées sur les Figures 0.16 et 0.17.

Sur la Figure 0.16, nous présentons les performances théoriques calculées analytiquement (par le biais du système $M-$PAM équivalent) ainsi que les performances obtenues par simulation pour des égaliseurs linéaires et widely linear appliquée au système FBMC-OQAM. Nous pouvons déduire d'après la Figure 0.16 que :

- Il y a un très bon accord entre les résultats analytiques et simulés pour les deux types d'égalisation,
- La performance du traitement widely linear est toujours meilleure que celle du traitement linéaire classique. Nous confirmons ainsi, l'intérêt et l'apport de l'égalisation widely linear dans le cas de la transmission d'un signal NSOC de type QR,
- La performance de l'égaliseur linéaire est fortement dépendante du nombre de sous-porteuses adjacentes actives autour de la sous-porteuse d'intérêt. Par contre, la per-

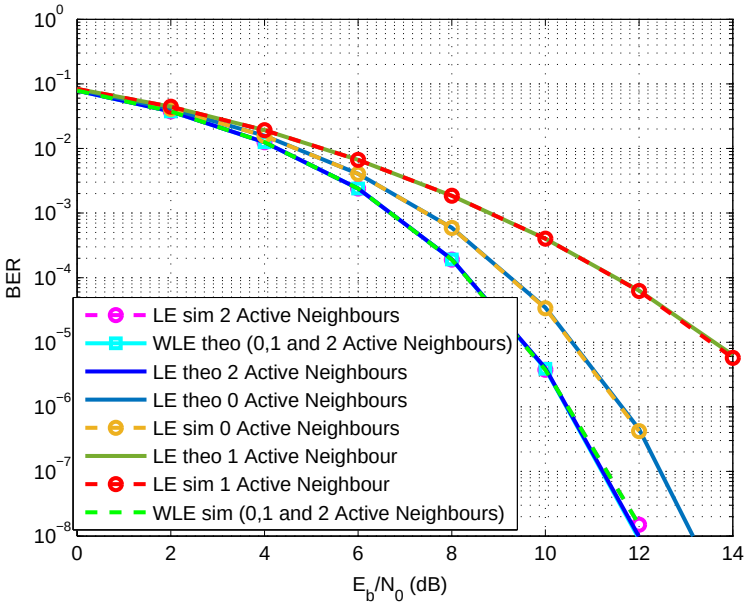

FIGURE 0.16: Performance des égaliseurs LE et WLE en terme de BER pour un canal flat fading.

formance de l'égaliseur widely linear est toujours égale à la performance dans le cas idéal quelque soit le nombre de sous-porteuses adjacentes actives.

La Figure 0.17 présente les performances dans le cas d'un canal sélectif en fréquence. La performance du traitement widely linear est toujours meilleure que celle du traitement classique et, cela, indépendamment du nombre de sous-porteuses adjacentes actives. Néanmoins, quand le nombre de sous-porteuses actives augmente, les performances des deux égaliseurs se rapprochent avec, toujours, une meilleure performance pour l'égaliseur WLE.

Performance des égaliseurs linéaire, widely linear et widely linear Fresh appliqués au système FBMC-OQAM avec plusieurs numérologies

Nous nous intéressons dans cette section à l'étude des différentes structures d'égalisation : linéaire, widely linear et widely linear Fresh sur un système FBMC-OQAM avec deux utilisateurs utilisant différentes numérologies. Le système modèle servant à cette étude est présenté sur les Figures 0.18 et 0.19.

La Figure 0.18 décrit le coté transmetteur du système FBMC-OQAM étudié. Il existe deux utilisateurs : le premier est considéré comme l'utilisateur d'intérêt (UOI) et le second représente l'utilisateur interféreur (UNOI). L'architecture du système de l'UOI est celle précédemment décrite dans la Figure 0.4. L'utilisateur d'interêt possède M_1 sous-porteuses avec un espacement de $\frac{1}{M_1}$ entre les sous-porteuses. Le filtre prototype de Phydyas est désigné par $p_1(m)$ et est de longueur $L_1 = KM_1$ où K est le facteur de chevauchement. L'utilisateur interféreur (UNOI) utilise une numérologie différente de celle de l'UOI. Cet

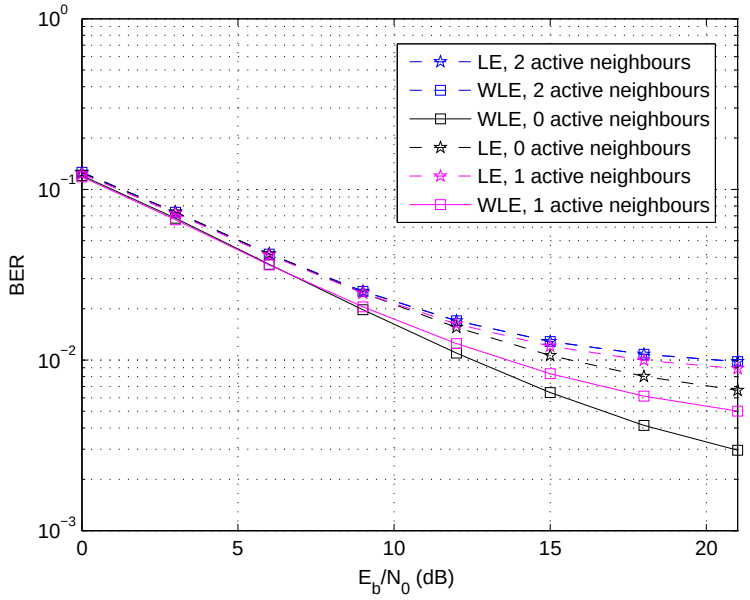

FIGURE 0.17: Performance des égaliseurs LE et WLE en terme de BER sur un canal sélectif en fréquence.

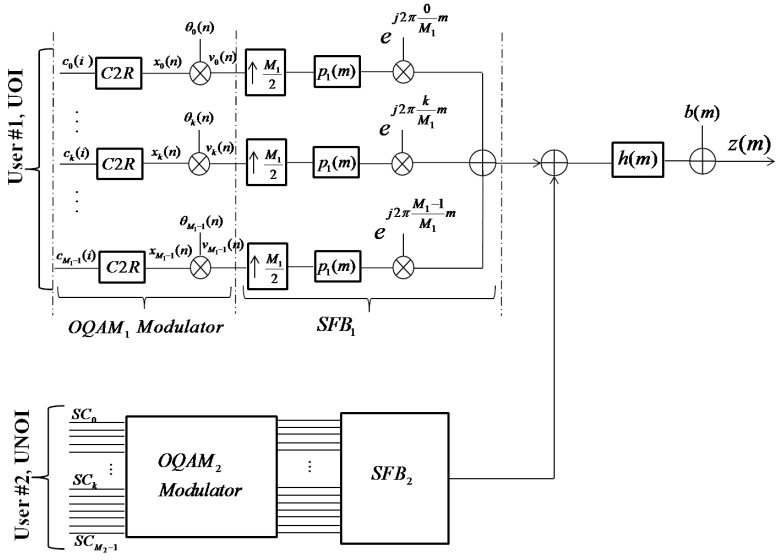

FIGURE 0.18: Le transmetteur du système FBMC-OQAM avec deux utilisateurs de numérologies différentes.

UNOI possède $M_2 > M_1$ sous-porteuses avec un espacement de $\frac{1}{M_2}$ entre les sous-porteuses. Le filtre prototype de Phydyas $p_2(m)$ est de longueur $L_2 = KM_2$.
La Figure 0.19 représente le récepteur FBMC-OQAM adapté à l'utilisateur d'intérêt avec la première numérologie. La perturbation venant du deuxième utilisateur sera évaluée dans le

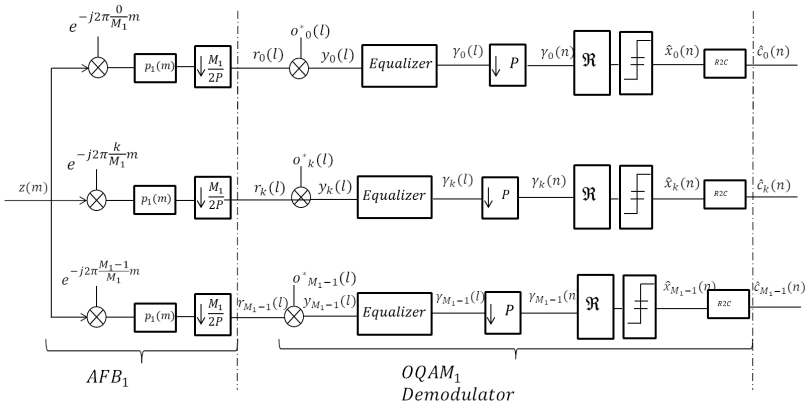

FIGURE 0.19: Le récepteur FBMC-OQAM pour l'utilisateur d'intérêt de numérologie 1.

cas d'une transmission synchrone (lien descendant de la station de base vers les terminaux mobiles) et d'une transmission asynchrone (lien montant des terminaux mobiles vers la station de base). Nous étudierons les performances en fonction de la bande de garde qui existe entre les deux utilisateurs. Cette configuration est illustrée dans la Figure 0.20.

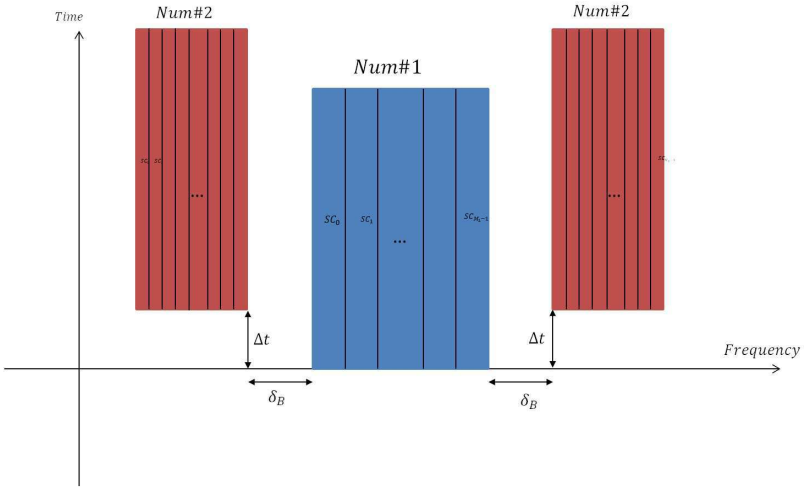

FIGURE 0.20: Le système FBMC-OQAM avec deux numerologies.

Transmission en sens descendant

Dans ce cas, les deux utilisateurs sont synchrones dans le temps. Le décalage temporel Δt dans la Figure 0.20 est donc nul.
Nous allumons, dans un premier temps, 5 sous-porteuses pour la première numérologie et

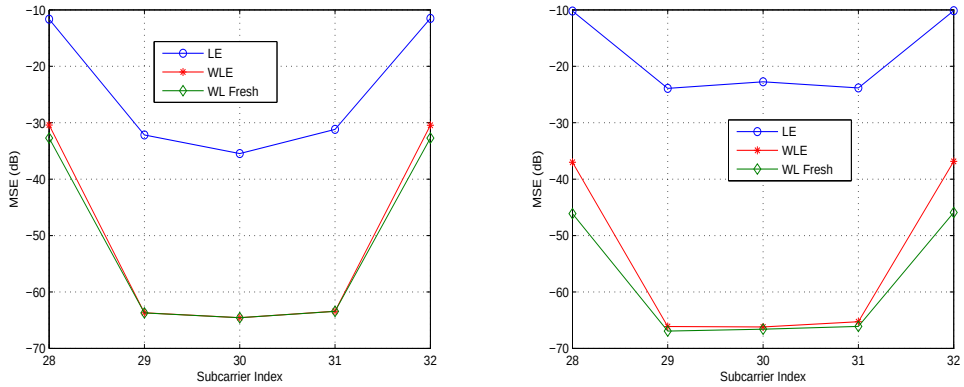

(a) $P = 1$ (b) $P = 8$

FIGURE 0.21: Performance des égaliseurs en terme de MSE en fonction des SPs actives du UOI en transmission idéale.

8 sous-porteuses pour la deuxième. La bande de garde est choisie égale à $\delta_B = \frac{1}{M_1}$. Nous comparons la performance des égaliseurs linéaire, widely linear et widely linear Fresh en mode SSE ainsi qu'en mode FSE. La performance obtenue en termes de MSE est donnée par la Figure 0.21.

Les principaux résultats que nous pouvons déduire de la Figure 0.21 sont :

— Les égaliseurs fractionnaires sont plus performants que ceux appliqués en mode SSE,
— Le traitement widely linear apporte du gain par rapport au traitement linéaire classique qui donne toujours de mauvaises performances,
— L'égaliseur WL Fresh est plus performant que le widely linear classique seulement pour les sous-porteuses de bord. Le traitement widely linear qu'il soit classique ou bien Fresh donne la même performance pour les sous-porteuses en milieu de bande de l'UOI.

Transmission en sens ascendant

Étant donné que seulement les sous-porteuses de bord sont impactées, nous allons étudier les performances des différents égaliseurs dans le cas où seulement une sous-porteuse est active pour l'UOI et pour l'UNOI. Cette étude se fera dans le cas d'un canal sélectif en fréquence. La bande de garde entre les deux utilisateurs est choisie égale à $\delta_B = \frac{2}{T_1}$. Les résultats de simulations sont présentés sur la Figure 0.22.

La Figure 0.22, montre que le traitement widely linear Fresh est le plus performant que le traitement classique. Cela est dû au caractère cyclo-stationnaire du signal FBMC-OQAM transmis. L'apport du traitement widely linear par rapport au traitement linéaire vient du caractère quasi-rectiligne du système FBMC. Nous constatons également d'après cette Figure, qu'avec l'égaliseur linéaire classique, nous ne pouvons pas récupérer les symboles transmis, même avec un fort $\frac{E_b}{N_0}$.

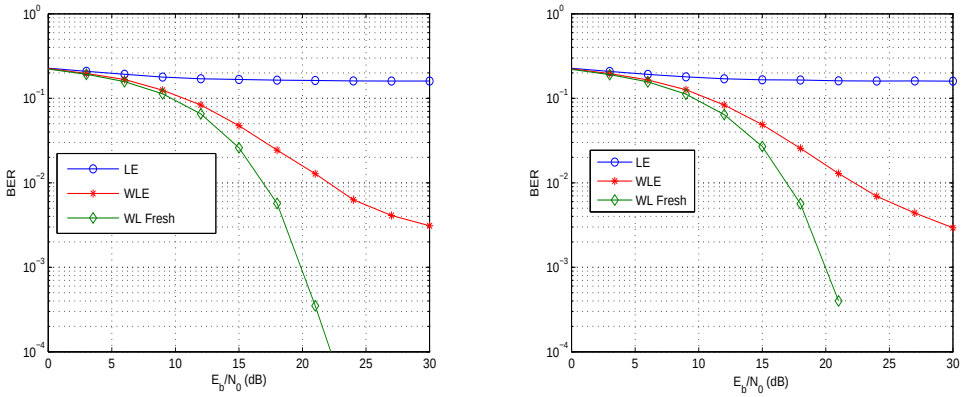

(a) Utilisateurs synchrones. (b) Utilisateurs asynchrones.

FIGURE 0.22: Performance des égaliseurs en terme de BER quand $\delta_B = \frac{2}{T_1}$.

Conclusions et Perspectives

Conclusions

Cette thèse a abordé le thème de l'égalisation des systèmes utilisant des modulations non circulaires au second ordre. Nous avons étudié la performance de différentes structures d'égalisation : linéaire, widely linear et widely linear Fresh, appliquées à un système utilisant la modulation $M-$PAM dans un premier temps et sur un système multi-porteuses FBMC utilisant la modulation OQAM. Motivé par le fait que la modulation OQAM peut être considérée comme la transmission de deux flux modulés en $M-$PAM, et que le traitement widely linear apporte du gain en performance par rapport au traitement linéaire classique, nous avons étudié l'apport du filtrage widely linear sur le système FBMC-OQAM.

Pour ce faire, nous avons tout d'abord commencé par présenter les notions de base et les concepts à utiliser tout au long de cette thèse. Dans le deuxième chapitre, nous avons introduit les concepts de la circularité et de la non circularité étudiés au second ordre. Nous avons également donné des exemples de modulations qui sont classées comme étant circulaires au second ordre (SOC) et autres non circulaires au second ordre (NSOC). Nous avons, aussi, décrit le système multi-porteuses à base de banc de filtre FBMC-OQAM ainsi que les canaux sélectifs en fréquence.

Dans le troisième chapitre de la thèse, nous avons introduit le concept de stationnarité. Les signaux peuvent être classés selon ce critère en des signaux stationnaires ou non stationnaires. Parmi les signaux non stationnaires une classe intéressante est celle des signaux cyclo-stationnaires. Bien étudier les propriétés statistiques du signal transmis permet de choisir le bon traitement d'égalisation selon les caractéristiques du signal. En effet, l'égaliseur linéaire est conçu pour égaliser des signaux SOC alors que pour les signaux NSOC, nous devons implémenter l'égaliseur widely linear. De plus, pour les signaux cyclo-stationnaires, nous pouvons implémenter l'égalisation Fresh qui prend en considération la corrélation entre les composantes spectrales du signal. Toutes ces structures d'égalisation sont étudiées en mode symbole (SSE) ou bien fractionnaire (FSE).

Les chapitres 4 et 5 sont dédiés à la présentation des contributions originales de la

thèse. Ces contributions consistent à appliquer les différentes structures d'égalisation sur un système utilisant une modulation rectiligne (chapitre 4) et sur un système utilisant une modulation quasi-rectiligne (chapitre 5).
Dans le chapitre 4, nous avons étudié, dans un premier temps, la performance des égaliseurs linéaire et widely linear en mode SSE, sur un système utilisant la modulation $M-$PAM en présence de K interférences. Que ce soit avec un canal plat ou bien sélectif en fréquence, le gain de l'égalisation widely linear est mis en évidence. Néanmoins, les performances de l'égaliseur widely linear se dégradent quand le nombre des interféreurs augmente. Dans un deuxième temps, nous avons testé la performance de l'égalisation Fresh et comparé les performances avec celles de l'égalisation classique dans le deux modes SSE et FSE. Nous avons montré que l'égaliseur Fresh fournit toujours la meilleure performance puisqu'il tient compte de la cyclo-stationnarité du signal.

Dans le chapitre 5, nous avons étudié l'égalisation linéaire, widely linear et widely linear Fresh appliquées sur le système FBMC avec l'utilisation de la modulation OQAM. Cette étude est faite en deux parties. Dans la première partie, nous avons étudié, pour un système FBMC avec un seul utilisateur, la performance des égaliseurs linéaire et widely linear appliqués en mode SSE avec la présence de ICI et/ou d'ISI. Nous avons également élaboré et proposé un système modèle équivalent au système FBMC reposant sur une modulation rectiligne de type $M-$PAM. Nous avons montré la bonne performance fournie par l'égaliseur widely linear en comparaison du traitement linéaire et, ce, en présence d'un canal sélectif en fréquence. Dans la deuxième partie du chapitre, nous avons étudié les comportements des égalisation linéaire, widely linear et widely linear Fresh (en mode SSE et FSE) pour un système FBMC-OQAM utilisant deux utilisateurs avec différentes numérologies. Nous avons testé la performance des différents égaliseurs dans les deux sens montant (UL) et descendant (DL). Dans tous les scénarios étudiés, la plus mauvaise performance est obtenue par le traitement linéaire. Le traitement widely linear dans sa version classique et Fresh est le plus performant. Nous avons également montré que la meilleure performance est fournie par l'égalisation Fresh du fait de l'exploitation de la cyclo-stationnarité du signal FBMC.

Perspectives

Cette thèse concerne l'étude de différentes structures d'égalisation appliqués à des signaux rectilignes (utilisant la modulation $M-$PAM) et quasi-rectilignes (avec l'utilisation de la modulation OQAM).

Ces égaliseurs sont calculés, dans cette thèse, en temps discret et en se basant sur le critère de minimisation de l'erreur moyenne quadratique (MSE) entre les symboles émis et les symboles égalisés.

Les performances obtenues par les égaliseurs basés sur le critère MSE, pourraient être comparées à celles obtenues par les filtres quasi optimaux en temps continu basés sur le critère de maximum de vraisemblance (ML), dérivés dans [24]. En particulier, il serait intéressant de comparer les performances des récepteurs MMSE WL FRESH, proposés au chapitre 5, à celles des récepteurs pseudo-ML, proposés dans [24], lors de la variation de la fréquence d'échantillonnage et/ou la longueur des égaliseurs. Cette comparaison doit prendre en compte le gain de complexité obtenu grâce à l'approche MMSE.

De plus, le traitement d'égalisation est basé sur l'étude des propriétés statistiques du

signal à l'ordre 2. Il serait intéressant d'étudier l'apport en termes de performance des égaliseurs exploitant les propriétés statistiques à un ordre supérieur à 2.

De plus, nous avons concentrés sur l'étude de la capacité des égaliseurs WL et WL Fresh à gérer l'annulation d'une ou plusieurs interférences co-canal de type rectiligne ou quasi-rectiligne. Malgré les bonnes performances fournies par ces égaliseurs, ils nécessitent encore des améliorations, surtout pour les signaux quasi-rectilignes. À cet égard, une nouvelle approche a été récemment proposée, appelée filtrage de Volterra (CV) complexe de troisième ordre [25, 26], exploitant à la fois la non-circularité et la gaussianité des signaux jusqu'au sixième ordre [27]. Par conséquent, il est recommandé d'étudier, pour un système FBMC-OQAM, la performance des égaliseurs basés sur le filtrage de Volterra (CV).

Dans le 4ème chapitre, nous avons développé des expressions analytiques afin d'étudier la performance des égaliseurs linéaire et widely linear, pour un système utilisant la modulation $M-$PAM perturbé par K interféreurs. L'égalisation dans ce cas est faite en mode SSE/FSE et en supposant une estimation parfaite du canal de transmission (CSI). Cependant, dans les systèmes de communication sans fils, le CSI n'est pas facile de l'avoir. Par conséquent, il est important d'étudier la performance donnée par les égaliseurs widely linear et widely linear Fresh en considérant CSI imparfaite.

Toutes les structures d'égalisation appliquées au système FBMC-OQAM, ne supposent aucune discordance entre les symboles OQAM transmis. Cela veut dire que la partie radio fréquence (RF) du système FBMC-OQAM ne montre pas d'imbalance I/Q. En pratique, pour ne pas avoir des systèmes multi-porteuses coûteux, des récepteurs zéros-IF (Fréquence intermédiaire) pourraient être attrayants puisqu'ils évitent les filtres IF coûteux [28]. Cependant, ces récepteurs pourraient impliquer une démodulation IQ à la RF, ce qui ne peut donc pas être fait numériquement et introduit donc une discordance IQ. Ainsi, il pourrait être intéressant d'étendre l'étude des performances des différents égaliseurs (linéaire, widely linear et widely linear Fresh) proposés pour le système FBMC-OQAM, à un scénario incluant un décalage I/Q.

Lors de ce travail de thèse, nous nous sommes concentrés seulement sur l'étude du système SISO. Il serait intéressant d'étendre les études des différents égaliseurs (linéaire, widely linear et widely linear Fresh) à des système FBMC-OQAM avec des liaisons MIMO.

Récemment, un grand intérêt a été accordé aux UAV (Unmanned Autonomous Vehicles) pour les services de la télédétection, observation de la terre (surveillance des frontières, inspections des bâtiments et des ponts...), pour les communications (par exemple dans le cas des catastrophes naturelles), etc. Pour la liaison de communication entre les UAV et le sol (ou bien le satellite dans le cas des zones dépourvues du réseau radio communication terrestre), les modulations à phases continues (CPM) ont été standardisées pour la liaison terrestre [29]. L'utilisation de la même modulation pour la liaison satellite est aussi envisagée car les modulations CPM sont connues par leur robustesse contre la non-linéarité des altérations grâce aux amplificateurs de haute puissance (HPA). Grâce à l'approximation de Laurent [30], les CPM peuvent être vues comme la somme de plusieurs signaux $M-$PAM. Dans le cas d'un canal sélectif en fréquence, le traitement widely linear peut être appliqué dans ce contexte.

Table des matières

Table des figures

Nomenclature

Abbreviations and Acronyms

AWGN	Additive White Gaussian Noise
BER	Bit Error Rate
BPSK	Binary Phase Shift Keying.
CP	Cyclic Prefix
DL	Downlink
EE	Energy Efficiency
eMBB	enhanced Mobile BroadBand
FBMC	Filter Bank based MultiCarrier
FFT	Fast Fourier Transform
FIR	Finite Impulse Response
Fresh	Frequency Shift
i.i.d.	independent and identically distributed
ICI	Inter-Carrier-Interference
IDFT	Inverse Discrete Fourier Transform
IEEE	Institute of Electrical and Electronics Engineers
IFFT	Inverse Fast Fourier Transform
IoT	Internet of Things
IOTA	Isotropic Orthogonal Transfer Algorithm
ISI	Inter-Symbol-Interference
IUI	Inter User Interference
LE	Linear Equalizer
LTE	Long Term Evolution
LTE-A	Long Term Evolution-Advanced
MC	Multicarrier
MIMO	Multiple-Input Multiple-Output
MISO	Multiple-Input Single-Output
ML	Maximum Likelihood
MMSE	Minimum Mean Square Error
mMTC	massive Machine Type Machine
MSE	Mean Square Error
MWF	Multicarrier Wave Form
OFDM	Orthogonal Frequency Division Multiplexing

OOB	Out Of Band
OQAM	Offset Quadrature Amplitude Modulation
NSOC	Non Second Order Circular
PAM	Pulse Amplitude Modulation
PDF	Probability Density Function
PHYDYAS	PHYsical layer for DYnamic spectrum AccesSand cognitive radio
PSD	Power Spectral Density
QAM	Quadrature Amplitude Modulation
QPSK	Quadrature Phase Shift Keying
SE	Spectral Efficiency
SINR	Signal-to-Interference-plus-Noise Ratio
SIR	Signal-to-Interference Ratio
SISO	Single-Input Single-Output
SIMO	Single-Input Multiple-Output
SNR	Signal-to-Noise Ratio
SOC	Second Order Circular
SNOI	Signal Of Non Interest
SOI	Signal Of Interest
SRRC	Square Root Raised Cosine
SU	Secondary User
UL	Uplink
UNOI	User of Non Interest
UOI	User Of Interest
UMTS	Universal Mobile Telecommunications System
WiMAX	Worldwide Interoperability for Microwave Access
WL	Widely Linear
WONG5	Waveforms MOdels for Machine Types CommuNication inteGrating 5G Networks
ZF	Zero Forcing

Notations

Vectors and matrices are denoted by bold letters (e.g. $\mathbf{X}$). Other notational conventions are summarized as follows :

$\mathbb{C}^{n\times 1}$, $\mathbb{R}^{n\times 1}$	The sets of columns vectors of length n, with complex and real elements.
$\mathbb{C}^{p\times n}$, $\mathbb{R}^{p\times n}$	The set of matrices with p rows and n columns, with complex and real elements.
$\mathbb{N}$	The set of positive integer elements.
x^*	Complex conjugate of the complex value x.
$\|x\|$	The absolute value of a scalar.
$\mathbb{E}\{\cdot\}$	The expectation operator.
$[\cdot]^T$	The transpose operator.
$[\cdot]^H$	The Hermitian operator (complex conjugate transpose operator).
$\mathbf{X}^{-1}$	The inverse of matrix $\mathbf{X}$.
$\mathbf{I}_n$	The identity matrix of size n.
$\|\mathbf{v}\|$	Euclidean norm of vector $\mathbf{v}$.
$\mathrm{Re}\{x\}$	Real part of the complex value x.
$\star$	Convolution operator.

Chapitre 1

Introduction

1.1 Background and Motivation

Nowadays, technical progress continues to develop and improve in order to cope with the various and huge user requirements and applications. Indeed, since 2G and beyond, there have been enormous changes and developments in many forms, e.g., the number of users and used applications, types of devices have been increased and continue to raise. Thus, in this context, the number of mobile users was 62.6 millions users in 2010, raised to 171 millions in 2014 and it is estimated to reach 285.6 millions users in 2023 [1]. Hence, to address the variety of user demands, enhancements in provided services should keep improved. In fact, among these services, the latency should be reduced, contrary to the energy efficiency (EE) and spectral efficiency (SE) that both should be enhanced. Moreover, for every wireless network generation (from GSM and beyond), the key challenges are mainly presented as supporting mobility, more frequency bands, increasing the peak data rate for both Uplink and Downlink directions, providing more security and reliability, reducing cost, changing the used waveforms [2] and so on, to adapt every current generation system needs.

To address this huge range of service requirements, from one generation to the next one, the used basis waveform has known many changes mainly the switch from the mono-carrier to the multi-carrier waveform (MWF). Besides, these MWFs are the basis shapes leading to wireless communications progress thanks to the different advantages provided from each one. Furthermore, among the MWFs, the widely adopted one is the orthogonal frequency division multiplexing (OFDM) [3, 15, 16], and it represents the fundamental WF for the 4^{th} generation systems. Indeed, OFDM becomes very popular and widely used in many wireless standards like long term evolution (LTE)- Advanced (LTE-A) and Wi-Fi. This wide use is related to the OFDM advantages presented in its simple implementation through the use of an inverse fast Fourier transform (IFFT) for the transmitter side, and through a FFT in the receiver side. Also, the insertion of the cyclic prefix (CP) guarantees a transmitted signal without inter-symbol-interference (ISI), meaning while an ISI-free transmission. Besides, in

CP-OFDM, the equalization is trivial with the use of one tap coefficient per sub-carrier [4].

Despite the many advantages that it presents, the OFDM waveform suffers from several limitations, making it incompatible with the requirements of all the scenarios envisioned in 5G and beyond [5–7, 31]. From these limitations, we can cite the poor frequency localization, related to the use of the rectangular prototype filter and the loss in terms of spectral efficiency, related to the use of cyclic prefix. Furthermore, the 5G required services can be classified into three main categories which are : massive machine type machine (mMTC) known as wide area Internet of things (IoT), enhanced mobile broadband (eMBB) and ultra reliable and low latency communications (URLLC) [2–8, 32–34]. It is worth mentioning that 5G applications belonging to the different classes of services have not the same communication requirements. In fact, applications belonging to eMBB category require high spectral efficiency and very high data rate featuring 20 Gb/s, larger bandwidth so low latency [5], whereas the ones belonging to mMTC require small sub-carrier spacing in order to support a massive connectivity devices with up to 10^6 devices/km^2 [9]. URLLC supports applications with high reliability and low latency less than 1 ms.

Here, the plain OFDM can not response to the multitude and diverse requirements of the 5G services, in a flexible way. Indeed, it is cumbersome to conceive a unified solution responding to all different service demands.

To cater for these diversity in the aforementioned services with eventually their different requirements, the third generation partnership project (3GPP) has introduced the standardization of the first release of 5G specification called Release 15 or New Radio (NR). Thus, the ongoing 5G wireless network is going to support a huge variety of services with eventually very different communications requirements for each service class. It will also, support asynchronous transmission scenarios as well as large bandwidth [4], and it will be open for supporting mixed numerologies within the same NR [3, 9].

In this context, many waveforms (called also post-OFDM MWFs) [35–38] have been introduced and proposed as candidates for the 5G system network [2]. Among these MWFs, the offset-quadrature amplitude modulation based filter-bank multi-carrier (FBMC-OQAM) has been proposed as an alternative to OFDM in order to overcome its drawbacks mainly presented in its bad frequency localization and high out-of-band (OOB) emission [10, 11]. Indeed, FBMC-OQAM is characterized by owning the best frequency localization, thanks to its prototype filter (Phydyas) [11], providing then the best performance in supporting asynchronous and mixed numerologies transmissions while ensuring high spectrum efficiency by avoiding the use of large guard bands and CP. Besides, with the use of the OQAM modulation, orthogonality -over a flat channel- is guaranteed in the real domain and the interferences are then imaginary ones. However, this orthogonality is lost under frequency selective channels which requires advanced equalization techniques.
Thus, in the equalization process, we must take into consideration signal properties in order to conceive the appropriate equalizer that mitigates many forms of interferences. Indeed, based on the analysis of the second order properties (SO) of the studied signal, the process differs from whether the signal is SO circular (SOC) or non SO circular (NSOC), whether it is stationary or not, etc... Indeed, for SOC modulation, the linear processing is sufficient whereas, in case of NSOC modulation , the widely linear equalization is required.

The main objective of this thesis is to study different types of equalization schemes applied to multi-carrier systems using FBMC-OQAM modulation. This latter modulation

can be seen as the transmission of two $M-$ary Pulse Amplitude Modulation ($M-$PAM) over the same sub-carrier. And since the widely linear processing gives better performance when compared to the classical linear equalization, we are interested mainly on the study of the widely linear processing applied over FBMC-OQAM system.

1.2 Thesis outline

Chapter 2 : is devoted to describe and introduce some concepts to be used throughout this thesis. Indeed, the concept of circularity and non circularity is described and based on this definition, some modulations are classified as either SOC or NSOC. Then, an overview of the multi-carrier FBMC-OQAM system is studied. Furthermore, a description of the frequency selective propagation channel is given.

Chapter 3 : In this chapter, another concept, leading to signal classification is introduced. This concept is the stationary one. Indeed, as an extension to the previous chapter, signals can be also classified as either stationary or non-stationary. Moreover, the concept of equalization is studied and described based on the transmitted signal second order properties.

Chapter 4 : concerns the study of the different described equalization schemes applied over a system using a NSOC modulation known as rectilinear one. With the use of the $M-$PAM modulation, the impact of the number of external interferences on the widely linear processing is studied. Besides, a comparison of the different equalization processes is done for single carrier system using the $M-$PAM modulation .

Chapter 5 : This chapter studies the equalization over a Multi-carrier system using a NSOC modulation and classified as quasi-rectilinear. This system is chosen thanks to its capability to support mixed numerologies and asynchronous transmission and known as FBMC-OQAM system. Considering the OQAM modulation as the transmission of two $M-$PAM modulations over the same sub-carrier, we will study the improvements achieved by the aforementioned equalization processes, when applied to the FBMC-OQAM system. Furthermore, an analysis of the equalizers performance is studied in different scenarios cases.

1.3 WONG5 Project

This thesis is supported by the WONG5 project from the French National Agency (ANR) (Waveforms MOdels for Machine Types CommuNication inteGrating 5G Networks), including two academic partners (CNAM Paris and SUPELEC Rennes), one industrial (THALES) and one research center (CEA LETI). The WONG5 project aims to study and propose post-OFDM waveforms (WFs) that best fits the 5G challenges in C-MTC context.

1.4 List of publications

Journal papers

1. H. Fhima, R. Zayani, H. Shaiek, D. Roviras, B. S. Chang and R. Bouallegue "Comparison of Linear, Widely Linear and Fresh Equalizers for FBMC-OQAM systems with different Numerologies", *submitted to Wireless Communications and Mobile Computing Journal.*
2. H. Fhima, D. Roviras and R. Bouallegue "Analysis of Fractionally Spaced Widely Linear Equalization over Frequency Selective Channels with Multiple Interferences ", *International Journal of Wireless and Mobile Networks (IJWMN), August 2019, vol. 11.*

Conference papers

1. H. Fhima, H. Shaiek, R. Zayani, D. Roviras, B. S. Chang and R. Bouallegue,"BER Analysis for Linear and Widely Linear Equalization over Frequency Selective Channels with Multiple Interference", *WIMOB 2018, Limassol, Cyprus.*
2. H. Fhima, B. S. Chang, R. Zayani, H. Shaiek, D. Roviras and R. Bouallegue : "Performance of Linear and Widely Linear Equalizers for FBMC/OQAM modulation", *ICT 2018, Saint Malo, France.*
3. B. S. Chang, C. A. F. da Rocha, H. Fhima, R. Zayani, H. Shaiek and D. Roviras, "On the Performance of a Widely Linear SC-FDE System Under Multiple Independent Interferences", *IEEE PIMRC 2017, Montreal, QC, Canada.*
4. H. Fhima, R. Zayani, H. Shaiek, D. Roviras, B. S. Chang and R. Bouallegue, "Widely Linear equalizer performance with multiple independent interferences", *IEEE ISCC 2017, Crete, Greece.*

Chapitre 2

Generalities : Circularity and Channel selectivity

Introduction

In this chapter, we give the background and some generalities and definitions that allows us to lead our research studies during this Ph.D thesis.
First of all, this thesis work is about Widely Linear equalization with application to FBMC-OQAM signals. It is well known that Widely Linear equalization is applicable and efficient for non-circular signals. So, the first section of this chapter gives a rapid overview of the circularity/ non-circularity concept and classify some modulations according to this concept. In the following section, we describe the FBMC-OQAM modulation which is a particular case of non-circular modulation. FBMC-OQAM modulation is a very well frequency localized modulation scheme and represents an alternative to the classical CP-OFDM for future wireless communication systems. In the third section, frequency selective propagation channels are described.

2.1 Circularity

The notion of circularity [39] was first studied and applied on Gaussian complex vectors by characterizing their probability density function, and then extended to Non Gaussian ones [40]. This concept is widely studied in literature mainly in detection/estimation processes [22, 41] where the second order properties are exploited.

2.1.1 Circularity of a complex vector

Definition1 : A random complex vector $\boldsymbol{z} \in \mathbb{C}^{N\times 1}$ is characterized as circular if $\boldsymbol{z}$ and $\boldsymbol{z}e^{j\theta}$ have the same probability distribution, for all θ [39]. In other words, $\boldsymbol{z}$ is called a circular vector if its characteristic function satisfies the following condition :

$$\Phi_{\boldsymbol{z}}(e^{j\theta}u) = \Phi_{\boldsymbol{z}}(u), \forall\theta \in [0, 2\pi[. \tag{2.1}$$

Definition2 : A random complex vector $\boldsymbol{z} = (z_1, z_2, .., z_N) \in \mathbb{C}^{N\times 1}$ is called circular of order r if the following condition is satisfied [40] :

$$\mathbb{E}\left[\prod_{\sum_{a_i=p}} z_i^{a_i} \prod_{\sum_{b_j=q}} z_j^{*b_j}\right] = 0, \tag{2.2}$$

$\forall(p, q) \in \mathbb{N}$ where $p + q \leqslant r$ and $p \neq q$ [42].
A particular case which is widely used in literature is when $r = 2$; in that case, if the vector $\boldsymbol{z}$ satisfies Eq (2.2), then it is characterized as a second order circular (SOC) vector. Otherwise, it is called a non second order circular (NSOC) one.
Hence, the necessary and sufficient condition of circularity at the second order can be deduced from Eq (2.2), when $r = 2$, where it is simplified to be :

$$\mathbb{E}[\boldsymbol{z}\boldsymbol{z}^T] = 0. \tag{2.3}$$

The matrix function $\mathbb{E}[\boldsymbol{z}\boldsymbol{z}^T]$ of the random complex vector $\boldsymbol{z}$, which we note it as $\boldsymbol{C}$, is then called pseudo-auto-correlation function, pseudo-covariance in [43], complementary covariance in [44] and relation function (RF) in [45]. This latter matrix characterizes the SO properties of the signal. Indeed, the signal, which is represented by a complex vector, can be either second order circular if it satisfies Eq (2.3), or non second order circular if it pseudo-covariance matrix is non null.

It is worth to mention that the second order properties of a random complex vector $\boldsymbol{z}$ are given by both the auto-correlation or covariance matrix, which we refer it by $\boldsymbol{R}$, as well as the pseudo-covariance one $\boldsymbol{C}$. These two matrices are given by the following equations :

$$R = \mathbb{E}\left[\boldsymbol{z}\boldsymbol{z}^H\right] \qquad \& \qquad C = \mathbb{E}\left[\boldsymbol{z}\boldsymbol{z}^T\right] \tag{2.4}$$

Therefore, when the complex signal is characterized as SOC, meaning that its pseudo-covariance matrix is null, the information carried by the second order properties is only contained in the covariance function. On the other hand, when the signal belongs to the NSOC family, its the pseudo-covariance matrix is non null ; thus, the information carried by the SO properties is contained in both the covariance and the pseudo-covariance matrices. In the latter case, the signal is correlated with its complex conjugate version [44].

It should be emphasized that the concept of circularity (non-circularity) in the second order is also referred as the notion of propriety as used in [46] (impropriety in [47, 48]). Hence, a complex vector satisfying Eq. (2.3) is classified as SOC or proper ; otherwise, it is called improper or NSOC.

2.1.2 Non-circularity coefficient

Similarly, a random complex variable z is said to be non second order circular, if $\mathbb{E}[z^2] \neq 0$. This non-circularity of order 2 can be measured through a non-circularity coefficient [12]

as given by :

$$\delta \triangleq \frac{\mathbb{E}[z^2]}{\mathbb{E}[|z|^2]} \triangleq |\delta| e^{j\phi}, \tag{2.5}$$

where $\phi \in [0, 2\pi)$ is referred to as the non-circularity phase of z. It is worth mentioning that the coefficient of non-circularity $|\delta| \in [0, 1]$ [13] informs about the type of the signal : whether it is circular or not.

Indeed, according to the value of $|\delta|$, we have [42] :

— If $|\delta| = 0$, then the signal is characterized as second order circular (SOC) or proper,

— If $|\delta| \neq 0$, then the signal is identified as non second order circular (NSOC) or improper,

— When $|\delta| = 1$, the NSOC signal is called rectilinear [14] and its circularity spectrum is maximum.

2.1.3 Examples of SOC and NSOC signals

Second order circular (SOC) modulations : $M-$QAM modulations

The $M-$ary quadrature amplitude modulation (QAM) belongs to the second order circular modulation family, where the baseband modulated signal can be written as follows :

$$s(t) = \sum_n a_n v(t - nT), \tag{2.6}$$

where T represents the symbol duration, $v(t)$ is the shaping filter and a_n are a series of complex transmitted QAM symbols. The complex $M-$QAM symbols a_n can be written as $a_n = a_n^R + j a_n^I$, where the amplitudes a_n^R and a_n^I belong to the set $\left\{\pm A, \pm 3A, .., \pm(\sqrt{M} - 1)A\right\}$. The representation of $4-$QAM and $16-$QAM constellations is given by Figure 2.1.

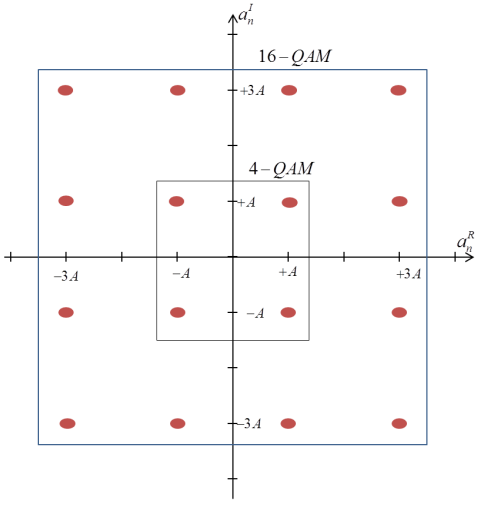

FIGURE 2.1: $4-$QAM and $16-$QAM constellations diagram.

NSOC modulations (Rectilinear)

We recall that the rectilinear (R) modulations (also known as one-dimensional ones) belong to the NSOC ones, with a maximum non-circularity coefficient (equal to 1). Among these R modulations, we find, $M-$ary pulse amplitude modulation ($M-$PAM) [14,49], where the modulated baseband signal is also given by Eq (2.6). In the case of $M-$PAM, the transmitted symbols a_n in Eq (2.6) are real valued and belong to the set $\{\pm A, \pm 3A, .., \pm(M-1)A\}$. We recall that the non circularity aspect of the $M-$PAM modulation can be seen through the non zeros value of the signal pseudo-covariance matrix. Indeed, using equation (2.6), the pseudo-covariance function is equal to :

$$\begin{aligned}\mathbb{E}[s(t)\, s^T(t)] &= \mathbb{E}\left[\left\{\sum_k a_k v(t-kT)\right\}\left\{\sum_{k'} a_{k'} v(t-k'T)\right\}\right], \\ &= \sum_k \mathbb{E}\left[a_k^2\right] v^2(t-kT), \\ &\neq 0,\end{aligned} \tag{2.7}$$

which proves that the $M-$PAM modulation belongs to the NSOC modulations family.
On the other hand, we have :

$$\begin{aligned}\mathbb{E}[s(t)\, s^H(t)] &= \mathbb{E}\left[\left\{\sum_k a_k v(t-kT)\right\}\left\{\sum_{k'} a_{k'}^* v^*(t-k'T)\right\}\right], \\ &= \sum_k \mathbb{E}\left[|a_k|^2\right] |v(t-kT)|^2.\end{aligned} \tag{2.8}$$

As the transmitted symbols a_k of the $M-$PAM are real values then :

$$\sum_k \mathbb{E}\left[|a_k|^2\right] |v(t-kT)|^2 = \sum_k \mathbb{E}\left[a_k^2\right] v^2(t-kT) = \mathbb{E}[s(t)\, s^T(t)]. \tag{2.9}$$

Therefore, using equations (2.8) and (2.9), we deduce the equality between the covariance function and the pseudo-covariance one of the $M-$PAM modulation. Thus, the non circularity coefficient of the $M-$PAM signal which is equal to the ratio between the equations (2.7) and (2.8) is equal to 1, which show that the modulation is a rectilinear one.

Quasi-rectilinear (QR) modulations

Quasi-rectilinear modulations belong to the NSOC modulation family. This modulation family is characterized by the fact that it can be considered, after a de-rotation process, as a one dimensional modulation or rectilinear one. Among this family, we find the offset quadrature amplitude modulation (OQAM) where the baseband modulated signal is given as follows :

$$s(t) = \sum_n a_n^R v(t-nT) + j a_n^I v(t-nT-\tfrac{T}{2}), \tag{2.10}$$

where T is the symbol period, $v(t)$ is the shaping filter, a_n^R and a_n^I are, respectively, the real and imaginary parts of the transmitted QAM symbols (a_n), meaning $a_n^R + j a_n^I = a_n$. The real and imaginary parts (a_n^R and a_n^I) of the QAM symbols are transmitted with a time shift of half a symbol period duration $\left(\frac{T}{2}\right)$. Likewise, the OQAM modulation can be seen as

the transmission of two PAM modulations (represented by both the flows a_n^R as well as a_n^I) transmitted with half symbol period shift. This description of the OQAM modulation can be modeled as shown in Figure 2.2.

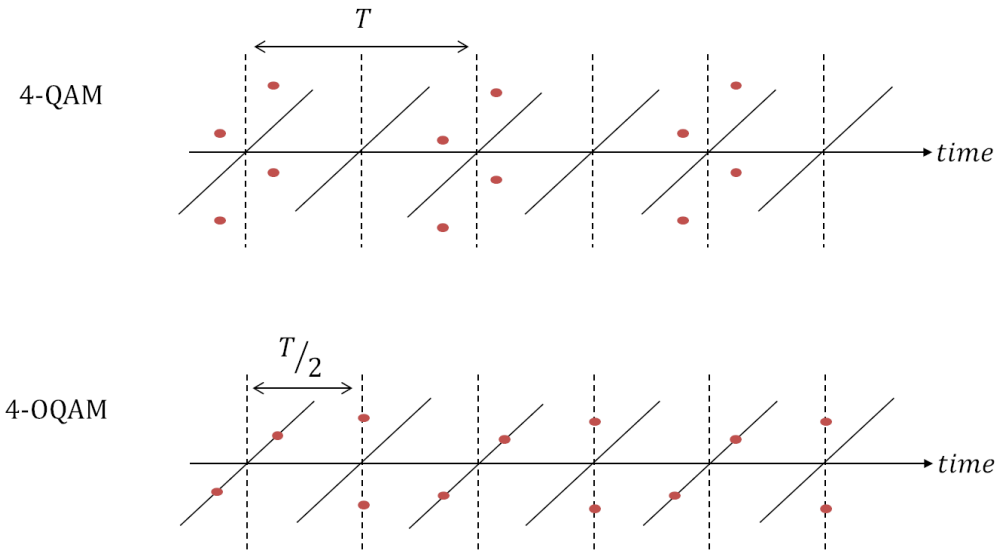

FIGURE 2.2: 4-QAM and 4-OQAM modulations.

Continuous Phase modulations (CPM)

Some of the continuous phase modulations (CPM) [50], [51], also know as non linear ones [52], belong to the NSOC family where, the baseband transmitted signal can be described as follows :

$$s(t) = \sqrt{\frac{E_s}{T}} e^{j\varphi(t,\boldsymbol{a})}, \tag{2.11}$$

where E_s is the symbol energy, T represents the symbol period and $\varphi(t, \boldsymbol{a})$ stands for the information-carrying phase which is expressed by :

$$\varphi(t, \boldsymbol{a}) = 2\pi h \sum_{i=0}^{\infty} a_i q(t - iT), \tag{2.12}$$

where $\boldsymbol{a} = \{a_i\}$ describes the information sequence and takes values from the set $\{\pm A, \pm 3A, .., \pm(M-1)A\}$. h denotes the modulation index, which is less than 1, $q(t)$ is the phase response and it represents a primitive of a normalized frequency pulse function noted $g(t)$:

$$q(t) = \int_0^t g(\tau) d\tau, \tag{2.13}$$

where $g(t)$ is defined for $t \in [0,\ LT]$, where $L \in \mathbb{N}^*$, and satisfies the following condition :

$$\int_0^{\infty} g(\tau) d\tau = \int_0^{LT} g(\tau) d\tau = \tfrac{1}{2}. \tag{2.14}$$

Among the CPM modulations, we find the case of the minimum shift keying (MSK) and the Gaussian minimum shift keying (GMSK). The MSK modulation could be considered as a quasi-rectilinear (QR) one belonging to the same family as the OQAM modulation, where with a simple de-rotation, the modulation becomes a one-dimensional one. Likewise, the GMSK could be considered, in an approximative way, as a QR modulation [53].

2.2 FBMC-OQAM

FBMC-OQAM modulation appears to be a promising alternative to replace the classical cyclic prefixed orthogonal frequency division multiplexing (CP-OFDM) systems [15], [16], in future communication systems. Indeed, CP-OFDM suffers from lack of flexibility and has a poor spectrum localization which are strongly expected in 5G systems. Thus, with FBMC system, there is no need to insert neither CP nor large guard bands which enhances the spectral efficiency when compared to the classical OFDM system. Moreover, regarding the out of band emission (OOB) which is very high in OFDM system ; with FBMC-OQAM, it is reduced. Besides, FBMC is less sensitive to the Doppler effect and it has the best frequency localization providing then the best performance in supporting asynchronous transmissions [54]. Hence, to overcome the OFDM shortcoming, and to respond to the necessity of having more frequency localization, a pulse shaping filter that is different from the rectangular one (used in OFDM) must be implemented. Many filters are designed in order to fulfil the criterion of enhancing the spectrum localization. Among these filters, there is the so called IOTA (Isotropic Orthogonal Transform Algorithm) [55, 56] prototype filter using an algorithm that converts the Gaussian pulse into an orthogonalized one [57]. Another popular prototype filter widely used in FBMC system is identified by PHYDYAS [10, 17–19, 58] (physical layer for dynamic spectrum access and cognitive radio) prototype filter. This latter, first introduced by Bellanger in [18], is based on the so-called frequency sampling technique [17]. In this dissertation, the used prototype filter is the PHYDYAS one.
The PHYDYAS prototype filter modelling depends on mainly three parameters, which are the overlapping factor K (set equal to $K = 4$), the number of the sub-carriers N and the roll-off parameter ζ, which is chosen to be $\zeta = 1$ in order to reduce the time impulse response length and the complexity implementation. Indeed, for the PHYDYAS filter with $\zeta = 1$, only the immediately adjacent sub-carriers are interacting and interfering with each other, i.e., the interference of the k^{th} sub-carrier is coming mainly from the $k^{th} - 1$ and $k^{th} + 1$ sub-carriers.
The design of the aforementioned filter starts with the determination of $L = KN$ desired frequency values $\bar{P}[k]$, $0 < k < L - 1$, where L represents the the length of the prototype filter. These coefficients are given as follows [19] :

$$\begin{cases} \bar{P}[0] = 1, \\ \bar{P}[1] = 0.97195983, \\ \bar{P}[2] = \dfrac{1}{\sqrt{2}}, \\ \bar{P}[3] = \sqrt{1 - \bar{P}[1]^2} = 0.23514695, \\ \bar{P}[k] = 0, k \geq 4. \end{cases}$$

Then, the continuous impulse response of the PHYDYAS prototype filter is determined

by an IDFT and is equal to :

$$p(t) = \begin{cases} \frac{1}{\sqrt{B}} \left[\bar{P}[0] + 2\sum_{k=1}^{K-1} (-1)^k \bar{P}[k] cos\left(\frac{2\pi kt}{KT}\right) \right], & t \in [0, KT] \\ 0, & \text{elsewhere} \end{cases}$$

where T is the symbol period and B represents the normalisation factor which is equal to :

$$\begin{aligned} B &= \int_0^{KT} \left[1 + 2\sum_{k=1}^{K-1} (-1)^k \bar{P}[k] cos\left(\frac{2\pi kt}{KT}\right) \right]^2 dt \\ &= KT \left[1 + 2\sum_{k=1}^{K-1} (-1)^k \bar{P}[k]^2 \right]. \end{aligned} \tag{2.15}$$

The time and frequency responses of PHYDYAS prototype filter as well as the rectangular one are presented in Figures 2.3 and 2.4, respectively.

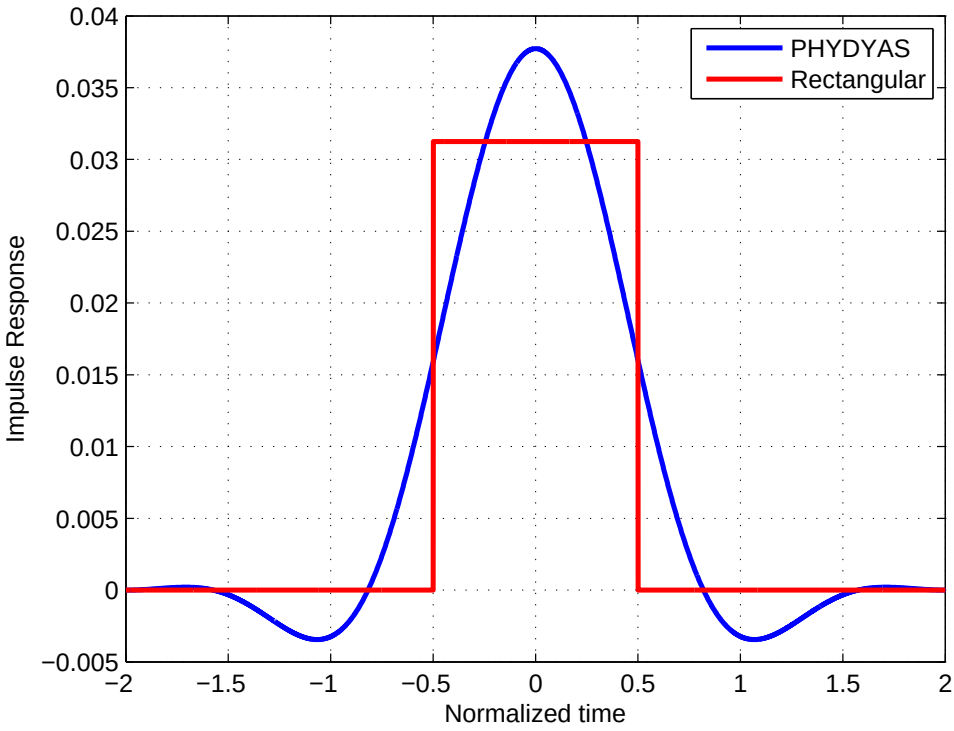

FIGURE 2.3: Time impulse response of PHYDYAS and Rectangular filters

From Figure 2.4, we clearly see that the PHYDYAS prototype filter is well localized in frequency compared to the rectangular one used in OFDM systems. Indeed, the FBMC-OQAM modulation using the aforementioned prototype filter (PHYDYAS) has one of the best frequency localizations providing very good performances in supporting asynchronous transmission while ensuring high spectrum efficiency by avoiding the use of cyclic prefix and large guard bands as it is the case in CP-OFDM.
Maximum spectral efficiency and orthogonality in the complex domain is only satisfied with

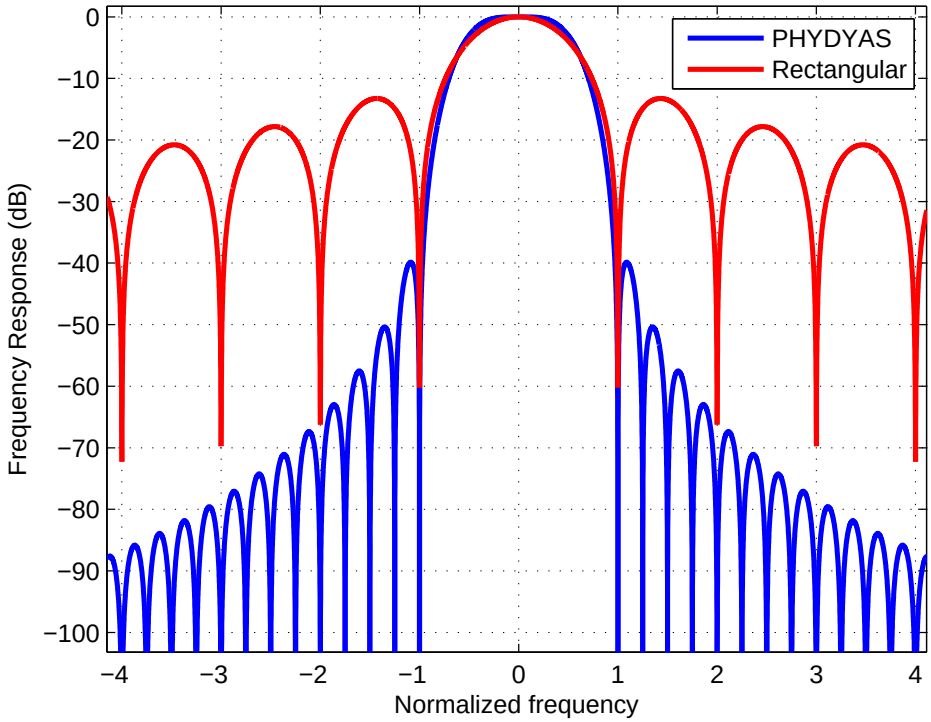

FIGURE 2.4: Frequency response of PHYDYAS and Rectangular filters

the rectangular shape filter of CP-OFDM modulation. For better frequency localization, it is necessary to drop either spectral efficiency or complex orthogonality [55]. For the case of PHYDYAS filter, spectral efficiency is still maximal but the orthogonality is verified and restricted in only the real domain. This latter condition is satisfied through to the use of the OQAM modulation. The time-frequency diagram of the OQAM modulation is shown in Figure 2.5. Hence, we recall that the principle of the OQAM modulation consists in transmitting staggered or offset QAM symbols instead of classical QAM ones. Meaning, transmitting the real and the imaginary parts of the QAM symbols shifted by half symbol period. The so-called OQAM pre-processing for both even and odd sub-carrier can be modeled as shown in Figure 2.6.

With the adoption of the OQAM modulation and the PHYDYAS prototype filter, the general scheme of the FBMC system with N sub-carriers is given by Figure 2.7.
Looking at Figure 2.7, the FBMC-OQAM system contains four main blocs [59], which are the OQAM modulator and the synthesis filter bank (SFB), that both constitute the FBMC-OQAM transmitter side, the analysis filter bank (AFB) and the OQAM demodulator, forming the FBMC-OQAM receiver. The FBMC transmitter and receiver, respectively, are detailed in Figures 2.8 and 2.9, respectively.

Regarding the FBMC modulator presented in Figure 2.8, the first operation is to convert the QAM complex symbols sent on the k^{th} sub-carrier $c_k(i)$ (with variance σ_c^2), to real symbols $x_k(n)$ (with variance σ_x^2). This operation is called the complex-to-real conversion $\mathbb{C}2\mathbb{R}$, and results in a doubled flow rate. Real and imaginary parts of $c_k(i)$ are sent every half sym-

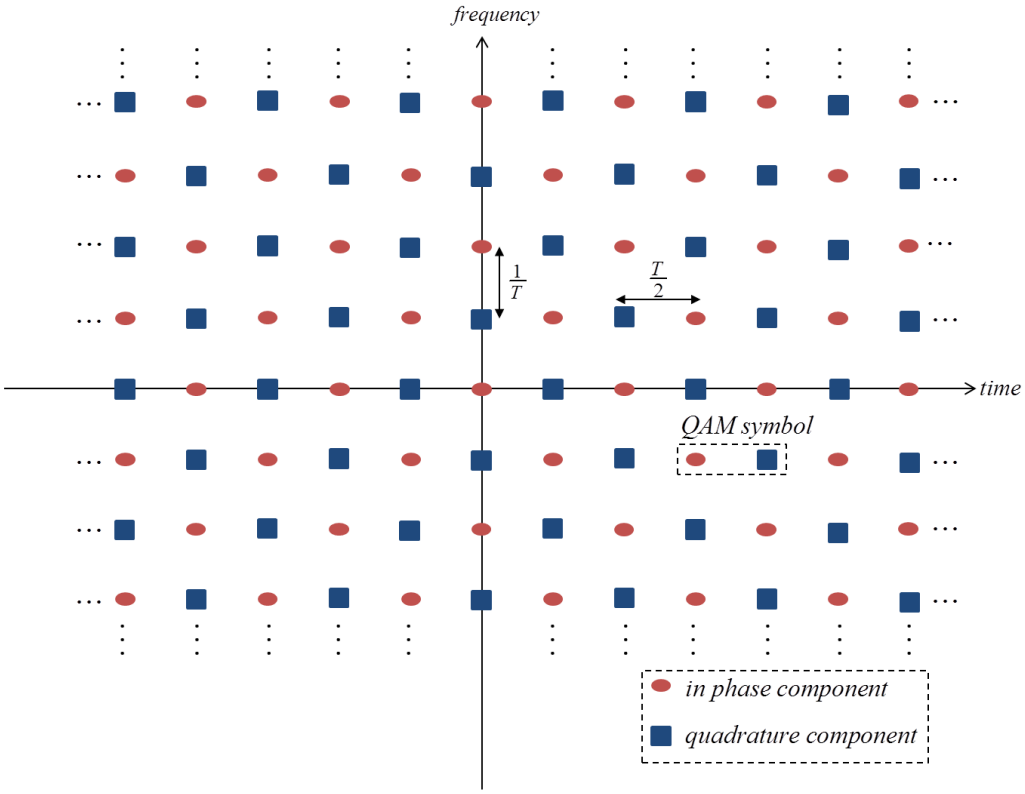

FIGURE 2.5: Time-frequency diagram of an OQAM modulation.

bol period (forming the Offset QAM transmission). The multiplicative factor $\theta_k(n)$ converts this real stream into either pure real or pure imaginary symbols $v_k(n)$. The multiplicative factor $\theta_k(n)$ at the k^{th} sub-carrier is given by :

$$\theta_k(n) = j^{k+n}. \tag{2.16}$$

In the SFB part, we first up-sample the flow on each sub-carrier by a factor $\frac{N}{2}$ before filtering it by a sharp frequency localized filter $p(m)$, which has a length equal to $L = KN$, where K represents the overlapping factor. Afterwards, the k^{th} sub-carrier signal is multiplied by $e^{j2\pi\frac{k}{N}m}$. Then, all the sub-carrier signals are added together, forming the SFB output signal which represents the transmitted signal $s(m)$. This latter signal passes through the propagation channel with impulse response $h(m)$ (with L_h taps) and is corrupted by a complex circular additive white Gaussian noise $b(m)$, with variance σ_b^2, to form the received signal $z(m)$. The expression of $z(m)$ is given by :

$$\begin{aligned} z(m) &= [s \star h](m) + b(m) \\ &= \sum_{i=0}^{L_h-1} h(i)s(m-i) + b(m), \end{aligned} \tag{2.17}$$

where $\star$ represents the convolution operation, and the expression of the SFB output signal

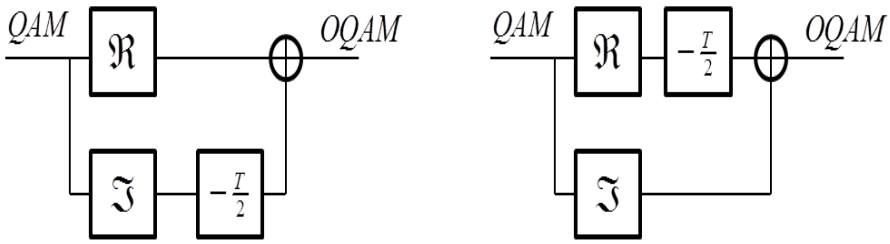

(a) Even sub-carrier. (b) Odd sub-carrier.

FIGURE 2.6: OQAM pre-processing for even and odd sub-carriers

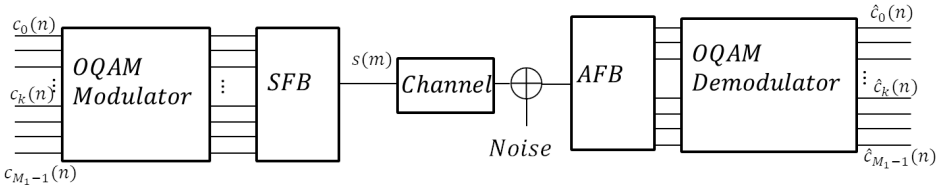

FIGURE 2.7: FBMC-OQAM system.

$s(m)$ is given as follows :

$$s(m) = \sum_{k=0}^{N-1} \sum_{n=-\infty}^{\infty} \left([x_k(n)\theta_k(n)]_{\uparrow \frac{N}{2}} \star p(m) \right) e^{j2\pi \frac{k}{N} m}. \tag{2.18}$$

At the receiver side (see Figure 2.9), the received signal, $z(m)$, is processed by the analysis filter bank (AFB). The output of the AFB gives rise to N parallel sub-carriers signals, that will be further processed by the OQAM demodulator.

In the receiver, the input signal of the k^{th} sub-carrier is first multiplied by the factor $e^{-j2\pi \frac{k}{N} m}$ then filtered by the PHYDYAS matched filter $p(m)$ and down-sampled by a factor $\frac{N}{2}$. In the OQAM demodulator, the first processing is to multiply the signal at the k^{th} sub-carrier by the factor $\theta_k^*(n)$, which is the complex conjugate of Eq. (2.16). With this multiplication, the signal is de-rotated. The de-rotated signal at the k^{th} sub-carrier $y_k(n)$ corresponds to the equalizer input. The signals γ_k and $\hat{x}_k$ are the equalized signals before and after decision process, respectively. The last operation, in the OQAM demodulator, is the real-to-complex conversion $\mathbb{R}2\mathbb{C}$, which is the inverse operation of the $\mathbb{C}2\mathbb{R}$ used in the OQAM modulator. This operation converts the real symbols $\hat{x}_k$ into complex ones $\hat{c}_k$.

It is worth to mention that the presented FBMC-OQAM system model given by Figures 2.8 and 2.9, respectively, will be adopted in this dissertation. In the case of an ideal transmission, i.e., $h(m) = \delta(m)$, the transmultiplexing table of the PHYDYAS prototype filter is presented in Table 2.1. If a symbol equal to 1 is sent on the k_0^{th} sub-carrier (SC) at time $n_0 \frac{T}{2}$, the received signals on neighbors SC for different times are given by table 2.1.

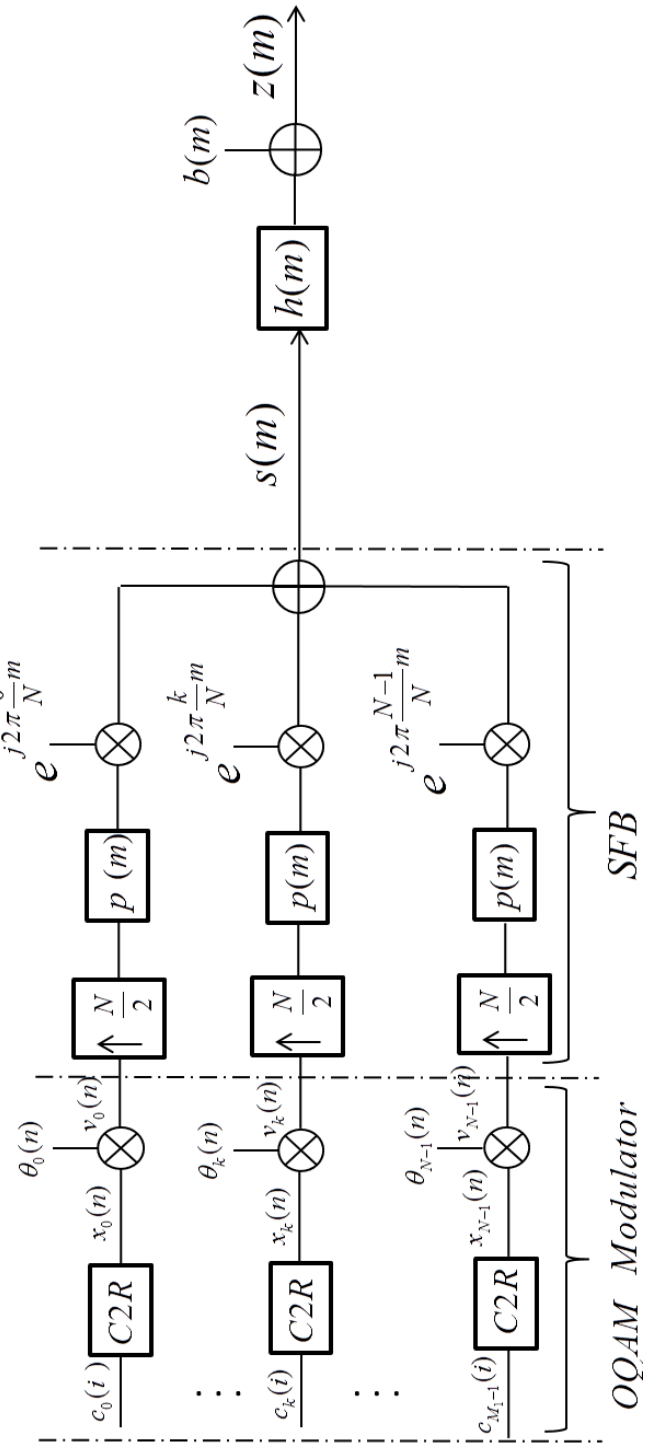

FIGURE 2.8: FBMC-OQAM transmitter

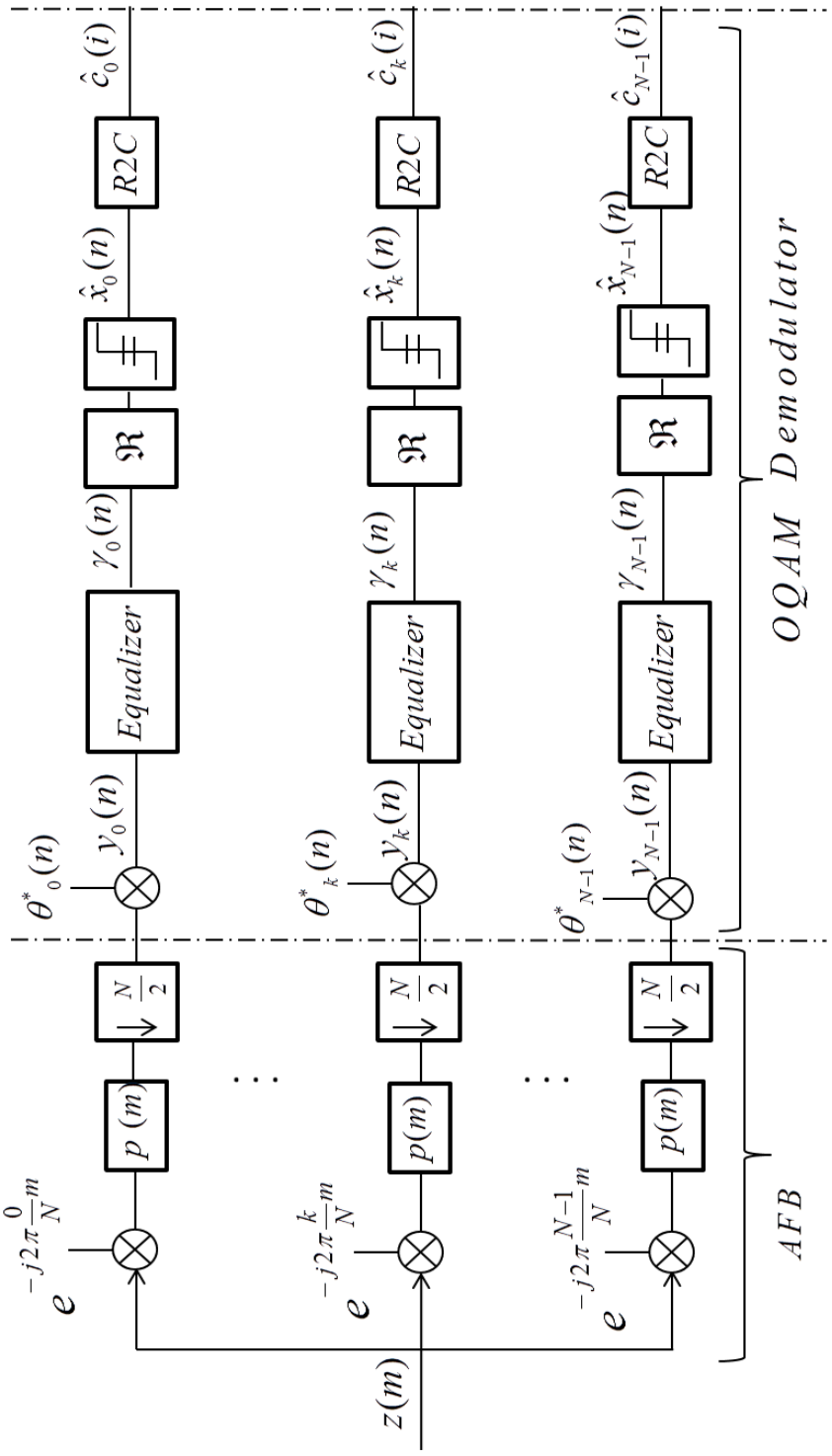

FIGURE 2.9: FBMC-OQAM receiver.

TABLE 2.1: FBMC-OQAM transmultiplexer response with the PHYDYAS prototype filter.

	n_0-3	n_0-2	n_0-1	n_0	n_0+1	n_0+2	n_0+3
k_0-2	0.0006	-0.0001	0	0	0	$-0,0001$	$0,0006$
k_0-1	0.0429j	-0.125	-0.2058j	0.2393	0.2058j	-0.125	-0.0429j
k_0	-0.0668	0.0002	0.5644	1	0.5644	0.0002	-0.0668
k_0+1	-0.0429j	-0.125	0.2058j	0.2393	-0.2058j	-0.125	0.0429j
k_0+2	0.0006	-0.0001	0	0	0	-0.0001	0.0006

Obviously, a value equal to 1 is received on the k_0^{th} SC at time $n_0\frac{T}{2}$. At time $n_0\frac{T}{2}+\frac{T}{2}$ or $n_0\frac{T}{2}-\frac{T}{2}$ a received value 0.5644 is received on the k_0^{th} SC. Because pure imaginary symbols are transmitted at these times, there is no interference on these time/frequency point. Using both table 2.1 and figure 2.5, it can be clearly seen that orthogonality is preserved in the real domain due to the OQAM procedure.

2.3 Propagation Channels

It is well known [20,60], that to transmit an information from a transmitter to a receiver, it passes necessary through a communication system with eventually a propagation channel. When passing through the channel, several phenomena can happen causing signal distortion and/or fading. These phenomena can be resumed in mainly : reflection, diffraction and scattering [20], [21].

Reflection : occurs when an electromagnetic wave propagates upon an obstacle (buildings par example) having very larger dimensions compared to the propagating wavelength.

Diffraction : occurs when the radio path between the transmitter and receiver is obstructed by a surface that has sharp irregularities (edges) [20]. It allows radio signals to propagate around the curved surface of the earth and to propagate behind obstructions. Thanks to this mechanism, the receiver, even with the absence of line of sight path with the transmitter, still receive information sent from the transmitter.

Scattering : occurs when the electromagnetic wave propagates upon rough surfaces, and upon smaller dimensioned-objects than the wavelength.

With these aforementioned mechanisms, the receiver gets many versions of the transmitted signal but with different amplitudes, phases and delays. This is known as the multi-path effect, where the different received signals are obtained from a direct path called line-of-sight (LOS) and others called non-line-of-sight (NLOS). Note that the LOS path does not always exist. Indeed, when the buildings and mountains are higher than the transmitter and the receiver antennas, it causes a loss of direct line of sight between the transmitter and the receiver. However, when it exists, the signal received from the LOS paths represents usually the most dominant signal [21]. Furthermore, these phenomena cause either attenuation called also, large-scale fading or small scale fading. Large-scale fading is caused by the long distance path that exists between the transmitter and the receiver antennas, engendering a loss of power. Small scale fading happens due to interference between two or more versions of the signal received with different delays.

The different phenomena can be modeled as shown in Figure 2.10.

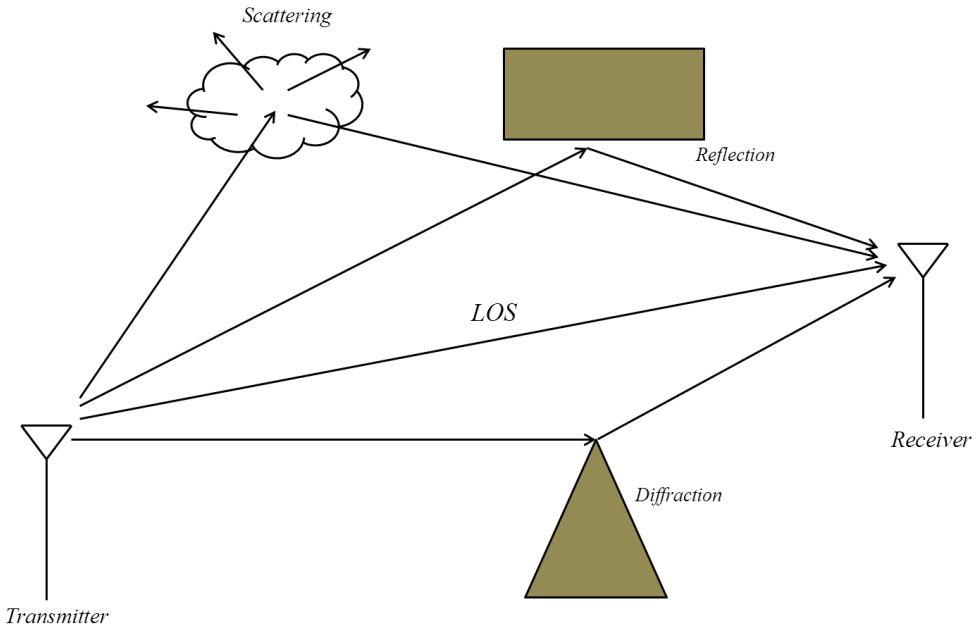

FIGURE 2.10: LOS and NLOS paths [21].

2.3.1 Channel characterization

Since reflection, diffraction and scattering cause the reception of many versions of the transmitted signal with different amplitudes, phases and delays arriving from multi-paths, the wireless multi-path channel can be modeled as a linear time varying (TV) filter, with the impulse response $h(t,\tau)$ [21] is given by :

$$h(t,\tau) = \sum_{k=0}^{L_h-1} a_k(t,\tau) e^{j\{2\pi f_h \tau_k(t) + \phi_k(t,\tau)\}} \delta(\tau - \tau_k(t)), \tag{2.19}$$

where, L_h represents the number of the paths, a_k, f_h and τ_k stand for the amplitude (real), the transmitted frequency and the excess delay of the k^{th} received path, respectively. The phase shift is presented by the term $\{2\pi f_h \tau_i(t) + \phi_i(t,\tau)\}$ and $\delta(.)$ is the Dirac delta function.

In order to characterize the wireless channel, we must introduce some parameters. These parameters are : the delay spread, the coherence bandwidth, which describe the time dispersive nature of the channel, the Doppler spread and the coherence time, which describe the time varying nature of the channel in a small scale region [20].

Delay spread

The delay spread is defined as the time difference between two different paths arriving at slightly different times. We distinguish three types of delay spread :

Mean excess delay : It represents the weighted average delay and is equal to :

$$\overline{\tau} = \frac{\sum_{k=0}^{L_h-1} a_k^2 \tau_k}{\sum_{k=0}^{L_h-1} a_k^2}. \tag{2.20}$$

Maximum excess delay : It represents the delay of the last arrived electromagnetic wave where its amplitude is not neglected compared to the first arrived one. We note it as τ_{max}.

Root mean square delay spread (RMS) : It is noted as : σ_τ or also τ_{RMS} and is given by :

$$\sigma_\tau = \sqrt{\overline{\tau^2} - \overline{\tau}^2}, \tag{2.21}$$

where

$$\overline{\tau^2} = \frac{\sum_{k=0}^{L_h-1} a_k^2 \tau_k^2}{\sum_{k=0}^{L_h-1} a_k^2}. \tag{2.22}$$

Coherence Bandwidth : B_c

The coherence bandwidth, referred as B_c, represents the frequency range where the channel is considered as flat. It is linked to the RMS delay spread given by Eq. (2.21), with the following expression :

$$B_c \simeq \frac{1}{\alpha_\tau \sigma_\tau}, \tag{2.23}$$

where $\alpha_\tau \in \mathbb{R}^{*+}$, so that the coherence bandwidth, depends on the frequency correlation function as cited in [20] and [21]. If the correlation function is above 0.9, then $\alpha_\tau = 50$ and if it is above 0.5 then, $\alpha_\tau = 5$.
It is worth mentioning that by using the coherence bandwidth, one can characterize if a channel is frequency selective or not. Indeed, if B_c is greater than the signal bandwidth B_s, then the channel is flat. However, when $B_c < B_s$, the channel is said to be a frequency selective one.

Doppler spread

The Doppler spread, noted B_D, is defined as the range of frequencies over which the received signal spectrum from a single frequency signal, also called Doppler spectrum, is essentially non-zero [20]. We define the Doppler shift, referred as f_d, as the frequency change of the electromagnetic wave, and expressed as :

$$f_d = \frac{v}{\lambda} cos(\theta), \tag{2.24}$$

where v, λ and θ represent, the velocity, the wavelength signal and the angle between the direction of mobile motion and the direction of wave arrival.
If the Doppler spread B_D is less than the signal baseband bandwidth, then, the channel is characterized as slow fading. In this case, at the receiver side, the Doppler spread effects are trifling and not considered. On the other hand, the channel is categorized as a fast fading channel if B_D is much higher than the signal bandwidth.

Coherence time : T_c

The coherence time, T_c, describes the time duration where the channel is considered to be invariant. It is inversely proportionally with the Doppler shift with the following expression :

$$T_c = \frac{1}{\alpha_f f_m}, \tag{2.25}$$

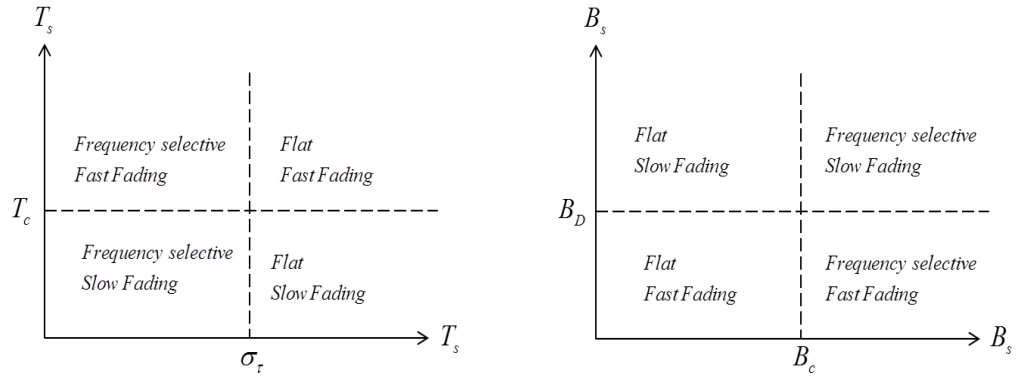

(a) Using transmitted symbol period (b) Using transmitted baseband signal bandwidth

FIGURE 2.11: Channel characterization [20]

where, f_m represents the maximum Doppler shift ($f_m = \frac{v}{\lambda}$), and α_f is a positive real coefficient depending on the time correlation function [20]. Using these aforementioned parameters, the channel classification can be resumed as follows :

— if $B_s \gg B_c$ or $T_s \ll \sigma_\tau$, the channel is a frequency selective one.
— if $B_s \ll B_c$ or $T_s \gg \sigma_\tau$, then the channel is characterized as flat.
— if $B_s \gg B_D$ or $T_s \ll T_c$, the channel is categorized as slow fading.
— if $B_s \ll B_D$ or $T_s \gg T_c$, the channel is characterized as fast fading.

These statements can be presented as given in Figure 2.11.

2.3.2 Channel taps distributions

As aforementioned before, we have modeled in equation (2.19) the wireless multi-path channel by a linear time-varying impulse response. Thus, for frequency selective channel, it is the sum of many delta functions that represent the signals on each path arrived at different instants with different amplitudes a_k. Hence, all signal amplitudes on all multi-path signals follow either the Rayleigh distribution or the Ricean one according to the absence or the presence of the LOS path.

Rayleigh distribution

The Rayleigh distribution is used, when there is no direct line of sight between the transmitter and the receiver, so all the paths are NLOS ones where the amplitudes and the phases are independent and uniformly distributed. The probability density function (pdf) of a Rayleigh random variable u is given as follow :

$$p(u) = \begin{cases} \frac{u}{\sigma^2} e^{-\frac{u^2}{2\sigma^2}}, & u \geq 0 \\ 0, & u < 0, \end{cases}$$

where, σ is the standard deviation of the real part of the random variable u.
The mean and variance, respectively, of a variable u with the Rayleigh distribution are given

by :

$$Mean : m_u = \mathbb{E}[u] = \sigma\sqrt{\tfrac{\pi}{2}}, \tag{2.26}$$

$$Variance : \sigma_u^2 = \mathbb{E}[u^2] - (\mathbb{E}[u])^2 = \sigma^2(2 - \tfrac{\pi}{2}). \tag{2.27}$$

Ricean distribution

The Ricean distribution is used when there is a LOS path between the transmitter and the receiver, which is considered as the dominant one. The pdf of the Ricean distribution of a random variable u is given by :

$$p(u) = \begin{cases} \frac{u}{\sigma^2} e^{-\frac{u^2+D^2}{2\sigma^2}} I_0(\frac{D\,u}{\sigma^2}), & u \geq 0, D \geq 0 \\ 0, & u < 0, \end{cases}$$

where σ^2 is the variance of either the real or the imaginary part, D is the magnitude of the LOS component and $I_0(.)$ is the modified Bessel function of the first kind and zero-order.

Nakagami$-m$ distribution

In most of the cases, the Rayleigh distribution and the Ricean one are sufficient to describe the fading distribution of signals in mobile channel. However, some channels are neither Rayleigh nor Rice. Indeed, this happens, for example, when two paths have almost the same powerful amplitude. In this case, neither the Rayleigh distribution nor the Ricean one can accurately describe the channel. Hence, an alternative to these two aforementioned distributions is the so-called the Nakagami$-m$ distribution, where the pdf is given by :

$$p(u) = \frac{2}{\Gamma(m)} \left(\frac{m}{\Omega}\right)^m u^{2m-1} e^{-\frac{m}{\Omega}u^2}, u \geq 0, \tag{2.28}$$

where $\Gamma(.)$ is the gamma function defined as follows : $\Gamma(x) = \int_0^{+\infty} e^{-t} t^{x-1} dt$.
$\Omega = \mathbb{E}[u^2]$ is the second moment and m is a parameter that defines the path depth [60].

2.4 Conclusion

In this chapter, we have introduced some generalities and concepts to be used throughout this Ph.D thesis.
We have started by defining the circularity and non circularity concept given in the second order and classifying some modulations with regard to this concept. Thus, this is done through the study of the second order properties of the transmitted signal. Indeed, according to the whether the pseudo-covariance matrix is null or not, the studied signal/modulation is characterized as either second order circular (SOC) or non second order circular (NSOC). In a second step, we have interested on a particular NSOC modulation also known as a quasi rectilinear one. This modulation is the FBMC-OQAM where we have described its principle and introduced the system using the FBMC-OQAM modulation. This modulation is characterized by owning a very well frequency localization which makes it an alternative modulation for future communication systems. Then, we have interested in the characterization of the wireless communication channels and the description of the frequency selective ones.

The next chapter will be a continuity of the current one. Indeed, the concept of stationarity and cyclo-stationarity will be introduced in chapter 3. Besides, we will introduce the equalization techniques and classify the signal equalizers according to the circularity and stationarity of the studied modulation.

Chapitre 3

Equalization techniques

Introduction

We have seen in the previous chapter that a signal can be classified according to the circularity concept of its second order statistical properties. Indeed, based on the pseudo-covariance matrix, the signal can be either characterized as second order circular (SOC) or non second order circular (NSOC). However, the circularity is not the only criterion that can be used to classify random processes. In fact, besides the circularity there are the so-called the stationarity properties [61], based on whether the signal statistical properties are time dependent or not.
On the other hand, when emitting a signal, it may suffer from some distortion, induced by the propagation channel, as aforementioned in the previous chapter. This requires a process called equalization at the receiver side, in order to limit and suppress the interference, to recover the original transmitted symbols.
Therefore, studying the statistical properties of the transmitted signal is fundamental to describe the best way to implement the equalization process in an efficient way by taking into account the signal properties In this chapter, we give more details about the stationarity concept, recall the different equalization processes required according to the signal nature and describe the behavior of the different equalizers.

3.1 Cyclo-Stationarity

3.1.1 Definition

Random processes can be classified according to the nature of their first and second order statistical properties. We recall that the first and the second order statistical properties are the mean and the covariance and pseudo-covariance matrix functions, respectively. Hence, if these latter are time invariant, i.e., if these properties keep the same value all the time and

do not change as function of time, the signals are then characterized as stationary. However, if this condition is not satisfied, meaning that the statistical properties are time dependent and they vary as function of time, in this case the signals are time variant and they are said to be Non-stationary.

For Non-stationary signals, there is a particular case, where the statistical properties of the first and the second order are time-periodic. Signals that have such characteristic are called Cyclo-stationary signals (in the wide sense). In this case, the mean and the covariance function (as well as the pseudo-covariance one) vary periodically with the period T.

Broadly speaking, if the signals $x(t)$ and $y(t)$ are classified as, respectively, stationary and cyclo-stationary with a period T, then it is possible to state the following properties :

— For the signal $x(t)$:

$$\mathbb{E}[x(t)] = m_x(t) = m_x \tag{3.1}$$
$$\mathbb{E}[x(t)x^*(t+\tau)] = R_x(t,\tau) = R_x(\tau), \quad \forall t \quad \text{or} \tag{3.2}$$
$$\mathbb{E}[x(t_1)x^*(t_2)] = R_x(t_1 - t_2) \tag{3.3}$$
$$\mathbb{E}[x(t)x(t+\tau)] = C_x(t,\tau) = C_x(\tau), \quad \forall t \quad \text{or also} \tag{3.4}$$
$$\mathbb{E}[x(t_1)x(t_2)] = C_x(t_1 - t_2), \tag{3.5}$$

— For the signal $y(t)$:

$$\mathbb{E}[y(t)] = m_y(t) = m_y(t+T) = \mathbb{E}[y(t+T)] \tag{3.6}$$
$$\mathbb{E}[y(t)y^*(t+\tau)] = R_y(t,\tau) = R_y(t+T,\tau), \quad \forall t \quad \text{or also} \tag{3.7}$$
$$\mathbb{E}[y(t_1)y^*(t_2)] = R_y(t_1,t_2) = R_y(t_1+T,t_2+T), \tag{3.8}$$
$$\mathbb{E}[y(t)y(t+\tau)] = C_y(t,\tau) = C_y(t+T,\tau), \quad \forall t \quad \text{or also} \tag{3.9}$$
$$\mathbb{E}[y(t_1)y(t_2)] = C_y(t_1,t_2) = C_y(t_1+T,t_2+T), \tag{3.10}$$

where m_x and m_y denote the mean of signals $x(t)$ and $y(t)$, respectively. Likewise, R_x and R_y designate the covariance function of respectively $x(t)$ and $y(t)$. C_x and C_y are the pseudo-covariance function of the signals $x(t)$ and $y(t)$, respectively. We recall that, if the signals $x(t)$ and $y(t)$ are SOC then C_x and C_y are null. The period T is defined as the cyclic period of the cyclo-stationary signal $y(t)$.
For the cyclo-stationary signal $y(t)$, since the auto-correlation (covariance) function as well as the pseudo-auto-correlation (pseudo-covariance) are periodic functions of time with a period T, then they can be represented as Fourier series expansions, given as follows :

$$R_y(t,\tau) = \sum_{\alpha_i \in \mathcal{A}_\alpha} R_y^{\alpha_i}(\tau) e^{j2\pi\alpha_i t} \tag{3.11}$$

$$C_y(t,\tau) = \sum_{\beta_i \in \mathcal{B}_\beta} C_y^{\beta_i}(\tau) e^{j2\pi\beta_i t} \tag{3.12}$$

where

— α_i are the non conjugate second order (SO) cyclic frequencies and are related to the cyclic period and its harmonics; i.e, $\alpha_i = \dfrac{i}{T}, i \in \mathbb{Z}$.

— β_i are the conjugate SO cyclic frequencies and they are equal to twice the carrier frequency (we note it Δ_f), possibly plus or minus the baud rate and its harmonics, [22], i.e, $\beta_i = 2\Delta_f + \frac{i}{T}, i \in \mathbb{Z}$.
— $\mathcal{A}_\alpha$ and $\mathcal{B}_\beta$ are defined as the sets of, respectively, all the non conjugate and conjugate SO cyclic frequencies, i.e., α_i and β_i, respectively.
— $R_y^{\alpha_i}(\tau)$ and $C_y^{\beta_i}(\tau)$ represent, respectively, the non conjugate cyclic auto-correlation and the conjugate cyclic pseudo-auto-correlation functions of the $T-$ cyclo-stationary signal $y(t)$. They are obtained as follows :

$$R_y^{\alpha_i}(\tau) = \frac{1}{T}\int_{\frac{-T}{2}}^{\frac{T}{2}} R_y(t,\tau)e^{-j2\pi\alpha_i t}dt \tag{3.13}$$

$$C_y^{\beta_i}(\tau) = \frac{1}{T}\int_{\frac{-T}{2}}^{\frac{T}{2}} C_y(t,\tau)e^{-j2\pi\beta_i t}dt \tag{3.14}$$

It is worth mentioning that the SO cyclic covariance and pseudo-covariance functions at the null non conjugate and conjugate SO cyclic frequencies ($(\alpha_i, \beta_i) = (0,0)$) represent, respectively, the conventional covariance and pseudo-covariance functions, meaning $R_y^{\alpha_i=0}(\tau) = R_y(\tau)$ and $C_y^{\beta_i=0}(\tau) = C_y(\tau)$.
When a signal $y(t)$ is characterized as cyclo-stationary with a cyclic period T, the cyclic auto-correlation function $R_y^{\alpha_i}(\tau)$ is non zero for some non zero values of α_i, i.e., there are some $\alpha_i \neq 0$ where $R_y^{\alpha_i}(\tau) \neq 0$. However, when a signal $x(t)$ is classified as stationary, the only non null cyclic auto-correlation function is when $\alpha_i = 0$, and for $\alpha_i \neq 0$, the cyclic auto-correlation functions are null. Hence, $R_x^{\alpha_i}(\tau) = 0$ for $\alpha_i \neq 0$ and $R_x^{\alpha_i=0}(\tau) \neq 0$. In this case, there is no correlation between the spectral components of the stationary signal.

It is worth emphasizing that contrary to the stationary signal, the cyclo-stationary one has correlation between its spectral components. In this case, the power spectral density (PSD) of the signal may be deduced from the cyclic-auto-correlation function. Indeed, with a simple Fourier transform of the cyclic auto-correlation function with respect to τ, we obtain the expression of the PSD, given as follows :

$$S_y(t,f) = \mathcal{TF}_\tau[R_y(t,\tau)] \tag{3.15}$$

The characteristics of the PSD are similar to those of the auto-correlation function. When the signal is stationary, the PSD is a function of frequency only and it is time-independent. This is opposite of the case of cyclo-stationary signals (with a cyclic period T), where the PSD is function of both frequency and time where it is T-periodic, i.e., :

$$S_y(t,f) = S_y(t+T,f); \forall t \tag{3.16}$$

Likewise, since the PSD is time periodic with the period T, then it can be written as the form of a Fourier series expansion, as shown in the following expression :

$$S_y(t,f) = \sum_{\alpha_i \in \mathcal{A}_\alpha} S_y^{\alpha_i}(f)e^{j2\pi\alpha_i t}, \tag{3.17}$$

where $S_y^{\alpha_i}(f)$ are called spectral correlation functions and they can be obtained by Fourier transform with respect to time t of the power spectral density of the signal $y(t)$:

$$S_y^{\alpha_i}(f) = \frac{1}{T}\int_{\frac{-T}{2}}^{\frac{T}{2}} S_y(t,f)e^{-j2\pi\alpha_i t}dt \tag{3.18}$$

Similarly to the cyclic auto-correlation functions, when a signal $x(t)$ is stationary, the cyclic spectral correlation functions are non null for only null cyclic frequency ; i.e : $S_x^{\alpha_i}(f) = 0$, when $\alpha_i \neq 0$ and $S_x^{\alpha_i}(f) \neq 0$, for $\alpha_i = 0$. For a cyclo-stationary signal $y(t)$ with the cyclic-period T, $\exists\ \alpha_i \neq 0$ where $S_y^{\alpha_i}(f) \neq 0$. Note that, if there is no $\alpha_i \neq 0$ where $S_y^{\alpha_i}(f) \neq 0$, the signal $y(t)$ becomes stationary.
The value of the cyclic spectral correlation functions $S_y^{\alpha_i}(f)$ can also be obtained by Fourier transform with respect to τ of the cyclic auto-correlation functions $R_y^{\alpha_i}(\tau)$:

$$S_y^{\alpha_i}(f) = \mathcal{TF}_\tau[R_y^{\alpha_i}(\tau)]. \tag{3.19}$$

Indeed, Eq. (3.19) can be deduced using Eqs. (3.13), (3.15) and (3.18), respectively, as follows :

$$\begin{aligned} S_y^{\alpha_i}(f) &= \mathcal{TF}_t[S_y(t,f)], \\ &= \mathcal{TF}_t\left[\mathcal{TF}_\tau\left[R_y(t,\tau)\right]\right], \\ &= \mathcal{TF}_\tau\left[\mathcal{TF}_t\left[R_y(t,\tau)\right]\right], \\ &= \mathcal{TF}_\tau\left[\underbrace{\mathcal{TF}_t\left[R_y(t,\tau)\right]}_{R_y^{\alpha_i}(\tau)}\right], \\ &= \mathcal{TF}_\tau[R_y^{\alpha_i}(\tau)]. \end{aligned} \tag{3.20}$$

The relations between the auto-correlation function, the PSD, the cyclic auto-correlation functions and the cyclic spectral correlation functions can be summarized as given in Figure 3.1.

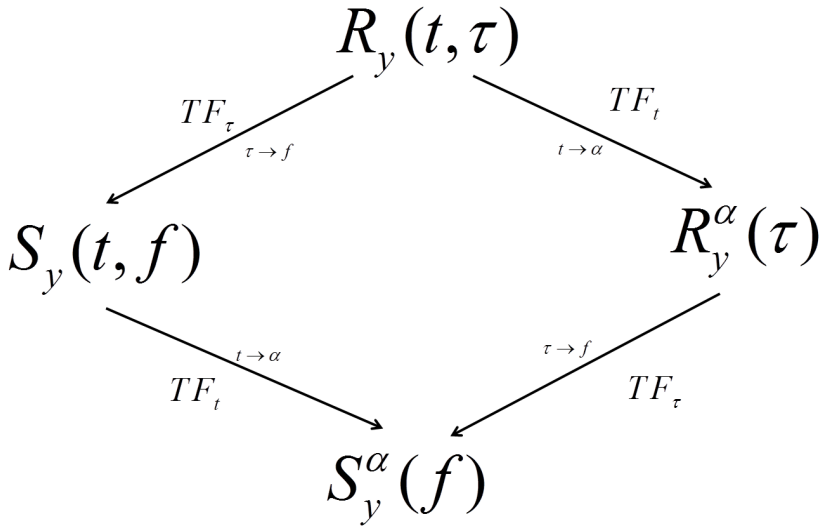

FIGURE 3.1: Relation between cyclo-stationary signal components.

We recall that for stationary signals [62], there is no correlations between the spectral

components of the signal. In this case, we have only one cyclic frequency $\alpha_i = 0$ and only one conjugate cyclic frequency $\beta_i = 0$ where we have energy ; i.e $R_y^{\alpha_i}(\tau)$ and $C_y^{\beta_i}(\tau)$ are non zero for, respectively $\alpha_i = 0$ and $\beta_i = 0$, and then $R_y^{\alpha_i}(\tau) = C_y^{\beta_i}(\tau) = 0$ for respectively, $\alpha_i \neq 0$ and $\beta_i \neq 0$. Consequently, $R_y(t,\tau) = R_y^0(\tau) = R_y(\tau)$ and $C_y(t,\tau) = C_y^0(\tau) = C_y(\tau)$.

It is worth mentioning that the aforementioned definition of a cyclo-stationary process is given when there is one set of cyclic frequency, meaning that, there is one baud rate. However, when there is more than one baud rate, more than one set of cyclic frequency exists ; the process in that case, is called poly-cyclo-stationary [63].
Hence, a process is characterized as poly-cyclo-stationary when the statistical properties of the first and the second order are time poly-periodic. Therefore, the set of the SO cyclic frequencies $\mathcal{A}_\alpha$ in Eq. (3.13), becomes : $\mathcal{A}_\alpha = \left\{ \frac{i}{T_1}, \frac{i}{T_2}, .., \frac{i}{T_N}, i \in \mathbb{Z} \right\}$, where $T_i \neq T_j$, for $i \neq j$.
Thus, a cyclo-stationary process is a particular case of a poly-cyclo-stationary process.

3.1.2 Examples

In this subsection, we present some examples in order to illustrate and represent the differences between stationary and poly-cyclo-stationary signals. The illustrations are based mainly on analysis of the cyclic auto-correlation and the spectral correlation functions.

A stationary signal

The stationary signal is chosen to be a proper additive white Gaussian complex noise (AWGN). We present in Figure 3.2 the SO non conjugate cyclic auto-correlation function, the conjugate cyclic pseudo-auto-correlation function and the cyclic spectral correlation function of the AWGN.

From Figure 3.2 we can clearly see that the only energetic cyclic frequency is $\alpha = 0$, where the other cyclic frequencies do not contain any information. This property characterizes the stationarity of the signal. Moreover, since the chosen signal is proper (SOC), the covariance matrix is null, That is why there is no energetic conjugate cyclic frequency, i.e., the absence of all β_i.

Case of a cyclo-stationary signal

For the representation of a cyclo-stationary signal [64], let us consider $u_1(t)$, a rectilinear signal filtered by a shaping filter with rectangular form $p_1(t)$. Without loss of generality, the rectilinear signal is chosen to have a BPSK modulation, where the symbol duration is set to be T_1. Hence, the generated signal expression is then :

$$u_1(t) = \sum_n a_n p_1(t - nT_1), \tag{3.21}$$

where $\{a_n\} \in \{\pm 1\}$.
The different signal components (cyclic auto-correlation and cyclic pseudo-auto-correlation functions and cyclic spectral correlation function) are given by Figure 3.3.

Regarding Figure 3.3, we can clearly see the difference between this signal and the stationary noise presented by Figure 3.2. Indeed, contrary to the previous case, where the

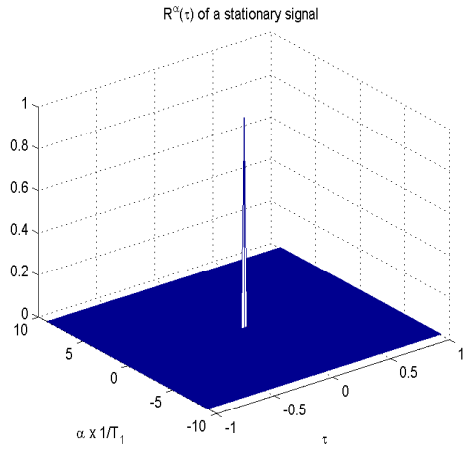

(a) $R^{\alpha}(\tau)$

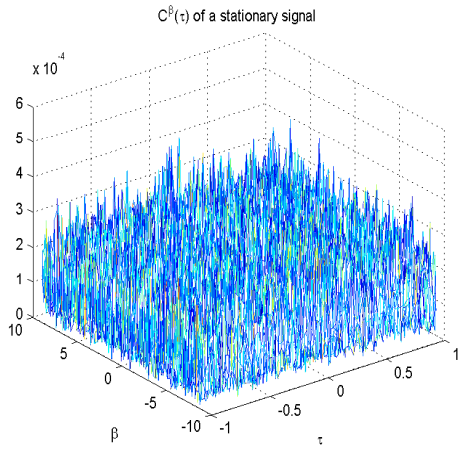

(b) $C^{\beta}(\tau)$

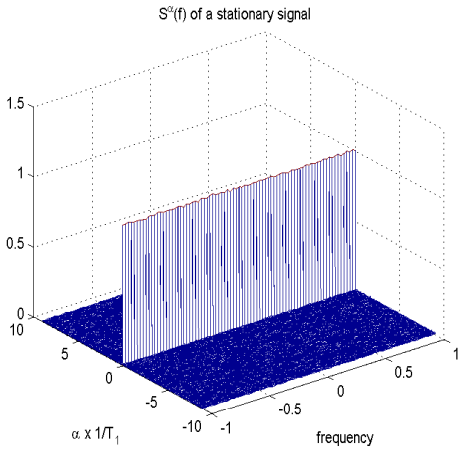

(c) $S^{\alpha}(f)$

FIGURE 3.2: SO cyclic covariance, pseudo-covariance and DSP functions of a stationary signal.

only energetic cyclic frequency is for $\alpha = 0$, other cyclic frequencies are present, for this signal. Besides, the energy is located at the cyclic frequencies $\frac{i}{T_1}, i \in \mathbb{Z}$.

Case of a Poly-cyclo-stationary signal

We can represent a poly cyclo-stationary signal as the sum of, for example, two (or more) cyclo-stationary signals with different symbol durations (various baud rates).
Thus let us consider $u(t)$, expressed as follows :

$$\begin{aligned} u(t) &= u_1(t) + u_2(t) \\ &= \sum_n a_n p_1(t - nT_1) + \sum_n b_n p_2(t - nT_2), \end{aligned} \tag{3.22}$$

where u_1 and u_2 are two rectilinear signals having a BPSK modulation with different symbol durations. $\{a_n\}$ and $\{b_n\} \in \{\pm 1\}$ represent the BPSK symbols of u_1 and u_2 respectively.

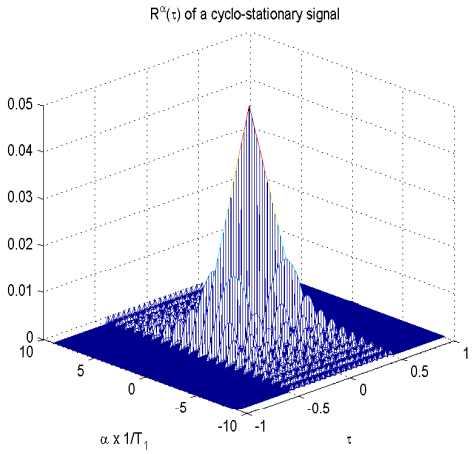

(a) $R^{\alpha}(\tau)$

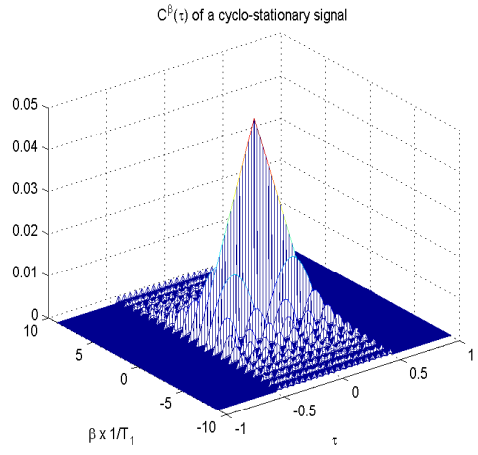

(b) $C^{\beta}(\tau)$

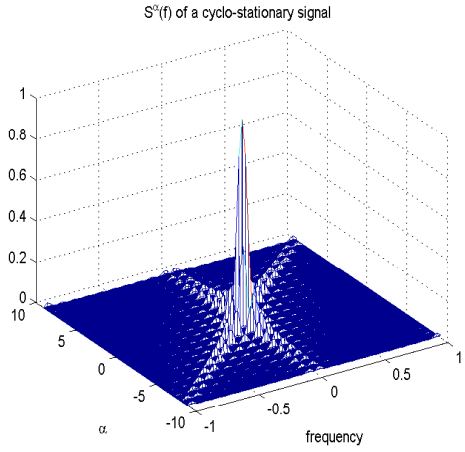

(c) $S^{\alpha}(f)$

FIGURE 3.3: SO cyclic covariance, pseudo-covariance and DSP functions of a cyclo-stationary signal.

p_1 and p_2 are the shaping filters and T_1 and T_2 are the symbol durations of the two cyclo-stationary signals, u_1 and u_2 respectively. In our example, we consider $T_2 = 2\,T_1$.
The cyclic auto-correlation, pseudo-auto-correlation and cyclic spectral correlation functions of the signal $u(t)$ are shown in Figure 3.4.

Regarding Figure 3.4, we can see that there are two sets of cyclic frequencies related to the different baud rates of the signal $u(t)$. Indeed, this set is equal to $\mathcal{A}_{\alpha} = \{\frac{i}{T_1}, \frac{i}{T_2}, i \in \mathbb{Z}\}$.

3.2 Equalization process

We recall that the equalization process is required when the transmitted signal arrives with some deformations and/or distortion at the receiver side. The source of distortion can be du to problems related to the wireless propagation channel (as described in the previous Chapter), and/or other external distortion caused by external interferer signals. Indeed, these phenomena can cause inter-symbol interference (ISI), inter-user interference (IUI),

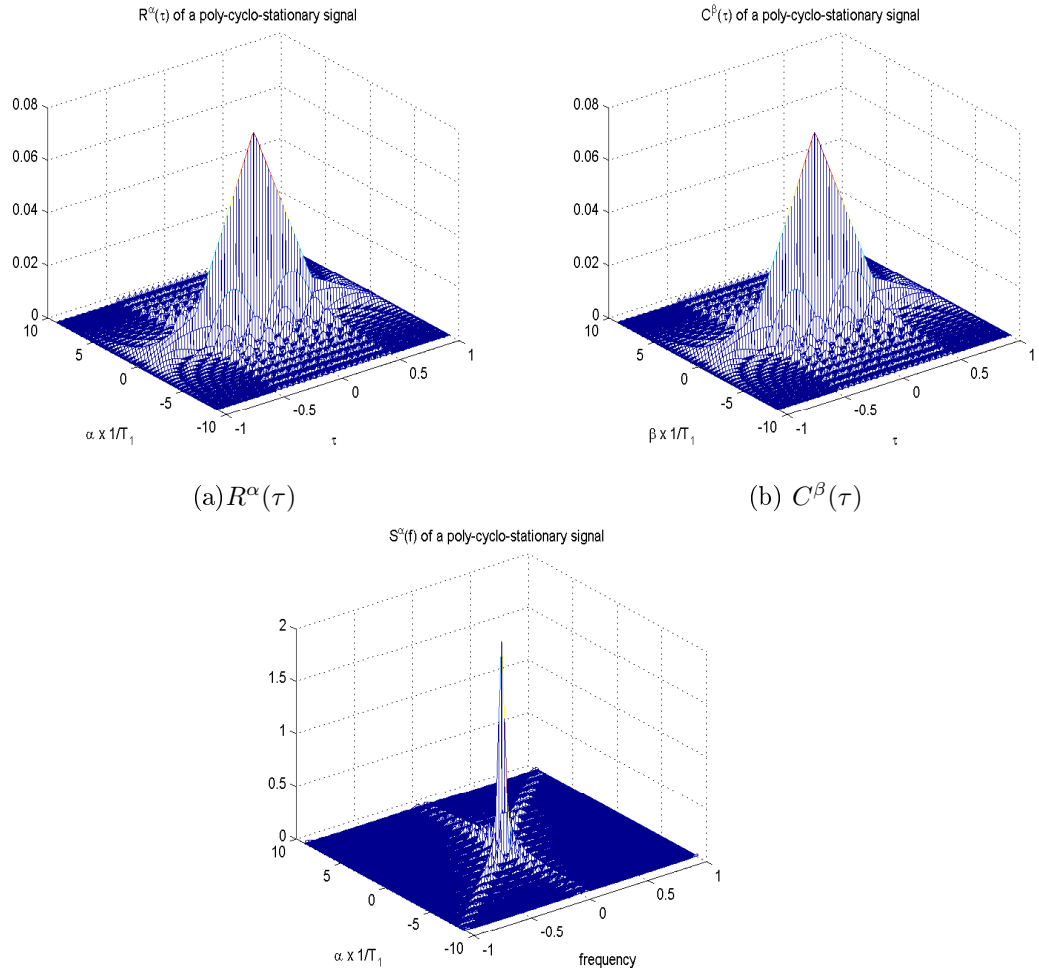

(a) $R^{\alpha}(\tau)$ (b) $C^{\beta}(\tau)$

(c) $S^{\alpha}(f)$

FIGURE 3.4: SO cyclic covariance, pseudo-covariance and DSP functions of a poly cyclo-stationary signal.

inter-carrier-interference (ICI),...
Therefore, at the receiver side, equalization should be implemented in order to deal with the different sources of interferences and recover the original transmitted symbols.

It is worth mentioning that since these sources of signal deformation, generated through the wireless channel transmission, are various and do not have a uniform character, finding an equalizer that can deal with all these non uniform interference is not a trivial solution. Hence, it is more realistic to conceive a solution that deal with some particular signal criteria. The role of the equalizer in that case is to optimize these criteria, called in the literature cost function.
Therefore, the first step of the equalization is to define and fix the optimization criterion. It can be, for example, Maximum Likelihood (ML), Maximum Ã Posteriori (MAP), mean square error (MSE), ...

3.2.1 Maximum Ã Posteriori (MAP)

The optimization of the criterion of the maximum a posteriori [65,66] consists of finding the transmitted symbol $x(n)$, in the alphabet of the M possible symbols, which maximizes the following conditional probability [67] : $\mathcal{P}_r\left(x(n) = m|y(1),..,y(n+K)\right)$, where y is the received symbol sequence :

$$x(n)^{MAP} = \underset{m\in M}{\arg\max}\, \mathcal{P}_r\left(x(n) = m|y(1),..,y(n+K)\right) \tag{3.23}$$

Using the Bayesian formula [68], the conditional probability can be written as follows :

$$\mathcal{P}_r\left(x(n) = m|y(1),..,y(n+K)\right) = \frac{\mathcal{P}_r\left(y(1),..,y(n+K)|x(n) = m\right)\mathcal{P}_r\left(x(n) = m\right)}{\mathcal{P}_r\left(y(1),..,y(n+K)\right)} \tag{3.24}$$

Therefore, maximizing Eq. (3.23) is equivalent to maximize the following equation :

$$x(n)^{MAP} = \underset{m\in M}{\arg\max}\, \mathcal{P}_r\left(y(1),..,y(n+K)|x(n) = m\right)\mathcal{P}_r\left(x(n) = m\right). \tag{3.25}$$

3.2.2 Maximum Likelihood (ML)

The Maximum Likelihood (ML) [69] criterion aims to find the transmitted sequence symbol in the alphabet of the M^K possible symbols which maximizes the following conditional probability :

$$\{x(1),..,x(K)\}^{ML} = \underset{m\in M^K}{\arg\max}\, \mathcal{P}_r\left(x(1) = m_1,..,x(K) = m_K|y(1),..,y(K)\right) \tag{3.26}$$

Likewise, using the Bayesian formula [68], maximizing Eq. (3.26) is equivalent to maximize the following expression :

$$\begin{aligned}\{x(1),..,x(K)\}^{ML} = \underset{m\in M^K}{\arg\max}\, &\mathcal{P}_r\left(y(1),..,y(K)|x(1) = m_1,..,x(K) = m_K\right)\times \\ &\mathcal{P}_r\left(x(1) = m_1,..,x(K) = m_K\right).\end{aligned} \tag{3.27}$$

3.2.3 Zero Forcing (ZF)

This criterion [70, 71] leads to suppress the interferences caused by the multi-path effect of the wireless propagation channel. If we assume that the channel can be represented by a linear filter (with $Z-$ transform is equal to $H(z)$), then the zero forcing (ZF) equalizing filter (with a $Z-$transform $W(z)$) is the inversion of this filter, meaning :

$$W(z) = \frac{1}{H(z)} \tag{3.28}$$

It is worth mentioning that, it is true that this equalizer is simple to implement and especially less complex than the two previous criteria. However, since it does not take into consideration the additive noise, it is not an optimal processing. Indeed, since it does the inversion of the channel, the noise could be increased, resulting to a performance degradation.

3.2.4 Mean Square Error (MSE)

The optimization of the mean square error (MSE) [72, 73] consists of minimizing the MSE between the transmitted symbols $x(n)$ and the equalized ones $\hat{x}(n)$, where the error is given by :

$$\epsilon_n = x(n) - \hat{x}(n) = x(n) - \boldsymbol{w}\, \boldsymbol{y}(n), \tag{3.29}$$

where $y(n)$ is the received symbol sequence and $\boldsymbol{w}$ the equalizer impulse response.
The MSE criterion aims to find a vector $\boldsymbol{w}$ verifying the following equation :

$$\underset{\boldsymbol{w}}{argmin}\, \mathbb{E}\left[||x(n) - \boldsymbol{w}\, \boldsymbol{y}(n)||^2\right], \tag{3.30}$$

where $\mathbb{E}$ stands for the expectation operator.

In this dissertation, we adopt the MSE criterion for minimizing the mean square error between the transmitted symbol and the received ones. Thus, more details on this equalization approach will be given in the following section.

3.2.5 Equalizers' types

Once the optimization criterion is fixed, the equalization process should also be adapted to the transmitted signal nature. Indeed, as mentioned before, the processing technique must be different for a signal that is SOC or NSOC, stationary or cyclo-stationary. Hence, taking into consideration the different characteristics of the transmitted signal allows us to design the appropriate equalizer.
Let us consider a system model where we can classify the equalizers according to the signal nature. This system model can be resumed as given in Figure 3.5 as follows : a signal is transmitted through a wireless propagation channel and is then corrupted by external interferences and noise. The receiver should differentiate and then extract the transmitted information from the corrupted received signal. This structure can be modelled as given in Figure 3.5.

FIGURE 3.5: system model.

In Figure 3.5 $x(n)$ represents the transmitted symbols emitted, with variance σ_x^2 and with symbol duration T_1. We assume that $T_1 = M_1 T_e$, where T_e is the sampling time. This signal is then filtered by a shaping filter, passes through a wireless propagation channel, and finally is corrupted by external interference and noise. At the receiver side, the signal is filtered with a filter matched to the one used at the transmitter side. The output of the matched filter $y(m)$ will be sampled with P samples per symbol before equalization. Finally, after equalization and the decision process, the signal $\hat{x}(n)$ represents the estimated symbols.

It is worth mentioning that for the equalization process, there are two types of MSEs : one is used in order to compute the equalizers' expressions and we note it MSE_γ, and the other one is used for evaluating the system performance and it is noted as MSE_q [49].

$$MSE_\gamma = \mathbb{E}[|\gamma(n) - x(n-\Delta)|^2], \tag{3.31}$$

$$\begin{aligned} MSE_q &= \mathbb{E}[|\text{Re}(\gamma(n)) - x(n-\Delta)|^2] \\ &= \mathbb{E}[|q(n) - x(n-\Delta)|^2], \end{aligned} \tag{3.32}$$

where Δ is a given decision delay for the decision procedure.

Note that the equalization process is different from an estimation process, as described in [74–76]. The equalizer delivers an output at the symbol rate. Even if the equalizer input rate is greater than the symbol rate, the performance of the equalizer in terms of MSE is quantified by the MSE_q between emitted and received symbols.

Symbol Spaced (SSE) and Fractionally Spaced Equalizations (FSE)

Regarding Figure 3.5, we down-sample the signal at the output of the matched filter. This operation consists in taking P samples for each symbol to construct the equalizer input signal. When P is equal to one, only one sample for each symbol is kept ; in this case, the equalization is called symbol spaced equalization (SSE), since we are working at the transmitted symbol rate. However, when P is higher than one, the process is called fractionally spaced equalization (P FSE) [77–81].
Note that since in FSE we use P times more samples per symbol than in SSE, we have P times more input information. In that case, the length of the FSE is P times higher than the SSE.

Classical Linear equalization (LE)

When the transmitted signal is characterized as second order circular, this means that the pseudo-covariance matrix of the received signal is null. Hence, the second order information is only carried by the covariance function. In that case, a minimum mean square error based linear equalization (MMSE-LE) [14, 23, 49] is required in order to eliminate the interference caused by the wireless propagation channel (ISI) and the noise.
Let us consider the vector $\boldsymbol{y_p}(l)$ of length L_e, defined as $\boldsymbol{y_p}(l) = [y_p(lT_1), y_p(lT_1 - T_e), ..., y_p(lT_1 - (L_e-1)T_e)]^T$.
The LE input signal is $y_p(l)$. As this equalizer uses only the information carried by the covariance function of the signal $y(l)$, the LE is a vector $\in \mathbb{C}^{1\times L_e}$ whose coefficients are given by [14] :

$$\boldsymbol{w_{LE}} = \boldsymbol{r}_{x\boldsymbol{y_p}} \boldsymbol{R}_{\boldsymbol{y_p}}^{-1}, \tag{3.33}$$

where $\boldsymbol{r}_{x\boldsymbol{y_p}} = \mathbb{E}[x(n)\boldsymbol{y_p^H}(l)]$ is a vector $\in \mathbb{C}^{1\times L_e}$ which represents the inter-correlation vector between the transmitted symbols and the equalizer input and $\boldsymbol{R}_{\boldsymbol{y_p}} = \mathbb{E}[\boldsymbol{y_p}(l)\boldsymbol{y_p^H}(l)]$ represents the covariance matrix $\in \mathbb{C}^{L_e\times L_e}$, of the equalizer input signal.

Widely Linear Equalization (WLE)

In case of a non second order circular signal (NSOC), the pseudo-covariance matrix of the signal is non null. Thus, the usage of a classical linear equalizer (LE) does not lead to

the best performance, since this equalizer does not take into consideration the whole SO information carried by the signal. Indeed, as it exploits only the information carried by the covariance function and neglects the one carried by the pseudo-covariance one, it results in non optimal solution for the equalization process. Therefore, in that case the process which takes into consideration both the SO statistical properties is called widely linear equalizer (WLE) [14, 59, 82, 83].
For the equalization process, the structure of the widely linear processing is described by Figure 3.6.

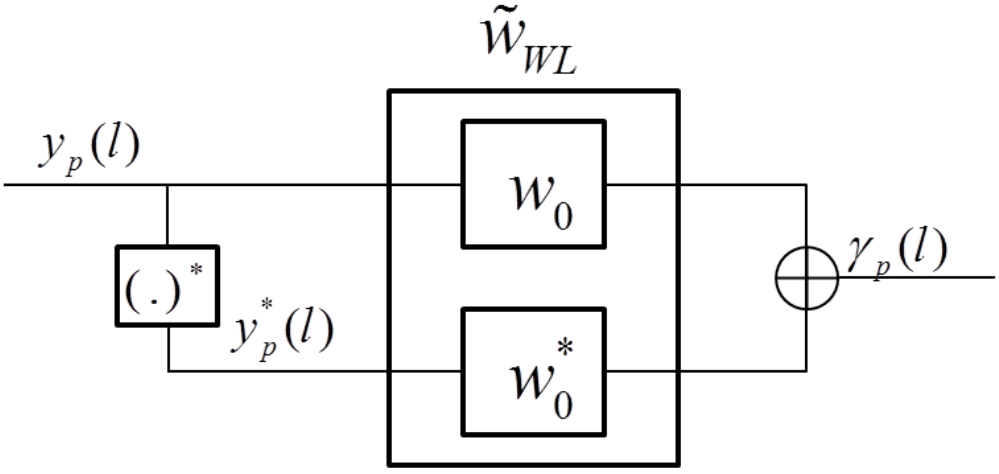

FIGURE 3.6: Widely linear equalization scheme.

Let us consider $\tilde{\boldsymbol{y}}_{\boldsymbol{p}}(l) = [\boldsymbol{y}_{\boldsymbol{p}}^{\boldsymbol{T}}(l), \boldsymbol{y}_{\boldsymbol{p}}^{*}(l)]^T$ to be a vector of length $2L_e$, which represents the WL equalizer input.
The widely linear equalizer length is twice the linear one. Indeed, since the number of the WLE input branches are doubled, compared to the classical linear processing, each branch (the signal and its conjugate version) will be fitted by a sub-equalizer having the same number of taps as the LE (i.e., L_e), resulting to an equalizer vector $\in \mathbb{C}^{1\times 2L_e}$, whose expression is given by [14] :

$$\tilde{\boldsymbol{w}}_{\boldsymbol{WL}} = \boldsymbol{r}_{x\tilde{\boldsymbol{y}}_{\boldsymbol{p}}} \boldsymbol{R}_{\tilde{\boldsymbol{y}}_{\boldsymbol{p}}}^{-\mathbf{1}}, \tag{3.34}$$

where $\boldsymbol{r}_{x\tilde{\boldsymbol{y}}_{\boldsymbol{p}}}$ is a vector $\in \mathbb{C}^{1\times 2L_e}$ and represents the inter-correlation vector between the transmitted symbols and the equalizer input in its widely linear version (i,e : $\tilde{\boldsymbol{y}}_{\boldsymbol{p}}(l)$). Besides, $\boldsymbol{R}_{\tilde{\boldsymbol{y}}_{\boldsymbol{p}}}$ is a matrix $\in \mathbb{C}^{2L_e\times 2L_e}$, called the covariance matrix of the signal $\tilde{\boldsymbol{y}}_{\boldsymbol{p}}(l)$. This matrix can be represented by :

$$\boldsymbol{R}_{\tilde{\boldsymbol{y}}_{\boldsymbol{p}}} = \mathbb{E}[\tilde{\boldsymbol{y}}_{\boldsymbol{p}}(l)\tilde{\boldsymbol{y}}_{\boldsymbol{p}}^{\boldsymbol{H}}(l)] = \begin{bmatrix} \boldsymbol{R}_{\boldsymbol{y}_p} & \boldsymbol{C}_{\boldsymbol{y}_p} \\ \boldsymbol{C}_{\boldsymbol{y}_p}^{*} & \boldsymbol{R}_{\boldsymbol{y}_p}^{*} \end{bmatrix}, \tag{3.35}$$

where $\boldsymbol{C}_{\boldsymbol{y}_p} = \mathbb{E}[\boldsymbol{y}_{\boldsymbol{p}}(l)\boldsymbol{y}_{\boldsymbol{p}}^{\boldsymbol{T}}(l)]$ represents the pseudo-covariance matrix ($\in \mathbb{C}^{L_e\times L_e}$) of the signal $\boldsymbol{y}_{\boldsymbol{p}}$.

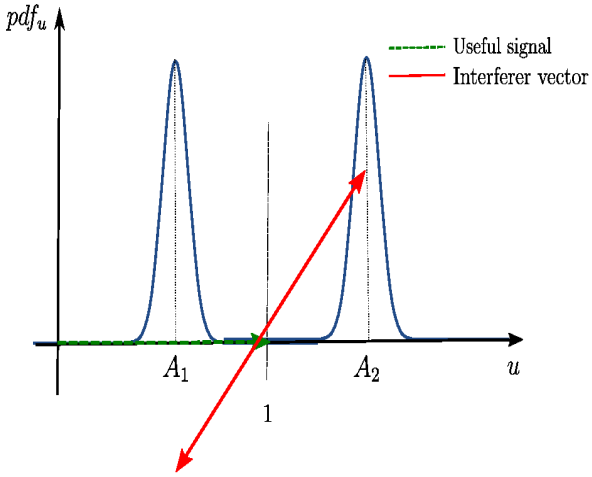

(a) Linear case

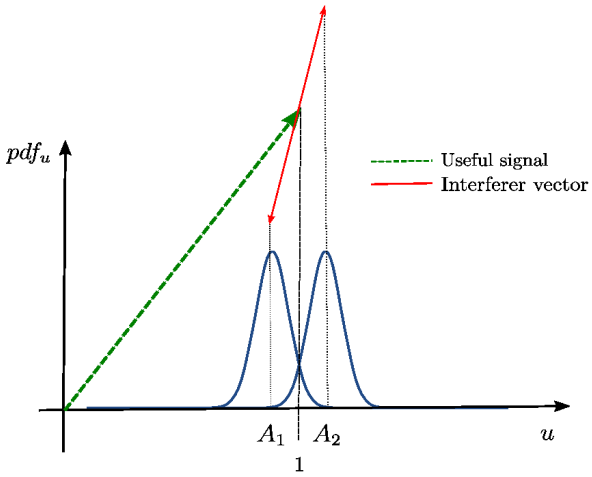

(b) Widely linear case

FIGURE 3.7: Illustration of Linear and Widely Linear Equalizers behavior with one interference.

In order to see and explain how do the two previous equalizers behave, let us consider a BPSK transmitted signal emitted through a flat fading channel, where the equalization is done in a SSE mode.

Figure 3.7 illustrates how LE and WLE are processing the input signal $\boldsymbol{y_p}(n)$. Because we have flat fading channels without ISI, the equalizer length L_e is set to one and $\boldsymbol{y_p}(n)$ is a complex vector of length equal to one.

In Figure 3.7, we show how the two equalizers operate (the interferer channel phase in this case is equal to $\frac{\pi}{4}$). In Figure 3.7, there are two interfering vectors (with red continued lines) depending on the value of the BPSK symbol (either $+1$ or -1). Using a LE with only one coefficient, the LE decision variables are the projections of the received vector $\boldsymbol{y_p}(n)$ on the real axis giving the two points A_1 (interferer -1) and A_2 (interferer $+1$). This behavior is different when using widely linear equalization. In fact, the process of the WLE has two steps : (1) multiplication by an optimal complex coefficient of the received vector $\boldsymbol{y_p}(n)$ followed by (2) projection of the rotated vector on the real axis in order to get the decision

variables A_1 and A_2, according to Figure 3.7(b). On each of the projected points (A_1 and A_2), we have an additive Gaussian noise vector which pdf is given by the blue Gaussian shapes centered on A_1 and A_2. For the WLE, the received signal $\boldsymbol{y_p}(n)$ is rotated by a complex multiplicative gain greater than one, yielding to an increased noise variance around A_1 and A_2. In conclusion, the interference plus noise pdf is the sum of two Gaussian pdf centered respectively on A_1 and A_2.

According to Figure 3.7, the variance of the pdf of interference plus noise has a "better shape" (more localized around +1 leading to lower BER) for the WLE compared to the LE. We can expect, based on this observation, that the WLE will achieve better performance, in terms of BER, when compared to the classical linear equalization.

Linear Fresh (L Fresh) and Widely Linear Fresh Equalization (WL Fresh)

We recall that when the signal is characterized as stationary, there is no correlation between the spectral components of the signal [22]. This is because the whole information is carried by the classical covariance and the pseudo-covariance matrices. We also reminisce that in case of stationary SOC signal, only a classical linear equalizer (LE) is required, contrary to the case of NSOC signal where the widely linear equalizer (WLE) remains the optimal solution.
However, when the signal is characterized as cyclo-stationary or poly-cyclo-stationary [84–87], contrary to stationary signals, there is correlation between the spectral components of the signal. Moreover, in case of NSOC signal, the covariance and the pseudo-covariance functions of the interferer signal, composed by the external interference plus the noise and called $I(l)$, are periodic functions of time [85]. Hence, based on equations (3.11) and (3.12), they can be represented as Fourier series expansions, given as follows :

$$\boldsymbol{R}_I(t,\tau) = \sum_{\alpha_i} \boldsymbol{R}_I^{\alpha_i}(\tau) e^{j2\pi\alpha_i t} \tag{3.36}$$

$$\boldsymbol{C}_I(t,\tau) = \sum_{\beta_i} \boldsymbol{C}_I^{\beta_i}(\tau) e^{j2\pi\beta_i t}. \tag{3.37}$$

Here, as mentioned in section 3.1, $\boldsymbol{R}_I^{\alpha_i}(\tau)$ and $\boldsymbol{C}_I^{\beta_i}(\tau)$ are defined, respectively, as the non-conjugate and conjugate cyclic correlation functions. Likewise, α_i and β_i are called the Second Order (SO) non conjugate and conjugate cyclic frequencies of the interferer signal.
If the transmitted signal is characterized as rectilinear and if we assume that the interferer has the same modulation with symbol duration T_I, then the SO cyclic frequencies have the following expressions :

$$\begin{cases} \alpha_i = \dfrac{i}{T_I} & \text{for } i \in \mathbb{Z} \\ \beta_i = \pm 2\Delta_f + \dfrac{i}{T_I} & \text{for } i \in \mathbb{Z}. \end{cases}$$

Δ_f stands for the interferer carrier frequency.

When the transmitted signal is characterized as quasi rectilinear (QR), then we have [85] :

$$\begin{cases} \alpha_i = \dfrac{i}{T_I} & \text{for } i \in \mathbb{Z} \\ \beta_i = \pm 2\Delta_f + \dfrac{2i+1}{2T_I} & \text{for } i \in \mathbb{Z}. \end{cases}$$

With an appropriate de-rotation (in order to make a quasi rectilinear signal as rectilinear one [59, 85]), the SO non conjugate and conjugate cyclic frequencies become the same as those corresponding to the rectilinear signal.

In case of SOC cyclo-stationary signal where the pseudo-covariance matrix is null, the classical LE only uses the information contained in the cyclic-frequency $\alpha = 0$. However, this solution is not an optimal solution. Indeed, as the SOC signal is also cyclo-stationary, the power spectral density is then scattered between the null SO cyclic frequency and other SO non conjugate and conjugate cyclic frequencies. Meaning that the whole energy is no more concentrated on $\alpha = 0$, but is shared with other non-null cyclic frequencies. In that case, exploiting only the information at the null cyclic frequency does not give good performance. Thus, the use of the information at the other energetic cyclic frequencies, in the equalization process, should be taken into consideration.

On the other hand, for a NSOC signal, the widely linear equalizer only exploits the information contained in the couple $(\alpha, \beta) = (0, 0)$. For a NSOC cyclo-stationary signal, since the most energetic conjugate cyclic frequency for rectilinear signal is $\beta = 2\Delta_f$ [85], then if the latter is not equal to zero, then the WLE is no longer the optimal solution. Moreover, if there is no energy at $\beta = 0$, then the WLE performs as well as the classical linear equalizer. Likewise, for QR signals, the most two energetic conjugate cyclic frequencies are $\beta = 2\Delta_f$ and $\beta = 2\Delta_f - \frac{1}{T_I}$, [84, 85]. Hence, if $\Delta_f \neq \frac{i}{2T_I}$, the WLE gives poor performance and becomes equivalent to the LE if there is no energy at the null conjugate cyclic frequency.
To better take into account the cyclo-stationarity of the signal, another structure of equalizer has been introduced, which exploits better the correlation between the spectral components of the signal. This structure is called FREquency SHift (FRESH) [85] equalizer.
Therefore, if the cyclo-stationary signal is characterized as SOC one, the Fresh equalizer is presented in its linear version where it is called Linear Fresh (L Fresh) equalizer. And in case of NSOC cyclo-stationary signal, the Fresh processing is implemented in its widely linear version and it is called widely linear Fresh (WL Fresh) equalizer.
The structures of the linear and widely linear Fresh equalizers, respectively, when using the most energetic cyclic frequencies, i.e., $(\pm\alpha_1, \pm\beta_1)$, are given by Figures 3.8 and 3.9, respectively :

In Figure 3.8, we use the most two energetic cyclic frequencies besides the null one to form an equalizer with 3 branches, so 3 times more taps than the classical LE. In Figure 3.9, with the use of the aforementioned most energetic cyclic frequencies besides the null ones $(\alpha = 0, \beta = 0)$, results to an equalizer with 6 branches, meaning 6 times more taps than the classical one.
Let us consider the following observation vectors $\boldsymbol{z_p}(l) = [\boldsymbol{z_1^T}(l), \boldsymbol{z_2^T}(l), \boldsymbol{z_3^T}(l)]^T$ and $\tilde{\boldsymbol{z}}_{\boldsymbol{p}}(l) = [\boldsymbol{z_1^T}(l), \boldsymbol{z_2^T}(l), \boldsymbol{z_3^T}(l), \boldsymbol{z_4^T}(l), \boldsymbol{z_5^T}(l), \boldsymbol{z_6^T}(l)]^T$, where $\boldsymbol{z_i}(l) = [z_i(lT_1), z_i(lT_1 - T_e), ..., z_i(lT_1 - (L_e - 1)T_e)]^T$, for $i = 1, .., 6$.
$z_i(l), i \in \{1, 3\}$ is the frequency shifted version of the received signal $y_p(l)$; this shift is done via the use of the cyclic frequencies $+\alpha_1, 0$ and $-\alpha_1$, respectively. Likewise, $z_i(l), i \in \{4, 6\}$ represents the frequency shifted version of the received signal complex conjugate $y_p^*(l)$ and that is done by the use of the following conjugate cyclic frequencies $+\beta_1, 0$ and $-\beta_1$.
Therefore, our linear and widely linear Fresh equalizers are given, respectively, by the Eqs.

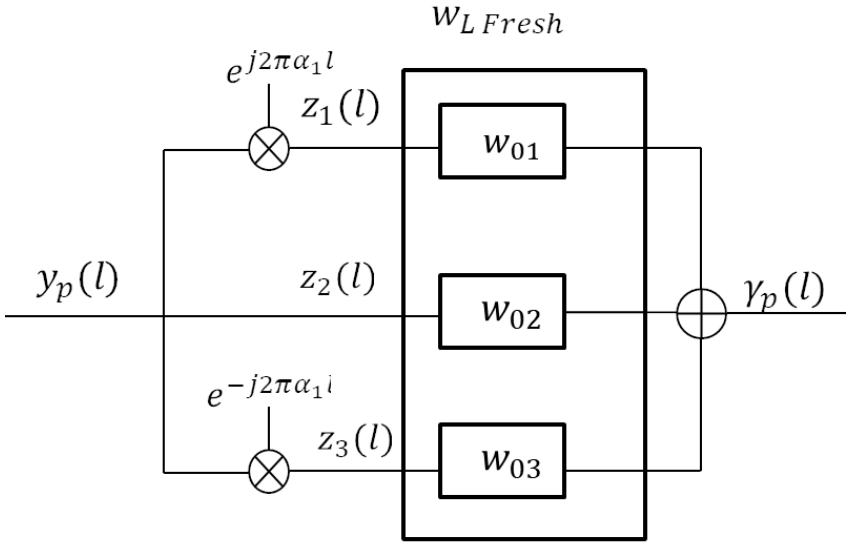

FIGURE 3.8: Linear Fresh equalization scheme.

(3.38) and (3.39) :

$$\boldsymbol{w_{LFresh}} = \boldsymbol{r}_{x\boldsymbol{z_p}}\boldsymbol{R}^{-1}_{\boldsymbol{z_p}}, \tag{3.38}$$

$$\tilde{\boldsymbol{w}}_{\boldsymbol{WLFresh}} = \boldsymbol{r}_{x\tilde{\boldsymbol{z}}_{\boldsymbol{p}}}\boldsymbol{R}^{-1}_{\tilde{\boldsymbol{z}}_{\boldsymbol{p}}}, \tag{3.39}$$

where $\boldsymbol{r}_{x\boldsymbol{z_p}}$ is a vector $\in \mathbb{C}^{1\times 3L_e}$ and $\boldsymbol{r}_{x\tilde{\boldsymbol{z}}_{\boldsymbol{p}}}$ is a vector $\in \mathbb{C}^{1\times 6L_e}$, they represent the inter-correlation vectors between the transmitted symbols and the equalizer inputs in the linear Fresh (i.e., $\boldsymbol{z_p}(l)$) and widely linear Fresh versions $\tilde{\boldsymbol{z}}_{\boldsymbol{p}}(l)$, respectively. Besides, $\boldsymbol{R}_{\boldsymbol{z_p}} = \mathbb{E}[\boldsymbol{z_p}(l)\boldsymbol{z_p^H}(l)]$ is a matrix $\in \mathbb{C}^{3L_e\times 3L_e}$ and $\boldsymbol{R}_{\tilde{\boldsymbol{z}}_{\boldsymbol{p}}} = \mathbb{E}[\tilde{\boldsymbol{z}}_{\boldsymbol{p}}(l)\tilde{\boldsymbol{z}}_{\boldsymbol{p}}^{\boldsymbol{H}}(l)]$ is a matrix $\in \mathbb{C}^{6L_e\times 6L_e}$, and they are defined as the covariance matrices of the signals $\boldsymbol{z_p}(l)$ and $\tilde{\boldsymbol{z}}_{\boldsymbol{p}}(l)$, respectively. As for the case of the stationary signal, when the signal is also NSOC, the widely linear outperforms the classical linear one. Likewise, for the case of cyclo-stationary signal, with the exploitation of other energetic cyclic frequencies besides the null ones, we can assure a better provided performance achieved by the Fresh processing. Indeed, additional information, non used by the classical equalizer, is exploited by the Fresh processing (either in its linear (L Fresh) or widely linear (WL Fresh) versions).

3.2.6 Equalization in FBMC-OQAM system

We recall that the orthogonality between the sub-carriers in FBMC-OQAM system is verified thanks to the use of the offset QAM (OQAM) modulation. When the signal is transmitted over a flat channel or over a moderate frequency selective one, the orthogonality between the sub-carriers still exist and only single tap frequency equalization is sufficient without the need for a time domain equalization process [59]. However, when the transmission channel is considered as high frequency selective one, the orthogonality between the sub-carriers is lost causing inter-carrier-interferences (ICI) besides the inter-symbol-interference

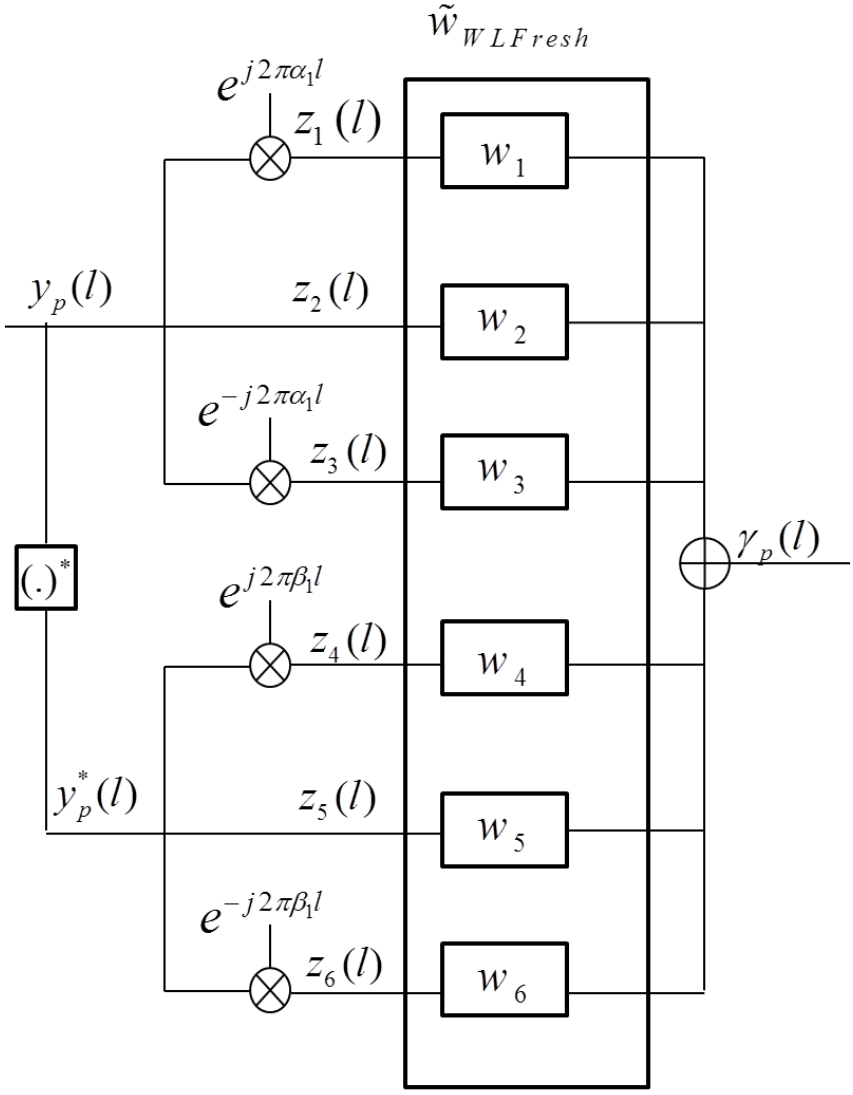

FIGURE 3.9: Widely linear Fresh equalization scheme.

(ISI) caused by the frequency selective channel. In this case, the implementation of a time domain equalizer on each sub-carrier is required in order to correct these forms of interferences.
In this context, many researchers showed their interest in studying the FBMC-OQAM system [56,88,89] and hence a few interested on the equalization side [24,90]. Indeed, researchers in [23] studied the performance of linear equalization in the SSE (symbol spaced) version using the criterion of minimizing the mean square error (MMSE) between the transmitted symbols and the equalized ones. The study of the performance of the widely linear equalizer in its classical version as for its Fresh (Frequency Shift) version is studied in [84, 85] using the maximum likelihood (ML) criterion in the equalization process. Moreover, while the the study of the linear equalizer based on the criterion of the MSE was done in [91], the study of a non linear equalizer based on MMSE criterion but with the use of the structure of decision feedback equalization was done in [92]. Besides the MSE criterion, the study of an equalizer based on the MLSE (Mean Least Square Error) criterion was done in [93]. Furthermore, in order to limit the ICI, researchers in [94], studied the linear equalization in a Fractionally rhythm.

3.3 Conclusion

In this chapter, we give a brief introduction to the cyclo-stationarity concept, where we explain how we can differentiate between a stationary signal and a poly-cyclo-stationary one. This explanation is given via equations as well as examples to better illustrate this phenomenon. Moreover, we present some equalization criteria, and define the best equalization strategy according to the signal nature and finally, we present a brief state of the art about equalization over FBMC-OQAM system.
After describing the equalization strategies involving the linear, widely linear and widely linear Fresh filters, we will apply, in the next chapter, these processing on different transmission scenarios.

Chapitre 4

Performance Analysis of Classical and Fresh equalizers in System with Rectilinear Modulation

Introduction

We recall that in literature [95], [96], [14], it is well known that when the transmitted signal is characterized as non second order circular, the linear equalization is not an optimal solution for reducing or omitting interferences. However, the widely linear processing, which is able to suppress one external interference, is required and it gives better performance when compared to the classical linear one.
Furthermore, we recall that, when the signal is also characterized as cyclo-stationary or poly-cyclo-stationary, the widely linear processing is non more an optimal solution and hence the Fresh processing should be implemented in order to have better performance.
Therefore, in this chapter, we will study the performance of the different aforementioned equalizers when applied to a signal using a rectilinear modulation. This study will be done in two parts. In the first part, as the widely linear equalizer can deal with one external interference, we will analyze how would be its behaviour when the transmitted signal is corrupted by more than one interference. In the second part, besides the classical linear and widely linear equalizers, we will analyze the performance of the Fresh filtering.

4.1 Performance of LE and WLE

In this first part, we study and analyze, theoretically, the performance of the classical linear and widely linear equalizers in a system having rectilinear modulation in presence of

multiple rectilinear interferences. Without loss of generality, the rectilinear modulation is chosen to be $M-$ary pulse amplitude modulation $M-$PAM. The PAM signal amplitudes belong to the set $\{\pm A, \pm 3A, .., \pm(M-1)A\}$.
The analysis of the equalizers' performance will be carried for two cases, depending on the propagation channel selectivity (Flat channels (subsection 4.1.2) or Frequency selective channels (subsection 4.1.3)).

4.1.1 System model and time domain equalizers expressions

The system model adopted in the study is presented by figure 4.1

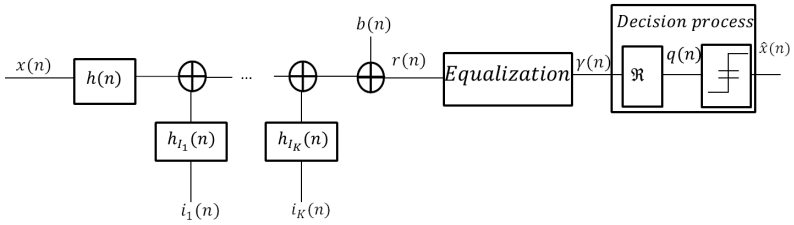

FIGURE 4.1: System model with K interferers.

In Figure, 4.1, we transmit the useful signal $x(n)$ at time n, with symbol-duration T and variance σ_x^2. $i_k(n)$ is the k^{th} interfering signal $(k = 1, ..., K)$ with variance σ_I^2. Without loss of generality, the studied modulation is the M-ary pulse amplitude modulation (M-PAM) where the signal amplitude $\in \{\pm A, \pm 3A, .., \pm(M-1)A\}$. We assume that all transmitted symbols are independent, and $h(l)$ and $h_{I_k}(l)$, $l \in \{0, 1, .., L-1\}$ are the discrete time domain channel impulse responses of, respectively, the useful signal and the k^{th} interferer. $b(n)$ is a proper complex white Gaussian noise with variance equal to σ_b^2. $r(n)$ is the equalizer input signal, $\gamma(n)$ and $q(n)$ are the equalizer outputs before and after taking its real part, respectively. Finally, $\hat{x}(n)$ is the estimated symbols after decision process.

The received signal $r(n)$ can be written as follows :

$$\begin{aligned} r(n) &= \sum_{l=0}^{L-1} h(l)x(n-l) + \sum_{k=1}^{K}\left[\sum_{l=0}^{L-1} h_{I_k}(l)i_k(n-l)\right] + b(n) \\ &= h(k_0)x(n-k_0) + \sum_{l=0, l\neq k_0}^{L-1} h(l)x(n-l) + \sum_{k=1}^{K}\left[\sum_{l=0}^{L-1} h_{I_k}(l)i_k(n-l)\right] + b(n) \\ &= \text{useful term} + \{\text{ISI} + \text{IUI}\} + \text{Gaussian Noise} \end{aligned} \tag{4.1}$$

Equalizers expressions

In order to compute the expressions of the equalizers, we adopt the criterion of minimizing the mean square error (MSE) between the transmitted symbols and the equalized ones. The MSE is given by equation (4.2)

$$MSE_\gamma = \mathbb{E}\left[|\gamma(n) - x(n-k_0)|^2\right], \tag{4.2}$$

where k_0 is the decision delay that should be well chosen [96], [97].

Let us express $\boldsymbol{r}(n)$ as a vector of length N given by $\boldsymbol{r}(n) = [r(n)\, r(n-1) ... \, r(n-N+1)]^T$. When applying classical linear processing [14], [23] to the received signal, the equalizer of length N (satisfying $\gamma(n) = \boldsymbol{f_L r}(n)$) is given by

$$\boldsymbol{f_L} = \boldsymbol{r_{xr}} \boldsymbol{R_{rr}^{-1}}, \tag{4.3}$$

where $\boldsymbol{R_{rr}} = \mathbb{E}[\boldsymbol{r}(n)\boldsymbol{r}^H(n)]$ is the covariance matrix and $\boldsymbol{r_{xr}} = \mathbb{E}[x(n-k_0)\boldsymbol{r}^H(n)]$ represents the inter-correlation vector of length N.

With widely linear processing [83], [14], [95], and when taking into account the received signal $\boldsymbol{r}(n)$ and its complex conjugate version $\boldsymbol{r}^*(n)$, the equalizing filters (satisfying $\gamma(n) = \boldsymbol{f_{1W} r}(n) + \boldsymbol{f_{2W} r}^*(n)$) are given as follows :

$$\boldsymbol{f_{1W}^H} = \left[\boldsymbol{R_{rr}} - \boldsymbol{C_{rr}} \boldsymbol{R_{rr}}^{-1*} \boldsymbol{C_{rr}}^*\right]^{-1} \left[\boldsymbol{r}_{\boldsymbol{r}x} - \boldsymbol{C_{rr}} \boldsymbol{R_{rr}}^{-1*} \boldsymbol{r}_{\boldsymbol{r}x}^*\right] \tag{4.4}$$

$$\boldsymbol{f_{2W}} = \boldsymbol{f_{1W}^*}, \tag{4.5}$$

where $\boldsymbol{C_{rr}} = \mathbb{E}[\boldsymbol{r}(n)\boldsymbol{r}^T(n)]$ is the pseudo-covariance matrix of rank N.

If we assume that the matrix $\boldsymbol{R_{rr}^{-1}}$ and $\boldsymbol{C_{rr}^{-1}}$, and the vector $\boldsymbol{r_{xr}}$ are already computed. The complexity to compute (4.3) (for the LE) and (4.4) (for the WLE) is asymptotically of order N^2 and N^3.

4.1.2 Equalizers performance over flat fading channels

In this section, we present a new method that aims to quantify the gain of WLE when compared to LE, in system using $M-$PAM modulation corrupted by multiple interferences, using the same modulation. This scheme can be found in filter bank multi-carrier modulation (FBMC) based systems [23, 90], where the useful signal is affected by interferences coming from adjacent sub-carriers. In order to focus on the impact of the external interferences on the WLE gain compared to LE, we have neglected, in this section, the multi-path effect. The impact of multi-path channels will be studied in section 4.1.3.

Equalizers expressions

As claimed before and without loss of generality, we have chosen flat fading channels for both useful signal and interferers, i.e., : $h(n) = \alpha_0 \delta(n)$ and $h_{I_k}(n) = \alpha_k \delta(n)$,$(k = 1, ..., K)$. The received signal $r(n)$, in this case, can be written as

$$r(n) = \alpha_0 x(n) + \sum_{k=1}^{K} \alpha_k i_k(n) + b(n). \tag{4.6}$$

We note ρ as the interference to useful signal power ratio. This ratio is equal to

$$\rho = \frac{P_{\text{Interferences}}}{P_{\text{Useful signal}}} = \frac{\sum_{k=1}^{K} |\alpha_k|^2}{|\alpha_0|^2}. \tag{4.7}$$

Without loss of generality, we have chosen a modulus equal to 1 and a phase equal to zero for α_0. In order to ensure that all the interferences are impacting similarly the useful signal, we suppose that all interferers have the same received power, meaning that channel gains

$\alpha_k (k = 1, \ldots, K)$ have a constant modulus equal to $|\alpha_k| = \sqrt{\frac{\rho}{K}}$ and a phase, φ_k, uniformly distributed over $[0, 2\pi[$.

Over flat fading channels, the expressions of, respectively, autocorrelation, pseudo-autocorrelation matrix and inter-correlation vector mentioned in equation (4.4), can be simply written as follows

$$\boldsymbol{R_{rr}} = E[\boldsymbol{r}\boldsymbol{r}^H] = (|\alpha_0|^2 + \sigma_b^2 + \sum_{k=1}^{K} |\alpha_k|^2)\boldsymbol{I}_N, \tag{4.8}$$

$$\boldsymbol{C_{rr}} = E[\boldsymbol{r}(n)\boldsymbol{r}^T(n)] = (\alpha_0^2 + \sum_{k=1}^{K} \alpha_k^2)\boldsymbol{I}_N, \tag{4.9}$$

$$\boldsymbol{r_{xr}} = E[x(n)\boldsymbol{r}^H(n)] = [\alpha_0^* \, 0..0], \in \mathbb{C}^{1\times N}. \tag{4.10}$$

where $\boldsymbol{I}_N$ represents the identity matrix of rank N

Performance Analysis

In this section, we evaluate the performance of both linear and widely linear equalizers in presence multiple interferers. Without loss of generality and for sake of simplicity, we consider $M = 2$ (which is equivalent to BPSK modulation). Nonetheless, the study and results remain valid for M-PAM modulation ($M > 2$) and other types of NSOC modulations (GMSK, MSK,...).
We have seen in a previous chapter the behaviour of both equalizers in presence of a single interference. Thus, in this analysis, we consider the case of multiple interferers with uniformly distributed phases, φ_k, over $[0, 2\pi[$.

Multiple Interferences ($K > 1$) with phases uniformly distributed over $[0, 2\pi[$

pdf estimation We add to the useful signal K interferers, having each a gain modulus equal to $\sqrt{\frac{\rho}{K}}$ and a phase angle φ_k uniformly distributed over $[0, 2\pi[$. We represent an interferer signal by a symbol that can take values from (+1 or −1) with equal probability. Then, we have 2^K possible vectors for the overall interference depending on the combinations of the BPSK interference symbols. This results into 2^K possible projections on the real axis, meaning that, for a given set of angles (φ_1, φ_2,...,φ_K) we have a sum of 2^K Gaussian pdfs. The resultant pdf of interference plus noise is then given by :

$$pdf(\varphi_1, ..., \varphi_K) = \frac{1}{2^K} \sum_{p=1}^{2^K} \frac{1}{\sqrt{2\pi\sigma_b'^2}} e^{-\frac{(u-A_p)^2}{2\sigma_b'^2}}, \tag{4.11}$$

where A_p is the p^{th} projection ($p = 1, ..., 2^K$) of the received vector $\boldsymbol{r}(n)$, and $\sigma_b'^2$ is the variance of the noise projection on the real axis.

For a given set of angles (φ_1, φ_2,...,φ_K), the appropriate pdf is expressed in (4.11). If we would like to estimate the average pdf of interference plus noise, we have to average the pdf of (4.11) over 'Γ' different realizations of the interference channels, as follows :

$$pdf_{est} = \frac{1}{\Gamma} \sum_{m=1}^{\Gamma} pdf(\varphi_{(m,1)}, ..., \varphi_{(m,K)}). \tag{4.12}$$

Assuming Γ is sufficiently large, the pdf of the interference plus noise for the linear and widely linear equalizers can be estimated by using (4.12).

pdf calculation by convolution In the linear case, it is possible to compute analytically the pdf of interference plus noise using convolution. According to Figure 4.1, the interference plus noise is given by

$$I(n) = \sum_{k=1}^{K} \alpha_k \; i_k(n) + b(n). \tag{4.13}$$

After linear equalization, $I(n)$ becomes $I_p(n)$ that is equal to

$$\begin{aligned} I_p(n) &= \sum_{k=1}^{K} \mathrm{Re}(\alpha_k) i_k(n) + b_p(n) \\ &= \sum_{k=1}^{K} (\sqrt{\frac{\rho}{K}} \cos\varphi_k) i_k(n) + b_p(n), \end{aligned} \tag{4.14}$$

where $b_p(n)$ is the real component of the additive complex Gaussian noise. Referring to (4.14), we see that $I_p(n)$ is a sum of $K+1$ independent random signals. The pdf of $I_p(n)$ is then equal to the convolution of the pdf of each term in the sum, i.e,

$$pdf_{conv} = pdf_1 \star pdf_2 \star ... \star pdf_K \star pdf_b, \tag{4.15}$$

where $(\star)$ represents the convolution operator, pdf_b is the pdf of $b_p(n)$ and pdf_k being the pdf of the k^{th} term of the sum in (4.14), given by

$$pdf_k = pdf(\sqrt{\frac{\rho}{K}} \cos\varphi_k) = \frac{1}{\pi} \frac{1}{\sqrt{\frac{\rho}{K} - u^2}}; \;\; |u| < \sqrt{\frac{\rho}{K}}. \tag{4.16}$$

Using (4.16) and (4.15), we are able to compute the pdf of the interference plus noise using multiple convolutions. When the number of interferers, K, increases, the pdf tends to a Gaussian law because of the central limit theorem given by (4.15) in the case of linear and widely linear equalizers.

BER Expressions

Because of α_0 is equal to one, the decision variable, after LE or WLE, is equal to one and the BER expressions are given by :

$$BER_{sim} = \frac{1}{2} Pr(1 + I_p(t) < 0) + \frac{1}{2} Pr(-1 + I_p(t) > 0), \tag{4.17}$$

$$BER_{est} = \int_1^{\infty} pdf_{est}(u) du, \tag{4.18}$$

$$BER_{conv} = \int_1^{\infty} pdf_{conv}(u) du. \tag{4.19}$$

The comparison of the shape of the pdf_{est} for LE and WLE will give us insight on the BER performance gain provided by the two equalizers.

Numerical Results

In this section, we present numerical results in order to validate our theoretical approach for LE and WLE. Indeed, we compare BER performance obtained by computer simulations

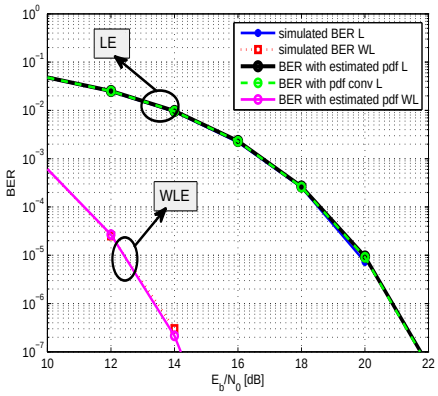

(a) Constant phase equal to $\frac{\pi}{4}$.

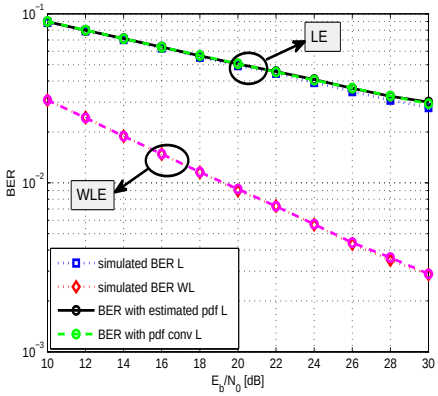

(b) Phase uniformly distributed over $[0, 2\pi[$

FIGURE 4.2: LE and WLE BER, $K = 1$, $\rho = 1$.

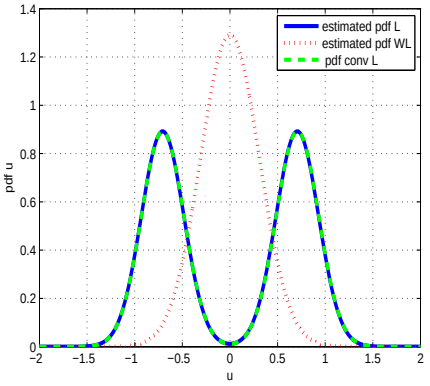

(a) Constant phase equal to $\frac{\pi}{4}$

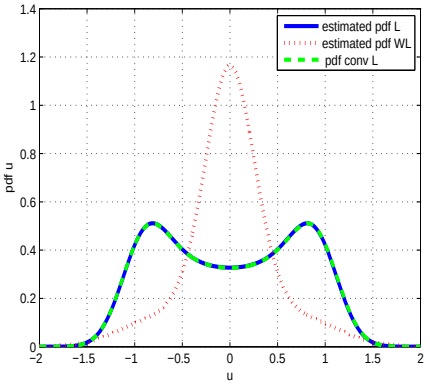

(b) Phase uniformly distributed over $[0, 2\pi[$

FIGURE 4.3: LE and WLE pdf at $\frac{Eb}{No} = 10$ dB, $K = 1$, $\rho = 1$.

(calculated using Eq. (4.17)) and theoretical ones performed using the expressions (presented in Eqs. (4.18) and (4.19)), calculated, respectively, with the estimated pdf (4.12) and the pdf obtained by convolution (4.15).

First, we consider a single interferer with either a constant phase or a phase uniformly distributed on $[0, 2\pi[$. A second part is devoted to the multi-interference case.

Single Interference ($K = 1$)

Constant phase $\varphi_1 = \frac{\pi}{4}$, $\rho = 1$ From Figure 4.2, we notice that the simulated curves match with the theoretical ones for both LE and WLE case. Moreover, the performance in terms of BER of the WLE is better than the conventional LE. This outperformance can be justified through the shape of the pdf of the interference plus noise. In fact, the pdf of the WLE is more concentrated around the decision variable than the one of the LE, as shown in Figure 4.3 (these curves are obtained for an $\frac{E_b}{N_0}$ equal to 10 dB).

Uniformly distributed phase φ_1 over $[0, 2\pi[$ and $\rho = 1$ When φ_1 is equal to 0 or $\frac{\pi}{2}$ the two equalizers provide the same performance (see Figure 3.7 in the previous chapter). For phase values close to 0 and $\frac{\pi}{2}$ the WLE has a better performance than the LE. The performance gap can be slight for phases closed to 0 or $\frac{\pi}{2}$ but can be greater for phases around $\frac{\pi}{4}$. Taking φ_1 uniformly distributed on $[0, 2\pi[$, we study the performance of the two equalizers. In Figures 4.2(a) and 4.2(b), the BER performance of the two equalizers is plotted. It is clear that the WLE outperforms the LE, and both the simulated BER (4.17) and the analytically computed BER with expressions (4.18) and (4.19) give similar results. For estimating (4.12), $5{\times}10^4$ realizations of the interference channel were done. Figure 4.3 illustrates the pdf of interference plus noise for the two equalizers for $\frac{E_b}{N_0} = 10$ dB. As stated before, we can see that the Widely Linear pdf has a better shape than the Linear one, which leads to lower BER. We deduce, from Figures 4.2 and 4.3, that Widely Linear processing, compared to the Linear one, remains the optimal solution whether the interference phase is constant or uniformly distributed, over $[0, 2\pi[$.

Multiuser interferences ($K > 1$)

We have shown, in Section 4.1.2, that the WLE outperforms the LE in the case where only one single interference is present. The goal of this section is to study and analyze the impact of increasing the number of interferences on WLE behaviour. All interferers have uniformly distributed phases φ_k over $[0, 2\pi[$.

In order to compare the performance of equalizers as a function of K, we have chosen, for each value of K, an interference power ρ giving mainly the same BER performance as for the LE. The chosen BER range for the LE has been taken arbitrarily equal to 2×10^{-3}. Then, we compare the BER gap between LE and WLE.

Figure 4.4 gives the pdf of interference plus noise for $K = 5$ at $\frac{E_b}{N_0}$ equal to 42 dB. We can see that the LE and WLE pdfs are mainly the same with a Gaussian shape giving thus similar performance in terms of BER. Nevertheless, zooming on the pdf tail, it can be noted that the WLE pdf exhibits a better shape (more concentrated in the center) than the LE one, giving thus better BER performance (see Figure 4.4). Figures 4.5(a) to 4.5(d) give the BER performance of the two equalizers for $K = 2$ to 5. We can see that the performance gap between LE and WLE decreases when the number of interferers grows. These results are very interesting, because they show that a WLE can perform better than its linear counterpart even in presence of multiple interferences. Concerning the pdf, when the number of interferers gets higher, the pdf of interference plus noise tends to be Gaussian because of the central limit theorem (see (4.18)).

4.1.3 Equalizers Performance Over Frequency selective channels

In the previous section, we have studied the performance of equalizers with the existence of only external interferences (IUI). With the corruption of both ISI and IUI, we will analyze, in this section, theoretically the performance of LE and WLE in terms of BER and MSE. In this analysis, the different channels are frequency selective. We have chosen this scenario in order to simulate a filter bank multi carrier-offset quadrature amplitude modulation (FBMC-OQAM) system [23]. With this multi-carrier system, QAM symbols are transmitted using two PAM modulations staggered by half a symbol period. Hence, the useful transmitted

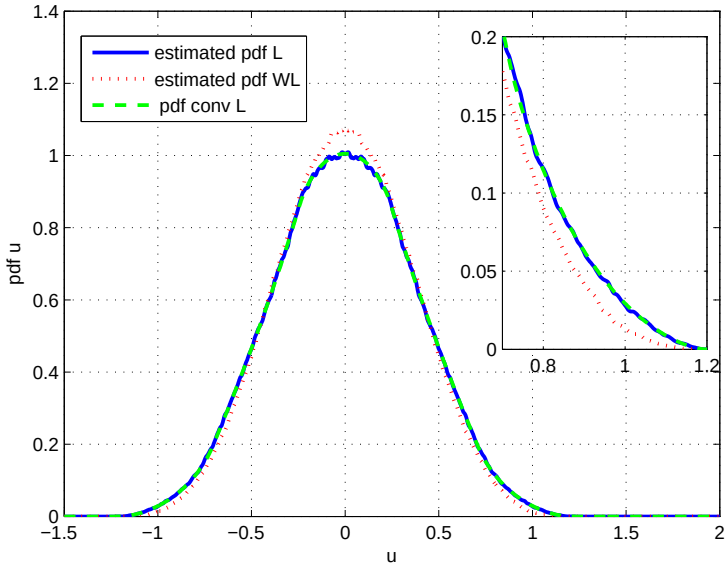

FIGURE 4.4: Interference plus Noise pdf at 42 dB with $K = 5$ Interferences which phases uniformly distributed over $[0, 2\pi[$.

signal can be seen as a PAM signal. When the transmission channel is frequency selective, adjacent carriers will interfere with the useful signal and are modeled, in our scenario, by IUI PAM interferences.

Performance Analysis

MSE expressions

In order to evaluate the system performance, we consider MSE_q as the mean square error according to the real part of the equalized signal

$$\begin{aligned} MSE_q &= \mathbb{E}\left[|\mathrm{Re}(\gamma(n)) - x(n-k_0)|^2\right] \\ &= \mathbb{E}\left[|q(n) - x(n-k_0)|^2\right]. \end{aligned} \tag{4.20}$$

It is worth noticing that the difference between (4.20) and (4.2) (which allows the derivation of the equalizers' responses) is only for the linear case, since the output of the WLE is real ($q(n) = \gamma(n)$ for the WLE case).

When the LE ($\boldsymbol{f_L}$) and WLE ($\boldsymbol{f_{1W}}$ and $\boldsymbol{f_{2W}}$) are computed, $q(n)$ can be written as

$$q(n) = \gamma'(n) + \gamma'^*(n) = \boldsymbol{f_1 r}(n) + \boldsymbol{f_2 r}^*(n),$$

where $\boldsymbol{f_1} = \boldsymbol{f_{1W}}$ for WLE, $\boldsymbol{f_1} = \frac{1}{2}\boldsymbol{f_L}$ for LE and $\boldsymbol{f_2} = \boldsymbol{f_1}^*$ for both equalizers cases. Therefore, $q(n)$ can be generated by using both the received signal and its complex conjugate. This configuration can be modeled as shown in Figure 4.6, where signals carried by the lower branch are the complex conjugate of those in the upper one. Note that this system model remains valid for both equalizers cases, by taking $f_1(n)$ and $f_2(n)$ equal to $f_{1W}(n)$ and

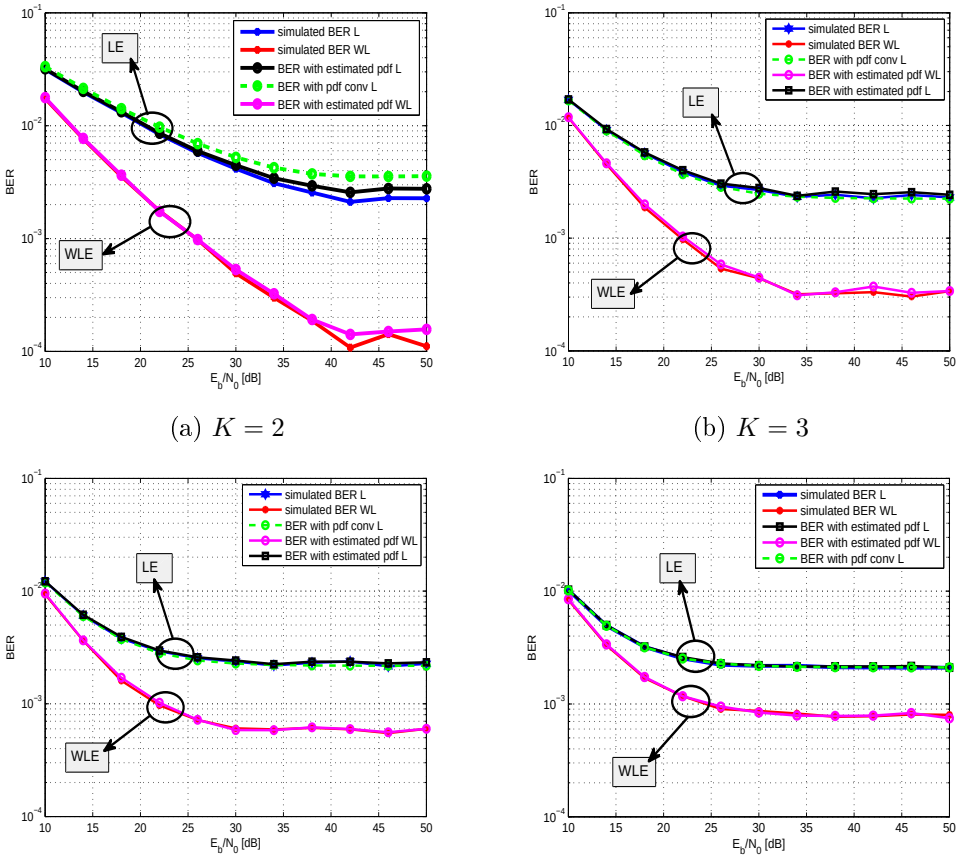

(a) $K = 2$ (b) $K = 3$

(c) $K = 4$ (d) $K = 5$

FIGURE 4.5: BER performance versus the number of interferences K.

$f_{2W}(n)$ given by (4.4) and (4.5) for the WLE, and $f_1(n) = \frac{1}{2} f_L(n)$ and $f_2(n) = \frac{1}{2} f_L^*(n)$ for the LE, where $f_L(n)$ is given by (4.3).

For the determination of the MSE in the time domain, we consider the real part of the equalized signal that can be written as follows :

$$q(n) = \alpha\, x(n - k_0) + n_E(n) + b_E(n), \tag{4.21}$$

where α is a real multiplicative coefficient applied to the useful signal. $n_E(n)$ and $b_E(n)$ are, respectively, the residual $ISI + IUI$ and noise, of variances σ^2_{NE} and σ^2_{BE}.
Thus, (4.20) can be rewritten as :

$$MSE_q = |\alpha - 1|^2 \sigma_x^2 + \sigma^2_{NE} + \sigma^2_{BE}. \tag{4.22}$$

Frequency domain equalizers and MSE expressions

In order to compute the value of MSE_q expressed in Eq. (4.22), we will first compute the power spectral density (PSD) of the error and then integrate it over the whole spectrum. To compute this PSD we must first derive the equalizers expressions in the frequency domain.

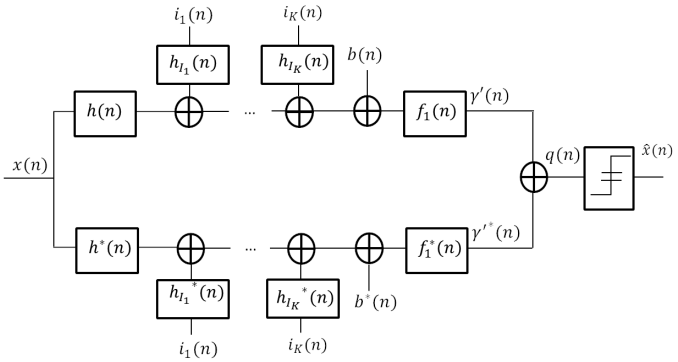

FIGURE 4.6: Equivalent system model scheme with K interferers.

As in the time domain, we distinguish two errors given by the following expressions

$$E_\Gamma(\omega) = \Gamma(\omega) - X(\omega)\, e^{-j\omega k_0 T} \tag{4.23}$$

$$\begin{aligned} E_Q(\omega) &= Q(\omega) - X(\omega)\, e^{-j\omega k_0 T} \\ &= \left[F_1(\omega)H(\omega) + F_1^*(-\omega)H^*(-\omega) - e^{-j\omega k_0 T}\right] X(\omega) \\ &+ \sum_{k=1}^{K} [F_1(\omega)H_{I_k}(\omega) + F_1^*(-\omega)H_{I_k}^*(-\omega)] I_k(\omega) \\ &+ F_1(\omega)B(\omega) + F_1^*(-\omega)B^*(-\omega), \end{aligned} \tag{4.24}$$

where $E_\Gamma(\omega)$, $E_Q(\omega)$, $\Gamma(\omega)$, $X(\omega)$, $Q(\omega)$, $F_1(\omega)$, $H(\omega)$, $H_{I_k}(\omega)$, $B(\omega)$ and $I_k(\omega)$, $k \in \{1, .., K\}$ are the Fourier transforms of respectively $e_\gamma(n)$, $e_q(n)$, $\gamma(n)$, $x(n)$, $q(n)$, $f_1(n)$, $h(n)$, $h_{I_k}(n)$, $b(n)$ and $i_k(n)$.
Since the WLE output signal is real ($(\gamma(n) = q(n))$), $E_\Gamma(\omega) = E_Q(\omega)$, whereas for the LE case, it is equal to :

$$E_\Gamma(\omega) = \left[F_L(\omega)H(\omega) - e^{-j\omega k_0 T}\right] X(\omega) \quad + \sum_{k=1}^{K} \left[F_L(\omega)H_{I_k}(\omega)\right] I_k(\omega) + F_L(\omega)B(\omega). \tag{4.25}$$

As in the time domain, to derive the expressions of the equalizers, we proceed by minimizing the power spectral density Se_Γ of the error $e_\gamma(n) = \gamma(n) - x(n - k_0)$ where

$$Se_\Gamma(\omega) = \mathbb{E}[|E_\Gamma(\omega)|^2] = \mathbb{E}\left[|\Gamma(\omega) - X(\omega)e^{-j\omega k_0 T}|^2\right]. \tag{4.26}$$

For the linear case, $E_\Gamma(\omega)$ is expressed by equation (4.25), whereas, for the widely linear case, it is given by equation (4.24) with $F_1(\omega) = F_{1W}(\omega)$.

The minimization of $\mathbb{E}\left[|\Gamma(\omega) - X(\omega)e^{-j\omega k_0 T}|^2\right]$ with respect to $F_L(\omega)$ gives the expression (4.27) which represents the MMSE-LE. The MMSE-WLE, corresponding to the widely linear equalizers are computed by minimizing $\mathbb{E}\left[|Q(\omega) - X(\omega)e^{-j\omega k_0 T}|^2\right]$ with respect to $F_{1W}(\omega)$ and they are expressed by (4.28) and (4.29).

Therefore, the expressions of the MMSE-LE and MMSE-WLE are given, respectively, by equations (4.27) and ((4.28) - (4.29)), respectively.

$$F_L(\omega) = \frac{\sigma_x^2 H^*(\omega)\, e^{-j\omega k_0 T}}{\sigma_x^2 |H(\omega)|^2 + \sigma_I^2 \sum_{k=1}^{K} |H_{I_k}(\omega)|^2 + \sigma_b^2}\ , \tag{4.27}$$

$$O(\omega) = \sigma_x^2|H(-\omega)|^2\left[\sigma_I^2\sum_{k=1}^{K}|H_{I_k}(\omega)|^2+\sigma_b^2\right]+\sigma_x^2|H(\omega)|^2\left[\sigma_I^2\sum_{k=1}^{K}|H_{I_k}(-\omega)|^2+\sigma_b^2\right]$$
$$+\sigma_b^2\left[\sigma_b^2+\sigma_I^2\sum_{k=1}^{K}\left(|H_{I_k}(\omega)|^2+|H_{I_k}(-\omega)|^2\right)\right]-2\sigma_I^2\sigma_x^2\mathrm{Re}\left(H(\omega)H(-\omega)\sum_{k=1}^{K}H_{I_k}^*(\omega)H_{I_k}^*(-\omega)\right)$$
$$+\sigma_I^4\left[\left(\sum_{k=1}^{K}|H_{I_k}(\omega)|^2\right)\left(\sum_{k=1}^{K}|H_{I_k}(-\omega)|^2\right)-\left|\sum_{k=1}^{K}H_{I_k}(\omega)H_{I_k}(-\omega)\right|^2\right] \tag{4.30}$$

$$F_{1W}(\omega) = e^{-j\omega k_0 T}\frac{\sigma_x^2H^*(\omega)\left[\sigma_b^2+\sigma_I^2\sum_{k=1}^{K}|H_{I_k}(-\omega)|^2\right]-\sigma_x^2\sigma_I^2H(-\omega)\sum_{k=1}^{K}H_{I_k}^*(\omega)H_{I_k}^*(-\omega)}{O(\omega)} \tag{4.28}$$

where $O(\omega)$ is expressed in equation (4.30), and

$$F_{2W}(\omega) = F_{1W}^*(-\omega). \tag{4.29}$$

Note that F_L, F_{1W} and F_{2W} (given by (4.27), (4.28) and (4.29)), represent the Fourier transforms of respectively f_L, f_{1W} and f_{2W} (given by (4.3), (4.4) and (4.5)). Once the equalizers are computed, the power spectral density Se_Q of the error $e_q(n) = q(n)-x(n-k_0)$ is expressed as $Se_Q(\omega) = \mathbb{E}[|E_Q(\omega)|^2]$, where $E_Q(\omega)$ is given by (4.24). Therefore, Se_Q is expressed as :

$$Se_Q(\omega) = |F_1(\omega)H(\omega)+F_1^*(-\omega)H^*(-\omega)-e^{-j\omega k_0T}|^2\sigma_x^2$$
$$+\sum_{k=1}^{K}|F_1(\omega)H_{I_k}(\omega)+F_1^*(-\omega)H_{I_k}^*(-\omega)|^2\sigma_I^2+\left[|F_1(\omega)|^2+|F_1^*(-\omega)|^2\right]\sigma_b^2, \tag{4.31}$$

where $F_1(\omega) = \frac{1}{2}F_L(\omega)$ for linear case and $F_1(\omega) = F_{1W}(\omega)$ for the widely linear case.
Referring to [98], the mean square error of the signal described by Figure 4.6 is expressed by (4.32).

Hence, we deduce the value of α by symmetry between Equations (4.22) and (4.32). This value is given by the following formula :

$$\alpha = \frac{T}{2\pi}\int_{-\frac{\pi}{T}}^{\frac{\pi}{T}} e^{j\omega k_0T}\left[F_1(\omega)H(\omega)+F_1^*(-\omega)H^*(-\omega)\right]dw. \tag{4.33}$$

Therefore, the BER expression of the studied system could now be derived.

BER

The expression of the BER related to the transmission of an M-PAM signal is given by the following equation

$$BER = \left[\frac{2(M-1)}{M\log_2(M)}\right]Pr\left(n_E(n)+b_E(n)>\alpha A\right). \tag{4.34}$$

$$
\begin{aligned}
MSE_q &= \frac{T}{2\pi}\int_{-\frac{\pi}{T}}^{\frac{\pi}{T}} Se_Q(\omega)\,dw. \\
&= \frac{T}{2\pi}\int_{-\frac{\pi}{T}}^{\frac{\pi}{T}} |F_1(\omega)H(\omega) + F_1^*(-\omega)H^*(-\omega) - e^{-j\omega k_0 T}|^2\sigma_x^2 \\
&+ \sum_{k=1}^{K} |F_1(\omega)H_{I_k}(\omega) + F_1^*(-\omega)H_{I_k}^*(-\omega)|^2\sigma_I^2 + \left[|F_1(\omega)|^2 + |F_1^*(-\omega)|^2\right]\sigma_b^2\,dw. \\
&= \frac{T}{2\pi}\int_{-\frac{\pi}{T}}^{\frac{\pi}{T}} \left|F_1(\omega)e^{j\omega k_0 T}H(\omega) + F_1^*(\omega)e^{j\omega k_0 T}H^*(-\omega) - 1\right|^2\sigma_x^2 \\
&+ \sum_{k=1}^{K} |F_1(\omega)H_{I_k}(\omega) + F_1^*(-\omega)H_{I_k}^*(-\omega)|^2\sigma_I^2 + \left[|F_1(\omega)|^2 + |F_1^*(-\omega)|^2\right]\sigma_b^2\,dw.
\end{aligned}
\tag{4.32}
$$

Since $n_E(n)$ and $b_E(n)$ are Gaussian, zero mean with variances, respectively, equal to σ_{NE}^2 and σ_{BE}^2, the BER expression can be written as

$$
\begin{aligned}
BER &= \left[\frac{2(M-1)}{M\log_2(M)}\right] Q\left(\frac{\alpha A}{\sqrt{\sigma_{NE}^2 + \sigma_{BE}^2}}\right) \\
&= \left[\frac{2(M-1)}{M\log_2(M)}\right] Q\left(\frac{\alpha A}{\sqrt{MSE_q - \sigma_x^2(\alpha-1)^2}}\right)
\end{aligned}
\tag{4.35}
$$

where A is equal to

$$
A = \sqrt{\frac{3}{M^2-1}\sigma_x^2}. \tag{4.36}
$$

It is worth noticing that the proposed method of computing the different terms expressed by (4.24), (4.31), (4.32), (4.33), (4.34) and (4.35) is given in a general way that remains valid for both MMSE-LE (when $F_1(\omega) = \frac{1}{2}F_L(\omega)$) and MMSE-WLE (when $F_1(\omega) = F_{1W}(\omega)$).

Numerical results

In this subsection, we present a comparison between the analytical expressions of BERs and MSEs given by (4.35) and (4.22), respectively and the simulated ones for both linear and widely linear equalizers. This comparison is done as a function of the number of channel taps L and the number of interferences K.

During simulations, the L taps of the channel impulse responses are chosen randomly having a Rayleigh modulus and a phase uniformly distributed in $[0, 2\pi]$ for each one. Likewise, these taps are kept constant during the transmission of the 10^6 M-PAM symbols. The equalizer length is set to $N = 30$, with the delay $k_0 = 20$. The simulation results are the average of 100 different channel realizations. The simulation parameters for Figure 4.7 are $L = 3$, $K = 1$ and $M = 4$, for Figure 4.8, $L = 10$, $K = 5$ and $M = 2$ and for Figure 4.9, $L = 3$, $K = 1$ and $M = 16$.

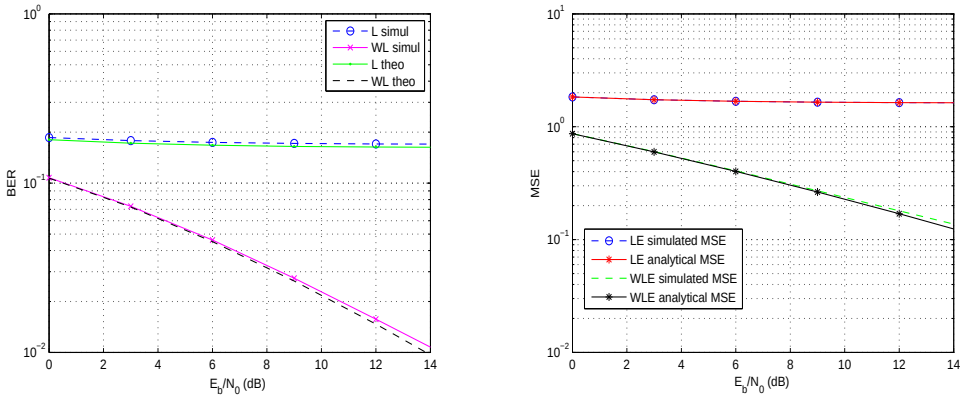

(a) BER (b) MSE

FIGURE 4.7: Error performance for $K = 1$, $L = 3$ and $M = 4$.

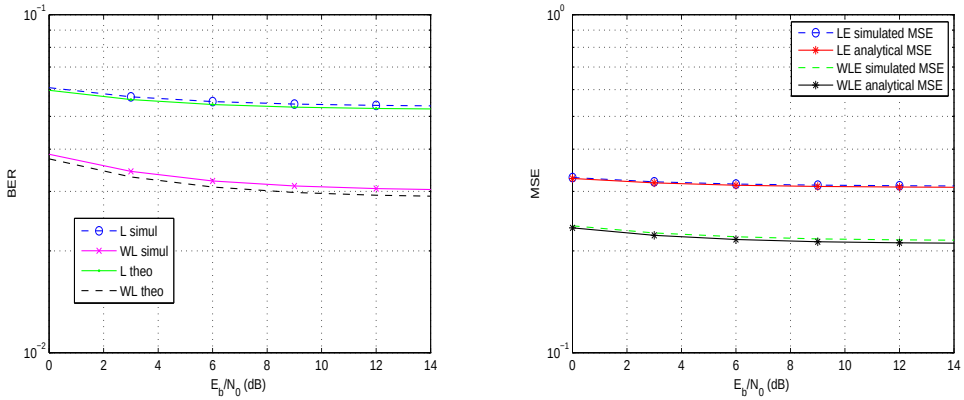

(a) BER (b) MSE

FIGURE 4.8: Error performance for $K = 5$, $L = 10$ and $M = 2$.

Through Figures 4.7 to 4.9, we show that the results provided by the theoretical expressions (4.35) and (4.22) match the simulated results for shorter or longer channel impulse responses, for a smaller or larger number of interfering signals, for 2−PAM, 4−PAM and 16−PAM and this remains valid for any PAM order, i.e. for all cases $(\forall L, \forall K, \forall M)$. From these figures, we can see the out-performance of the widely linear processing compared to the classical linear one, and this out-performance decreases as the interferers number increases. In the considered scenario, with the existence of both IUI and ISI, the error performance of the MMSE-LE is limited. Indeed, even with a large number of interferers, the system using a MMSE-WLE outperforms the one using a MMSE-LE.

4.2 Performance Analysis of LE, WLE and Fresh equalization

In this section, besides the classical linear and widely linear equalizers, we implement the Fresh equalizers, introduced in the previous chapter. These equalizers are implemented

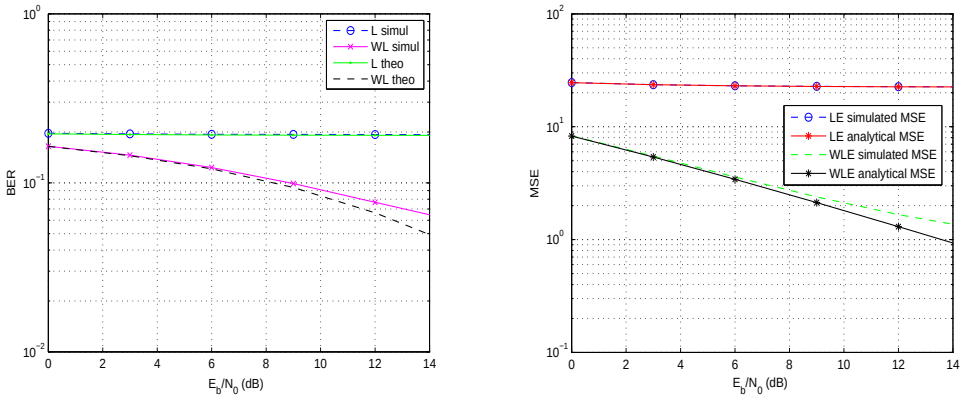

(a) BER (b) MSE

FIGURE 4.9: BER performance for $K = 1$, $L = 3$ and $M = 16$.

in their fractionally spaced mode (FSE). Thus, we study the performance of the aforementioned processing and analyze the gain of the Fresh equalizer in a rectilinear downlink (DL) transmission, i.e., a system having two users transmitting rectilinear signals. One of the users is considered as the primer user (PU) or also called user of interest (UOI), the second one is called user of non interest (UNOI) which represent an interferer to the UOI. Without loss of generality, we have chosen an $M-$ary pulse amplitude modulation ($M-$PAM) for the rectilinear modulation.

4.2.1 System model

In order to evaluate the performance of the different equalizers, a downlink (DL) transmission scheme is considered, where the system model is depicted by Figure 4.10.

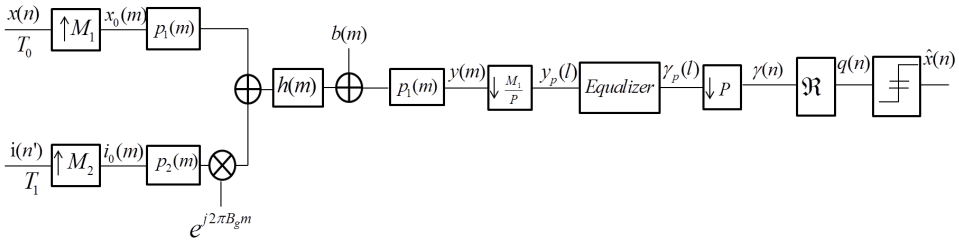

FIGURE 4.10: Rectilinear system model with two users.

For the UOI, we transmit $M-$PAM symbols $x(n)$, with variance σ_x^2 and symbol-duration T_0. $x_0(m)$ is then a series of Dirac impulses with multiplicative coefficients equal to the $M-$PAM symbols $x(n)$, and spaced by T_0. The signal $x_0(m)$ represents an oversampled version of $x(n)$, with a factor M_1, called signal of interest (SOI), is then filtered by the shaping filter, with impulse response $p_1(m)$. Likewise, $i(n')$ represent the $M-$PAM symbols transmitted by the interferer, with variance σ_i^2 and symbol-duration equal to T_1. In the following, w.l.g, we will assume that $T_1 > T_0$. $i_0(m)$ is called the signal of non interest (SNOI) and it is a series of Dirac impulses with multiplicative coefficients equal to the $M-$PAM

interferer symbols, $i(n')$, and spaced by T_1. We assume that $T_0 = M_1 T_e$ and $T_1 = M_2 T_e$, where T_e is the sampling time. The SNOI is also filtered by a shaping filter with impulse response $p_2(m)$.

As we have considered a DL transmission, the SNOI is synchronous in the time domain with the SOI. In the frequency domain, the SNOI is frequency shifted by B_g, which represents the Guard Band (GB) between the two users. $h(m)$ is the impulse response of the propagation channel. The channel output is corrupted by a circular and stationary complex Additive White Gaussian Noise (AWGN) $b(m)$, with variance σ_b^2. The receiver front end is composed of a filter matched to the shaping filter of the UOI, $p_1(m)$. The output of this matched filter, $y(m)$, will be sampled with P samples per symbol before processing by the equalizer. Finally, after equalization and decision process, the signal $\hat{x}(n)$ represents the received $M-$PAM symbols.

4.2.2 Expressions of the different equalizers

Regarding the expressions of the different equalizers (LE, WLE, L Fresh and WL Fresh), since the same equalization criterion is adopted which is minimizing the mean square error (MSE) between the transmitted useful signal $x(n)$ and the equalized one $\gamma(n)$, the same equalizers as given in the previous chapter are still applicable in the case of this system model.

We rewrite the expressions of the different equalizers as given and modeled in the previous chapter as follows :

— **Linear equalizer (LE)** :

$$\boldsymbol{w_{LE}} = \boldsymbol{r}_{x\boldsymbol{y_p}} \boldsymbol{R}_{\boldsymbol{y_p}}^{-\mathbf{1}}, \tag{4.37}$$

— **Widely Linear equalizer (WLE)**

$$\tilde{\boldsymbol{w}}_{\boldsymbol{WL}} = \boldsymbol{r}_{x\tilde{\boldsymbol{y}}_{\boldsymbol{p}}} \boldsymbol{R}_{\tilde{\boldsymbol{y}}_{\boldsymbol{p}}}^{-\mathbf{1}}, \tag{4.38}$$

where $\boldsymbol{y_p}(l)$ and $\tilde{\boldsymbol{y}}_{\boldsymbol{p}}(l)$ are vectors of length, respectively, L_e and $2L_e$, defined as : $\boldsymbol{y_p}(l) = [y_p(lT_1), y_p(lT_1 - T_e), ..., y_p(lT_1 - (L_e - 1)T_e)]^T$ and $\tilde{\boldsymbol{y}}_{\boldsymbol{p}}(l) = [\boldsymbol{y}_{\boldsymbol{p}}^{\boldsymbol{T}}(l), \boldsymbol{y}_{\boldsymbol{p}}^{*}(l)]^T$, respectively.

With the use of one SO non conjugate and conjugate cyclic frequencies, the expressions of the Fresh equalizers are given by :

— **Linear Fresh (L Fresh) equalizer** :

$$\boldsymbol{w_{LFresh}} = \boldsymbol{r}_{x\boldsymbol{z}_{\boldsymbol{p}}} \boldsymbol{R}_{\boldsymbol{z}_{\boldsymbol{p}}}^{-\mathbf{1}}, \tag{4.39}$$

— **Widely Linear Fresh (WL Fresh) equalizer** :

$$\tilde{\boldsymbol{w}}_{\boldsymbol{WLFresh}} = \boldsymbol{r}_{x\tilde{\boldsymbol{z}}_{\boldsymbol{p}}} \boldsymbol{R}_{\tilde{\boldsymbol{z}}_{\boldsymbol{p}}}^{-\mathbf{1}}, \tag{4.40}$$

where $\boldsymbol{z_p}(l) \in \mathbb{C}^{1\times 3L_e}$ and $\tilde{\boldsymbol{z}}_{\boldsymbol{p}}(l) \in \mathbb{C}^{1\times 6L_e}$ defined as follows : $\boldsymbol{z_p}(l) = [\boldsymbol{z_1^T}(l), \boldsymbol{z_2^T}(l), \boldsymbol{z_3^T}(l)]^T$ and $\tilde{\boldsymbol{z}}_{\boldsymbol{p}}(l) = [\boldsymbol{z_1^T}(l), \boldsymbol{z_2^T}(l), \boldsymbol{z_3^T}(l), \boldsymbol{z_4^T}(l), \boldsymbol{z_5^T}(l), \boldsymbol{z_6^T}(l)]^T$, where $\boldsymbol{z_i}(l) = [z_i(lT_1), z_i(lT_1 - T_e), ..., z_i(lT_1 - (L_e - 1)T_e)]^T$, for $i = 1, .., 6$.

The signal $z_i(l), i \in \{1, 3\}$ represents the frequency shifted version of the received signal $y_p(l)$ using the cyclic frequencies $+\alpha_1, 0$ and $-\alpha_1$, respectively. Likewise, the signal $z_i(l), i \in \{4, 6\}$ is the frequency shifted version of the received signal complex conjugate $y_p^*(l)$ using the conjugate cyclic frequencies $+\beta_1, 0$ and $-\beta_1$, respectively.

4.2.3 Simulation results

We recall that the chosen rectilinear modulation is the $M-$PAM. In order to simplify our analysis and without loss of generality, we have chosen $M = 2$ which is equivalent to the binary phase shift keying (BPSK) modulation. Thus, the reported results and conducted conclusion remain valid for any $M-$PAM modulation with $M > 2$.
For the simulation parameters, we consider that the interferer user (UNOI) is transmitting with a symbol duration which is twice the one of the primary user (UOI) ; meaning that $T_1 = 2T_0$, leading to $M_2 = 2M_1$. Moreover, the pulse shaping filters of the two users are chosen to be rectangular ones.
The performance evaluation of the BPSK system is done in two phases. First, we analyze the impact of the guard band (GB) between the two users. Then, we study the impact of the number of samples (P) on the performance of the different studied equalization schemes. As aforementioned in chapter 3, P denotes the number of samples for each symbol taken, after down-sampling operation, in order to construct the equalizer input signal.

Impact of Guard Band

Here, we evaluate the system performance with respect to the guard band (GB), in order to study the impact of this GB on the equalizer behaviors. Thus, we do that at a fixed signal to noise ratio : $\frac{E_b}{N_0} = 20$ dB and over a fixed frequency selective channel. The channel is modeled as a finite impulse response (FIR) filter with $3 \times M_1$ taps, in order to reproduce the effects of multi-path propagation encountered in wireless communication systems. The channel coefficients are chosen randomly and kept constant during the transmission of 10^4 symbols. The UOI transmitted symbol has $M_1 = 32$ samples, P is chosen to be equal to 16 and the linear equalizer (LE) length $L_e = 15 \times P$ for all simulation results.

Hence, the performance of the different studied equalizers (LE, WLE, L Fresh and WL Fresh) with respect to the guard band is given by Figure 4.11. Regarding the Fresh equalizers, we recall that the SO non conjugate and conjugate cyclic frequencies are equal to $\alpha_1 = \frac{1}{T_1}$ and $\beta_1 = 2\,B_g + \frac{1}{T_1}$. We recall that for L Fresh equalizer, only α_1 is used, where both α_1 and β_1 are exploited for the WL Fresh equalizer.

From results depicted in Figure 4.11, one can note that :

— The WLE outperforms the linear one because of the channel multi-path effect and the non-circularity of the chosen modulation : Indeed, since the modulation is NSOC and the channel is frequency selective, the WL gives better performance compared to the classical LE one. This result is well known as published in [96], [49].

— The WL Fresh filter outperforms the widely linear equalizer because of the cyclo-stationarity characteristic of the transmitted signals. Indeed, as the transmitted signal is poly-cyclo-stationary one, then the signal energy is not contained in only the null SO cyclic frequencies but spread in other non null ones. In this sense, since our WL Fresh equalizer exploits the spectral energies contained in the other used cyclic frequencies, it outperforms the classical widely linear equalizer which exploits only the energy contained in the null SO cyclic frequencies (i.e., $\alpha_0 = 0$ and $\beta_0 = 0$).

— The WL Fresh gives better performance when compared to the linear Fresh (L Fresh) because of the nature of the signal when combining the effect of NSOC and poly-cyclo-stationarity. Indeed, as the emitted signal is considered as both NSOC and

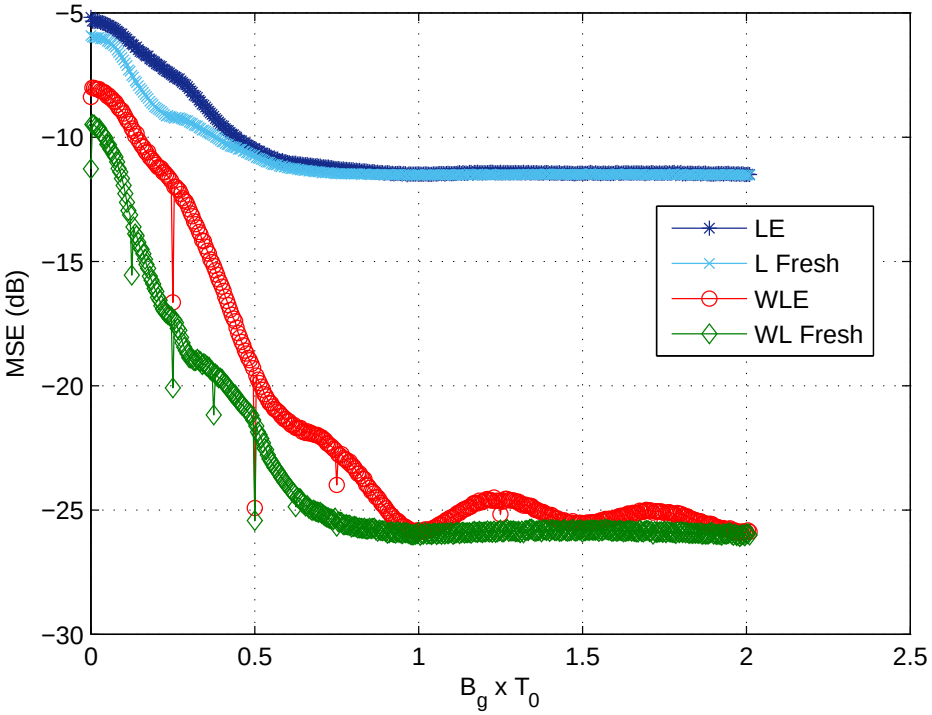

FIGURE 4.11: MSE Performance system with respect to GB for $\frac{E_b}{N_0} = 20$ dB.

also a poly-cyclo-stationary one, resulting in out-performance of the widely linear processing when compared to the linear one, in its Fresh version.

In addition to these expected results, interesting and new remarks compared to the existing literature can be highlighted :

— There are notches in the WLE curve when $B_g = \frac{i}{4T_0}$ in which the WLE performance increases. This fact can be explained as follows : we have shown, previously, that rectilinear SO cyclic frequencies are :

$$\begin{cases} \alpha_i = \frac{i}{T_1} \\ \beta_i = \pm 2B_g + \frac{i}{T_1} \end{cases}$$

and since the WLE exploits the energy contained at the null conjugate frequency; i.e., $\beta_i = 2B_g + \frac{i}{T_1} = 0 \Leftrightarrow B_g = \frac{i}{2\,T_1}$. As $T_1 = 2T_0$ then it performs better when $B_g = \frac{i}{4\,T_0}$.

We move now to the WL Fresh equalizer where another interesting and new remark can be added :

— The WL Fresh equalizer has also notches when $B_g = \frac{i}{8T_0} = \frac{i}{4T_1}$. This can be explained as done in the previous item. Indeed, as the most energetic conjugate SO cyclic frequencies are equal to $\beta_i = \pm 2\,B_g + \frac{i}{T_1}$, after frequency shifting equal to $\pm\beta_1$, the most energetic conjugate cyclic frequencies become located at frequencies $\beta_i \pm \beta_1 =$

$\pm 4B_g + \frac{i}{T_1}$ which are null for $B_g = \dfrac{i}{4\,T_1} = \dfrac{i}{8\,T_0}$.
To the best of our knowledge, the two previous findings have never been highlighted before in the literature.

It is worth mentioning that the notches for both WLE and WL Fresh are not related to the selectivity of the propagation channel.

Impact of P

To analyze the impact of the number of samples per symbol on the behavior of the different described equalizers, we study the MSE performance at a fixed $\dfrac{E_b}{N_0} = 20$ dB and over a frequency selective channel. To avoid being inside a notch for both WL cases, we consider for example $B_g = \dfrac{0.65}{T_0} \neq \dfrac{i}{8T_0}, \forall\, i$. In the simulation, we have taken $M_1 = 64$ and the channel is chosen to be frequency selective; it is modeled as a FIR filter with $3 \times M_1$ taps. Likewise, the channel coefficients are chosen randomly and kept constant during the transmission of 10^4 UOI symbols.

Figure 4.12 shows the MSE performance of LE, WLE, L Fresh and WL Fresh equalizers versus the number of samples per symbol P.

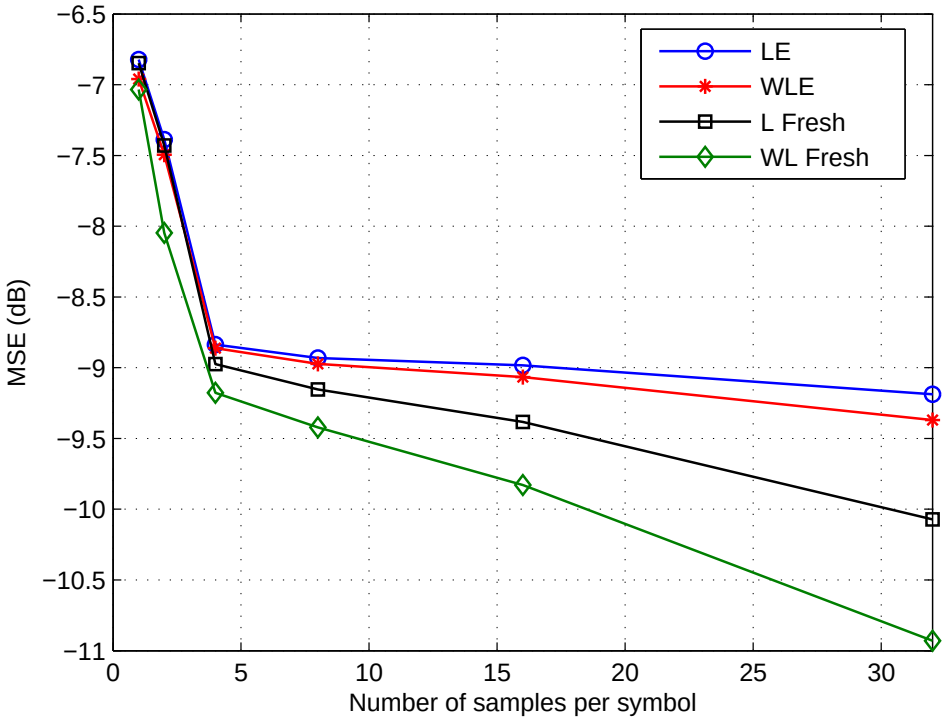

FIGURE 4.12: Impact of P on equalizers performance at $\dfrac{E_b}{N_0} = 20$ dB and $B_g = \dfrac{0.65}{T_0}$.

We deduce, from the results presented in Figure 4.12, that the WL Fresh equalizer outperforms all the other equalizers for any value of P, and that the LE has the worst performance. Moreover, the higher P is, the higher gap in performance is achieved. This

is related to the fact that when P is larger, the equalizer receives more signal information, leading to better performance.

Conclusion

In this chapter, a fair comparison between MMSE-LE and MMSE-WLE performance, in their SSE mode, was done in a system using rectilinear modulation corrupted by multiple external rectilinear interferences. We evaluated analytically the out-performance of the MMSE-WLE when compared to the classical MMSE-LE and showed the degradation of the WLE performance when the number of interferers got large.
On the other hand, besides the performance of the classical linear (LE) and widely linear (WLE) equalizers, the study of the contribution of the Fresh equalizers was done with the same system model. For all equalizers, we studied the impact of SSE/FSE processing and the impact of the guard band between UOI and interferer. New and original results are related to the existence of notches where MSE performance for WL processing-based equalizers increase considerably for particular guard band values. This can be explained by the fact that these particular guard band values result in null conjugate second order cyclic frequencies. Moreover, the worst performance is given by the classical linear equalizer (LE), whereas the best performance is provided by the WL Fresh equalizer, since it exploits the cyclo-stationarity properties of the transmitted signal. Additionally, we have confirmed that increasing the number of samples per symbol (FSE processing) enhances the performance for the two WL processing-based equalizers compared to the linear ones.

Chapitre 5

Equalization over a Quasi-Rectilinear signal : Application to FBMC-OQAM system

Introduction

This chapter studies the performance of the different aforementioned equalization processes (MMSE-LE, MMSE-WLE and the Fresh equalizer) applied on FBMC-OQAM systems with mixed numerologies transmission. This study will be done in two phases. The first one will be the analysis of the classical equalizers used in their SSE version for FBMC-OQAM systems, where only ICI and/or ISI are present. Here, we first derive an equivalent system model using rectilinear modulation. Then, with the presence of one user and one interferer with different numerologies, (i.e., with the presence of ISI, ICI and also inter-user-interferences (IUI)), we aim to analyze the performance of the classical equalizers (LE and WLE) and the widely linear Fresh one. For the proposed equalizers, both symbol spaced (SSE) and fractionally spaced (FSE) processing will be evaluated, in synchronous downlink (DL)/uplink (UL) and asynchronous UL scenarios.

5.1 FBMC-OQAM system model

As an application of the different equalization process, we aim to study the performance of the linear (LE), widely linear (WLE) and widely linear Fresh (WL Fresh) equalizers over a FBMC-OQAM system. To do so, we adopt the case where two users (User #1 which is

considered as the user of interest (UOI) and User #2 called User of non interest (UNOI)), which are transmitting simultaneously using different numerologies. We recall that different numerologies correspond to different parameter settings for the multi-carrier waveform, such as sub-carrier spacing, symbol duration and cyclic prefix (CP) length. The adopted configuration can be modeled as depicted in Figures 5.1 and 5.2, where the transmitter and the receiver are described, respectively.

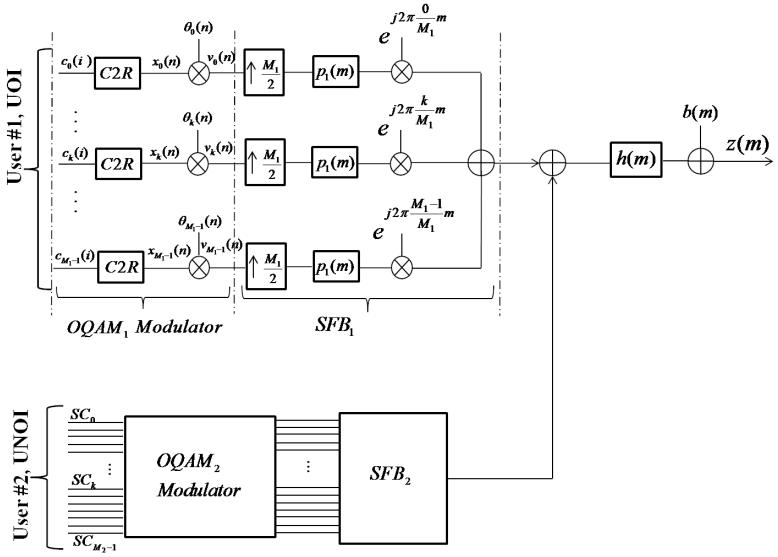

FIGURE 5.1: FBMC-OQAM system transmitter with two users having different numerologies.

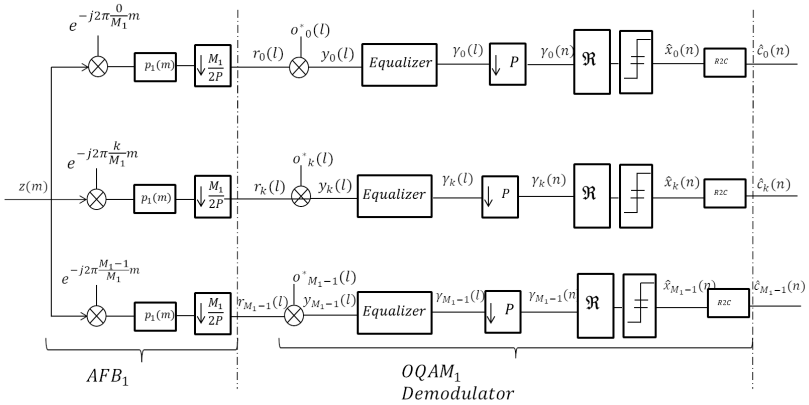

FIGURE 5.2: FBMC-OQAM system receiver for intended UOI having numerology 1.

Looking at Figures 5.1 and 5.2, the FBMC modulator contains two main blocs, which are the OQAM modulator and the synthesis filter bank (SFB), while the demodulator contains

two dual blocks, which are the analysis filter bank (AFB) and the OQAM demodulator. For clarity reasons, only User #1 modulator has been detailed in Figure 5.1. Modulator of User #2 is similar but adapted for a different numerology, i.e : M_2 instead of M_1, $p_2(m)$ instead of $p_1(m)$.
In this configuration, the first user, which is considered as the User of Interest (UOI) has inter-carrier spacing equal to $\frac{1}{M_1}$, whereas the second one called UNOI, has inter-carrier spacing equal to $\frac{1}{M_2}$. Without loss of generality we assume that $M_2 > M_1$.

It is worth mentioning that while the FBMC-OQAM system model given in chapter 2 is described in its SSE version, Figure 5.2 represents the FBMC-OQAM receiver in its $P-$FSE version. Hence the same transmitter description (eventually with the adapted parameters for the two users) is still applicable on Figure 5.1. The filters for the UOI and the UNOI have, respectively, length $L_1 = KM_1$ and $L_2 = KM_2$, where K is the aforementioned overlapping factor.

The outputs of the two SFBs (User #1 and User #2) are added together before the convolution with the channel impulse response and the corruption by the complex AWGN (see Figure 5.1). At the receiver side (see Figure 5.2), the received signal $z(m)$ is processed by the analysis filter bank number 1 (AFB_1, since we consider User#1 as the UOI). The output of the AFB_1 gives rise to M_1 parallel sub-carriers signals, that will be further processed by the OQAM_1 demodulator.

In the demodulator, the input signal of the k^{th} sub-carrier is first multiplied by the factor $e^{-j2\pi\frac{k}{M_1}m}$ then filtered by the PHYDYAS matched filter $p_1(m)$ and down-sampled by a factor $\frac{M_1}{2P}$, where P is the number of samples per symbol for the equalization process. In the OQAM_1 demodulator (part of Figure 5.2), the first operation is to de-rotate the signal on each sub-carrier. This de-rotation is done by multiplying the stream of the k^{th} AFB_1 output at time l by a factor $o_k^*(l)$, given by :

$$o_k^*(l) = j^{-\left(\frac{k+l}{P}\right)}. \tag{5.1}$$

After de-rotation, the resultant signal $y_k(l)$ corresponds to the equalizer input for the k^{th} sub-carrier branch. We note that the equalization process is done for each sub-carrier. The signals γ_k and $\hat{x}_k$ are the equalized signals before and after decision process, respectively. The decision process consists in taking the real part of $\gamma_k(n)$ before making the decision. It has to be noted that $\gamma_k(l)$ and $\gamma_k(n)$ are the same signal but with different rates ($\gamma_k(l)$ is sampled at $\frac{T_0}{P}$ and $\gamma_k(n)$ is sampled at T_0). The last operation consists in converting the real symbols $\hat{x}_k$ into complex ones $\hat{c}_k$, with a dual real-to-complex conversion $\mathbb{R}2\mathbb{C}$.

The underlying idea of de-rotating the AFB_1 output, is to transform the quasi-rectilinear system into a rectilinear one [84]. Therefore, we will, first, clarify this conversion (from quasi-rectilinear into rectilinear signal) by deriving an equivalent system model of the FBMC-OQAM trans-multiplexer (TMUX), resulting in the transmission of a $M-$PAM modulation. This study will be done for the case where only one user is transmitting. Indeed, we will first focus on the impact of the inter-carrier-interference of one user, which mainly comes from the adjacent sub-carriers. We will eventually study the performance of the MMSE-LE and MMSE-WLE used in the SSE mode.

5.2 Performance of MMSE-LE and MMSE-WLE for single user transmission

Since we focus here on the performance analysis of MMSE-LE and MMSE-WLE used in the SSE mode (where only one user is transmitting), we consider $P = 1$ and we ignore the signal transmitted by the second user (UNOI), see Figures 5.1 and 5.2. To do so, let us consider the following equations

$$g_k(m) = p_1(m)e^{j\frac{2\pi k}{M_1}(m-\frac{L_1-1}{2})}, \tag{5.2}$$

$$f_k(m) = g_k^*(L_1 - 1 - m). \tag{5.3}$$

$g_k(m)$ and $f_k(m)$ represent, respectively, the SFB and AFB for the k^{th} sub-carrier.

An equivalent model for the cascade of the SFB, the channel h and the AFB can be written as follows [23] :

$$q_{ji}(n) = (g_i \star h \star f_j)(m)_{\downarrow \frac{M_1}{2}}, \tag{5.4}$$

where $\star$ denotes the convolution operator and $g_i(m)$ and $f_j(m)$ represent the SFB and the AFB at the i^{th} and j^{th} sub-carrier, respectively.

Using the equivalent model presented in (5.4), the signal at the output of the AFB on the k^{th} sub-carrier can be given as :

$$r_k(n) = \sum_{i=0}^{M_1-1} q_{ki} \star v_i(n) + (b \star f_k(m))_{\downarrow \frac{M_1}{2}} \tag{5.5}$$

where

$$v_i(n) = \theta_i(n)x_i(n). \tag{5.6}$$

Also, we can model the filtered noise as the convolution of a Gaussian noise $b_1(n)$ with an equivalent filter $f_q(n)$, where

$$f_q(n) = \sqrt{\frac{M_1}{2}}\ (f_k(m))_{\downarrow \frac{M_1}{2}}. \tag{5.7}$$

With this filtered noise, (5.5) becomes

$$r_k(n) = \sum_{i=0}^{M_1-1} (q_{ki} \star v_i)(n) + (f_q \star b_1)(n). \tag{5.8}$$

We recall that the trans-multiplexer response of the FBMC-OQAM system given by Table 2.1 in Chapter 2, is the response given by the term q_{ji} when $h(m) = \delta(m)$. It also represents the interference table.

5.2.1 Equivalent M-PAM Model

On one hand, we can notice through Table 2.1 in Chapter 2 that the main interferences come from the immediately adjacent sub-carriers of the active one. This means that the index i in (5.5) can be limited to $[k-1, k, k+1]$. On the other hand, the OQAM modulation can be seen as the transmission of two M-PAM modulations on the same sub-carrier. Hence,

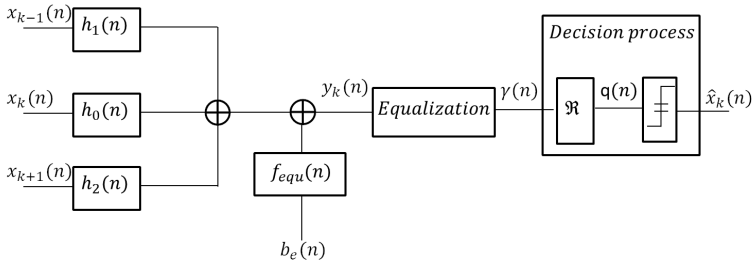

FIGURE 5.3: FBMC-OQAM equivalent system using only M-PAM modulations.

the FBMC-OQAM system for any given sub-carrier can be seen as the equivalent model shown in Figure 5.3.

In this Figure, the M-PAM signal on the k^{th} sub-carrier $x_k(n)$ is transmitted through the channel $h_0(n)$, and it is contaminated by two $M-$PAM interferences : $x_{k-1}(n)$ and $x_{k+1}(n)$ coming from the $k^{th}-1$ and $k^{th}+1$ sub-carriers, respectively. This reflects what can be seen in the interference table for a FBMC-OQAM trans-multiplexer. $h_1(n)$ and $h_2(n)$ represent the channel impulse responses of the interferences $x_{k-1}(n)$ and $x_{k+1}(n)$, respectively.

The expressions of $h_0(n), h_1(n)$, $h_2(n)$ and $f_{equ}(n)$ are obtained as follows. Note that L_q is the length of both q_{ki} and f_q. The received signal after de-rotation can be written as :

$$
\begin{aligned}
y_k(n) &= \theta_k^*(n)\, r_k(n) \qquad (5.9)\\
&= \theta_k^*(n) \left[\sum_{i=k-1}^{k+1} q_{ki} \star v_i(n) \right] + \theta_k^*(n) \left[f_q \star b_1(n) \right] \\
&= j^{-(k+n)} \left[\sum_{i=k-1}^{k+1} \sum_{l=0}^{L_q-1} q_{ki}(l) j^{(i+n-l)} x_i(n-l) \right] + j^{-(k+n)} \left[\sum_{l'=0}^{L_q-1} f_q(l') b_1(n-l') \right] \\
&= \sum_{l=0}^{L_q-1} \left[q_{k,k-1} j^{-(l+1)} x_{k-1}(n-l) \right] + \sum_{l=0}^{L_q-1} \left[q_{kk}(l) j^{-l} x_k(n-l) \right] \\
&+ \sum_{l=0}^{L_q-1} \left[q_{k,k+1} j^{-(l-1)} x_{k+1}(n-l) \right] + \sum_{l'=0}^{L_q-1} \left[j^{-(k+l')} f_q(l') b_1(n-l') j^{-(n-l')} \right] \\
&= \sum_{l=0}^{L_q-1} \left[h_0(l) x_k(n-l) + h_1(l) x_{k-1}(n-l) + h_2(l) x_{k+1}(n-l) \right] + \sum_{l'=0}^{L_q-1} f_{equ}(l') b_e(n-l')
\end{aligned}
$$

where $h_0(l) = j^{-l} q_{kk}(l), h_1(l) = j^{-(l+1)} q_{k,k-1}(l)$, $h_2(l) = j^{-(l-1)} q_{k,k+1}(l)$, $f_{equ}(l) = j^{-(k+l)} f_q(l)$, for $l = 0, .., L_q - 1$ and $b_e(n) = j^{-n} b_1(n)$ is still a Gaussian noise.

Finally, we get the equivalent received signal $y_k(n)$ at the k-th sub-carrier contaminated by the interference from the neighboring ones, given by

$$
y_k(n) = (h_0 \star x_k)(n) + (h_1 \star x_{k-1})(n) + (h_2 \star x_{k+1})(n) + f_{equ} \star b_e(n). \qquad (5.10)
$$

LE and WLE expressions

In this subsection, we develop expressions for linear and widely linear equalizers using the proposed FBMC-OQAM system model. We minimize the mean square error (MSE)

between the equalizer output signal (see Figure 5.3) and the transmitted one $x_k(n)$, which is expressed as follows [96]

$$MSE_\gamma = \mathbb{E}\left[|\gamma(n) - x_k(n-\Delta)|^2\right], \tag{5.11}$$

where Δ is the decision delay.

The equalizer length (L_e) is chosen so as to obtain the best compromise between performance and complexity. Let us consider the vector $\boldsymbol{y_k}(n)$, of length L_e given by $\boldsymbol{y_k}(n) = [y_k(n)\ y_k(n-1)\dots\ y_k(n-L_e+1)]^T$.

We recall that the expressions of both MMSE-LE and MMSE-WLE are given previously in Chapter 3 by, respectively, Eqs. (3.33) and (3.34). In our case, they are expressed as follows :

— MMSE-LE :

$$\boldsymbol{w_{LE}} = \boldsymbol{r}_{x\boldsymbol{y_k}}\boldsymbol{R}_{\boldsymbol{y_k}}^{-1}, \tag{5.12}$$

— MMSE-WLE :

$$\tilde{\boldsymbol{w}}_{\boldsymbol{WL}} = \boldsymbol{r}_{x\tilde{\boldsymbol{y}}_{\boldsymbol{k}}}\boldsymbol{R}_{\tilde{\boldsymbol{y}}_{\boldsymbol{k}}}^{-1}, \tag{5.13}$$

Regarding Figure 3.6 in chapter 3, the sub-equalizer $\boldsymbol{w_0}$ of the widely linear one expressed in Eq. (5.13) verifies also the following equation [83] :

$$\boldsymbol{w_0}^H = \left[\boldsymbol{R}_{\boldsymbol{y_k}} - \boldsymbol{C}_{\boldsymbol{y_k}}\boldsymbol{R}_{\boldsymbol{y_k}}{}^{-1*}\boldsymbol{C}_{\boldsymbol{y_k}}{}^*\right]^{-1}\left[\boldsymbol{s}_{x\boldsymbol{y_k}} - \boldsymbol{C}_{\boldsymbol{y_k}}\boldsymbol{R}_{\boldsymbol{y_k}}{}^{-1*}\boldsymbol{s}^*_{x\boldsymbol{y_k}}\right] \tag{5.14}$$

where $\boldsymbol{C}_{\boldsymbol{y_k}} = \mathbb{E}[\boldsymbol{y_k}(n)\boldsymbol{y_k}^T(n)]$ is the pseudo-covariance matrix of the signal $\boldsymbol{y_k}$.

Theoretical BER performance of LE and WLE equalizers in FBMC-OQAM systems

In order to show more insights on the developed widely linear processing scheme, in this subsection the performance of LE and WLE equalizers is analyzed in terms of BER. To facilitate the analysis, we consider Σ as the convolution between the channel h_0 and the equalizer ($\boldsymbol{w_{LE}}$ if LE chosen or $\boldsymbol{w_0}$ and $\boldsymbol{w_0}^*$ if WLE is considered). The lower efficiency of LE equalizer compared to the WLE one [14], which is related to the non-circularity of FBMC-OQAM signals, leads to a Σ with $N_c > 1$ non-null coefficients (i.e., the ISI still exist after equalization). Then, the filtered noise can not be necessarily considered as Gaussian distributed but the sum of N_c Gaussian laws. Thus, without loss of generality the BER expression for 2−PAM can be seen as the sum of 2^{N_c-1} Q−functions as shown by

$$BER_{\mathrm{LE}} = \frac{1}{2^{N_c-1}}\sum_{i=1}^{2^{N_c-1}} Q\left(\frac{\zeta_i}{\sqrt{\Sigma_0}}\right), \tag{5.15}$$

where $\Sigma_0 = \frac{1}{2}10^{\frac{-E_b/N_0}{10}} \times \sum_{j=1}^{L_e}(|\boldsymbol{w_{LE}}(i)|^2)$ and ζ_i are the positive values of the equalizer output when a M-PAM modulation is used.

Concerning the widely linear scheme, it is worth noticing that the residual ISI is negligible and the filtered noise can be represented as a Gaussian one. Thus, the BER expression is given by equation (5.15) with only one term for the sum and $\Sigma_{0,WL} = 10^{\frac{-E_b/N_0}{10}} \times \sum_{j=1}^{L_e}(|\boldsymbol{w_0}(i)|^2)$ instead of Σ_0.

5.2.2 Simulation Results

In this section, we evaluate the performance of the studied widely linear equalizer compared to the linear one, when considering or not interferer neighbors (adjacent sub-carriers). We set the equalizers length to $L_e = 3$. In order to validate our analytical study, theoretical results obtained with the equations presented in the previous section are compared to the ones obtained by simulations.

One tap deterministic flat channel ($h = 1$)

In order to compare the BER obtained when using WLE and LE for FBMC-OQAM signals, we consider a $4-$OQAM (which is equivalent to $\sqrt{4}-$PAM meaning a BPSK) modulation and a frame of 2×10^7 samples using $M_1 = 16$ sub-carriers. It is worth noticing that since the interference comes from the two neighboring sub-carriers, the number of total sub-carriers does not matter. We recall that the PHYDYAS prototype filter is considered with an overlapping factor of $K = 4$. In this subsection, we consider a one tap deterministic channel which is constant over the frame. Under these assumptions, Fig. 5.4 shows the evaluation of the BER at the output of the considered equalizers (LE and WLE) for three cases : (1) no interferer neighbor, (2) one interferer neighbor and (3) two interferer neighbors.
From these results, we can easily note a good agreement between analytical (5.15) and simulation results in all cases that validates our theoretical analysis. It is worth noticing that WLE outperforms the LE in the cases when no interferer neighbor and only one interferer neighbor is activated. This can be explained by the fact that WLE can efficiently suppress the negative impact of ISI in all cases, since it can take into account the imaginary part of the equivalent channel (Equation (5.4)) and then takes benefit from the information in the pseudo-autocorrelation matrix $\mathbf{C}_{\mathbf{y_k}}$. In contrast, with two interferer neighbors (i.e. the two adjacent sub-carriers are switched on) the performance of WLE and LE are similar. This is an unexpected and non-intuitive result. In this case, the interference coming from the two adjacent sub-carriers becomes very high and is totally orthogonal (imaginary) to the signal of interest. With such high imaginary interference, the number of LE taps (see Figure 5.5) tends to a single tap different from zero and all other taps equal to zero. This is due to an autocorrelation matrix close to an identity matrix. Moreover, a single real tap LE equalizer with an imaginary interference yields the performance of an AWGN channel.

Frequency Selective Channel

Figure 5.6 presents BER simulation results when h is a selective channel. h has been taken as $[\xi_1\, 0\, 0\, \xi_2]$, a 4 tap channel where ξ_1 and ξ_2 are two random variables with Rayleigh modulus distribution and a phase uniformly distributed between 0 and 2π. Results on Figure 5.6 are averaged over 500 random channels. Now, the ICI is no longer purely imaginary and we can see clearly the impact of the real ICI. When there are no active neighbors only ISI is present and WLE outperforms LE [96]. When there is one active neighbor, we have both ISI and one interferer. Here, WLE also performs better than LE because it is well known that WLE can suppress efficiently one interferer [14]. Finally, when we have two active neighbors, the performance gap between LE and WLE disappears because ICI cancellation

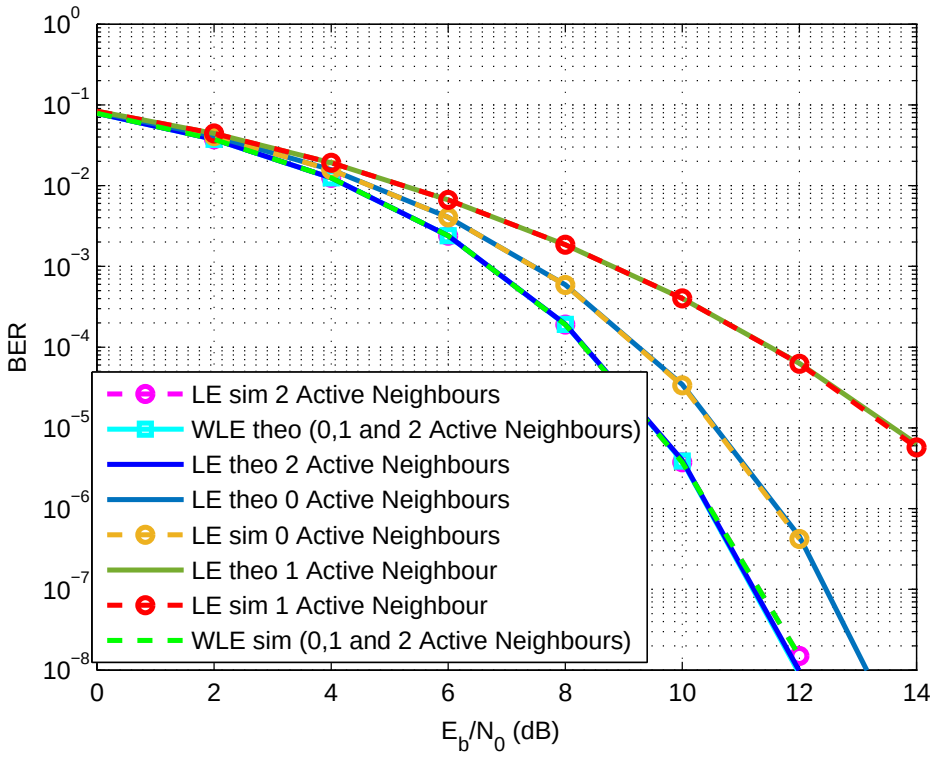

FIGURE 5.4: BER for $h = 1$ for single user transmission scenario.

is not possible anymore with two interferers.

5.3 Performance of linear, widely linear and WL-Fresh equalization in FBMC-OQAM with different Numerologies

After studying the performance of the classical equalizers (LE and WLE) in their SSE mode and in presence of ISI and ICI, we move now to study the impact of these interferences in addition to the inter-user-interference (IUI) coming from another user. Hence, at this stage, we aim to study the performance of linear (LE), widely linear (WLE) and widely linear Fresh (WL Fresh) equalizers in FBMC-OQAM system with two users. Motivated by the fact that the latter system has a well localized prototype filter (the PHYDYAS one) in the frequency domain, this leads the system to support asynchronous and mixed numerologies transmissions, which is very required in the upcoming wireless communication systems. Here, we adopt the FBMC based system model, with two different numerologies given in $2D$, Time/Frequency, as shown by Figure 5.7.

In Figure 5.7, we present a FBMC system having two users (UOI and UNOI) with QR modulation of the type OQAM, with eventually two different numerologies. The system with Numerology 1 is considered as the UOI and it has $M_1 = 64$ sub-carriers (SCs), whereas

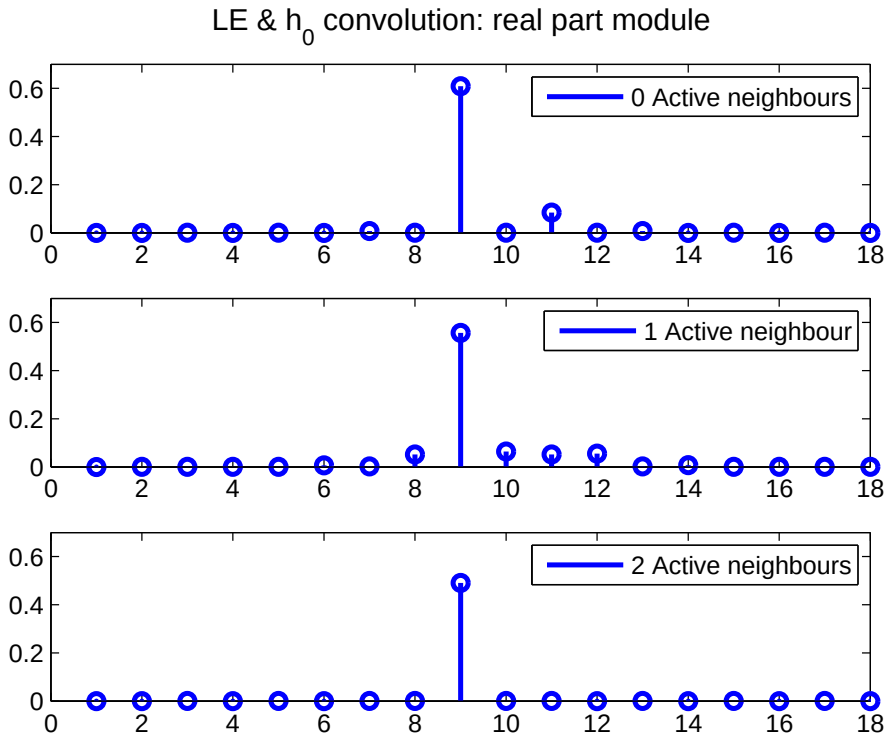

FIGURE 5.5: LE and equivalent channel convolution as a function of the number of active adjacent sub-carriers.

the second system (UNOI) with the second numerology has twice the number of UOI's sub-carriers, meaning $M_2 = 2 \times M_1 = 128$. Δt is the time shift between the two user signals, describing the asynchronism between the UNOI and UOI. If $\Delta t = 0$, the two users are synchronous, otherwise, they are transmitting asynchronously. δ_B denotes the guard band between the two users. The modulation is chosen to be $64-$OQAM. Note that the presented results are still valid for any $M-$OQAM modulation order. When using the WL Fresh equalizer, the SO non conjugate and conjugate cyclic frequencies used are given by :

$$\begin{cases} \alpha_1 = \dfrac{1}{T_1} \\ \beta_1 = 2\delta_B + \dfrac{1}{T_1}. \end{cases}$$

In the following, we study the performance of the FBMC-OQAM system in both the down-link (DL) and up-link (UL) cases.

Down-Link "DL" case

Since in the DL, the base station BS serves the two users synchronously, we consider that $\Delta t = 0$ in this case. First, we activate only 5 SCs for the UOI (using numerology #1) and 8 SCs for the UNOI (using numerology #2). δ_B is chosen to be equal to the one UOI sub-carrier spacing ($\delta_B = \dfrac{1}{M_1}$). We study how can the LE, WLE and WL Fresh equalizers,

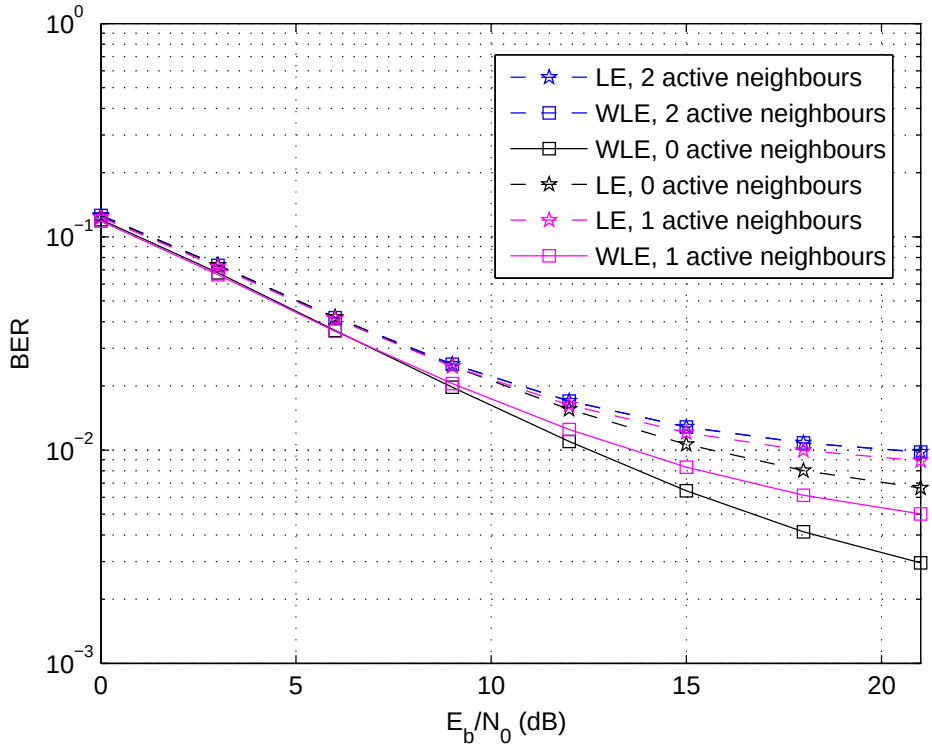

FIGURE 5.6: BER over a frequency selective channel for single user transmission scenario.

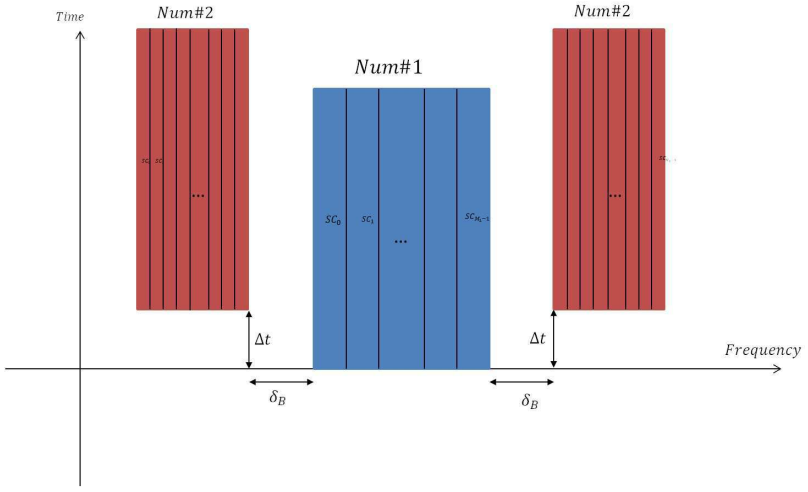

FIGURE 5.7: FBMC-OQAM systems with two numerologies.

in their SSE as well as FSE versions, perform to recover the UOI original symbols in presence of an adjacent UNOI using a different numerology. This performance is evaluated in terms of MSE. An ideal noiseless channel is considered, in order to clearly see the impact of the

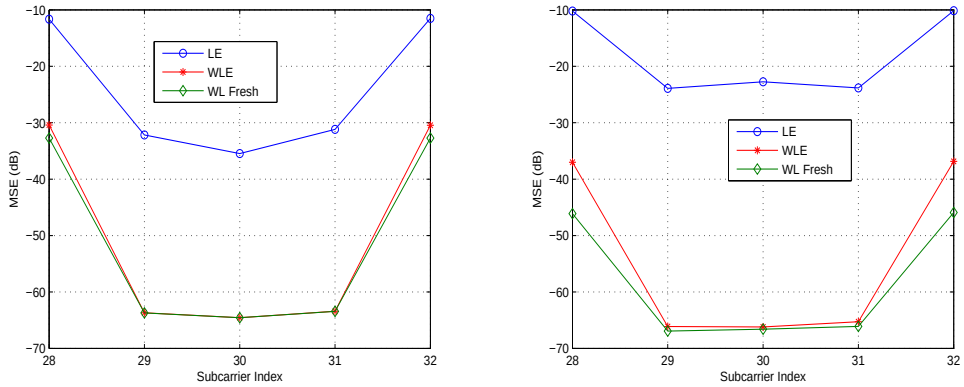

(a) $P = 1$ (b) $P = 8$

FIGURE 5.8: MSE performance versus UOI active sub-carriers over an ideal noiseless channel.

mixed numerologies on the different equalizers' performance. Results are depicted in Figure 5.8, where the performance of the different equalizers are given in terms of MSE for the two modes : SSE (Figure 5.8(a)) and FSE (Figure 5.8(b)). Sub-carriers 28 and 32 are the edge SCs of the UOI, while SC 30 is the middle one. Regarding these results, one can note that :

- The classical LE equalizer provides the worst performance, even for the sub-carriers in the middle of the band.
- WL Fresh outperforms the WLE when considering the sub-carriers in the edge of the band. We note about 2 dB and 6 dB of gain when $P = 1$ and 8, respectively.
- When the number of samples per symbol increases (in FSE mode), the performance of WLE and WL Fresh get better, while the LE one gets worse. It is worth mentioning that the gain between WL Fresh and WLE increases when P gets higher.
- In contrast to the classical LE equalizer, WLE and WL Fresh perform in the same way, providing excellent performance for the sub-carriers located in the middle of the band, enabling them to recover the performance of FBMC-OQAM over an ideal noiseless propagation channel.

We move now to study the performance of the considered equalizers under a realistic channel model, where new findings will be given. Since only the SCs in the edge of the band are affected, we have focused on the following simulations, on the impact of one UNOI SC on one UOI SC. Hence, we study the performance of the different equalizers in rejecting the interference, presented in the form of the near UNOI sub-carrier. We can model this by activating only one sub-carrier for User #1 and one SC for User #2 with $\Delta t = 0$ and with guard band equal to one UOI sub-carrier spacing. The channel in this case is chosen to be a frequency selective one. It is a FIR filter with 8 taps, which are chosen randomly. Thus, the BER performance of the SSE equalizers as well as the FSE equalizers are presented in Figures 5.9(a) and 5.9(b), respectively.

It is clear, from Figure 5.9, that the WL Fresh equalizer outperforms both the LE and WLE, whereas the worst behavior is provided by the LE. This is true for both SSE and FSE cases. Eventually, when P increases, the WLE and WL Fresh equalizers performance increases, and the WL Fresh gives always the best performance since it exploits the cyclo-stationarity properties of the signal.

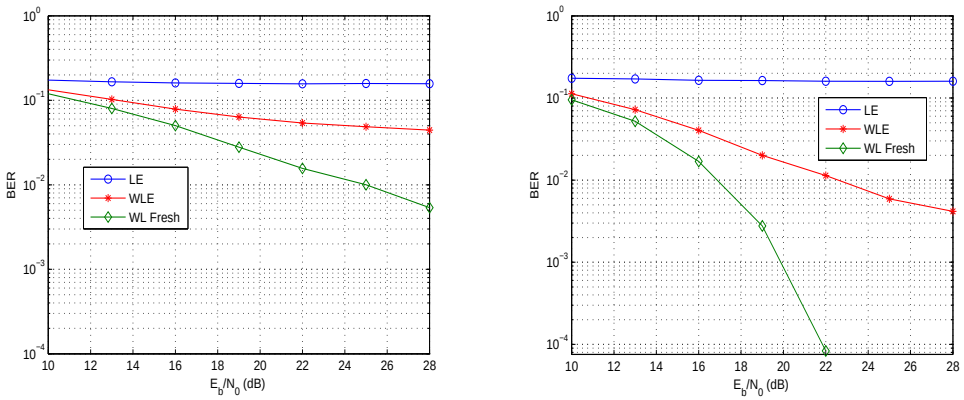

(a) $P = 1$ (b) $P = 8$

FIGURE 5.9: BER performance over a frequency selective channel.

Up-Link "UL" case

For the UL case, users are not necessarily synchronous in time. Thus, we will study the impact of this asynchronism as well as of the guard band on the system performance for LE, WLE and WL Fresh equalizers in their FSE version with $P = 8$.

As done in the DL case, we first activate the same 5 UOI SCs and the same 8 UNOI SCs. We study the impact of the δ_B on the MSE performance for the three equalizers. In a first test, we evaluate the MSE performance when the two users are synchronous (Figure 5.10) and the other results are given when the UNOI and UOI are transmitting asynchronously, which are presented in Figure 5.11. Without loss of generality, simulations of Figure 5.11, the asynchronism is half an UNOI symbol period $\left(\Delta t = \frac{T_1}{2}\right)$. In the two contexts, an ideal channel is considered in order to see the impact of mixed numerologies on the different equalizer behaviors.

Figures 5.10(a) and 5.11(a) show the performance of the classical linear equalizer for each active UOI sub-carrier in the synchronous $(\Delta t = 0)$ and asynchronous $\left(\Delta t = \frac{T_1}{2}\right)$ cases, respectively. In the same way, Figures 5.10(b) and 5.11(b) represent the behavior of the widely linear equalizer (WLE). Finally, the behavior of the WL Fresh equalizer is given in Figures 5.10(c) and 5.11(c).

From Figures 5.10 and 5.11, we can deduce that for all equalizer cases, only the SCs in the edge are affected by the interferer, in contrast to the SCs in the middle of the band. This remark remains true independently to the δ_B size as well as to the asynchronism time. Moreover, the WLE and the WL Fresh provide the same MSE performance when considering the SCs in the middle, which are equivalent to the ideal case.

When focusing on the SCs in the edge, we can see from the color degradation that the LE gives the worst performance in the two scenario cases (see Figures 5.10 and 5.11) when compared to the WLE and WL Fresh. Furthermore, an interesting and new finding can be deduced from Figure 5.10 : when the users are synchronous we can note a notch when the $\delta_B = \dfrac{3}{2T_1}$, where the performance of WLE and WL Fresh equalizers are very close. This can be explained by the fact that when $\delta_B = \dfrac{3}{2T_1}$ (related to the set of $\delta_B = \dfrac{i}{2T_1}$, where

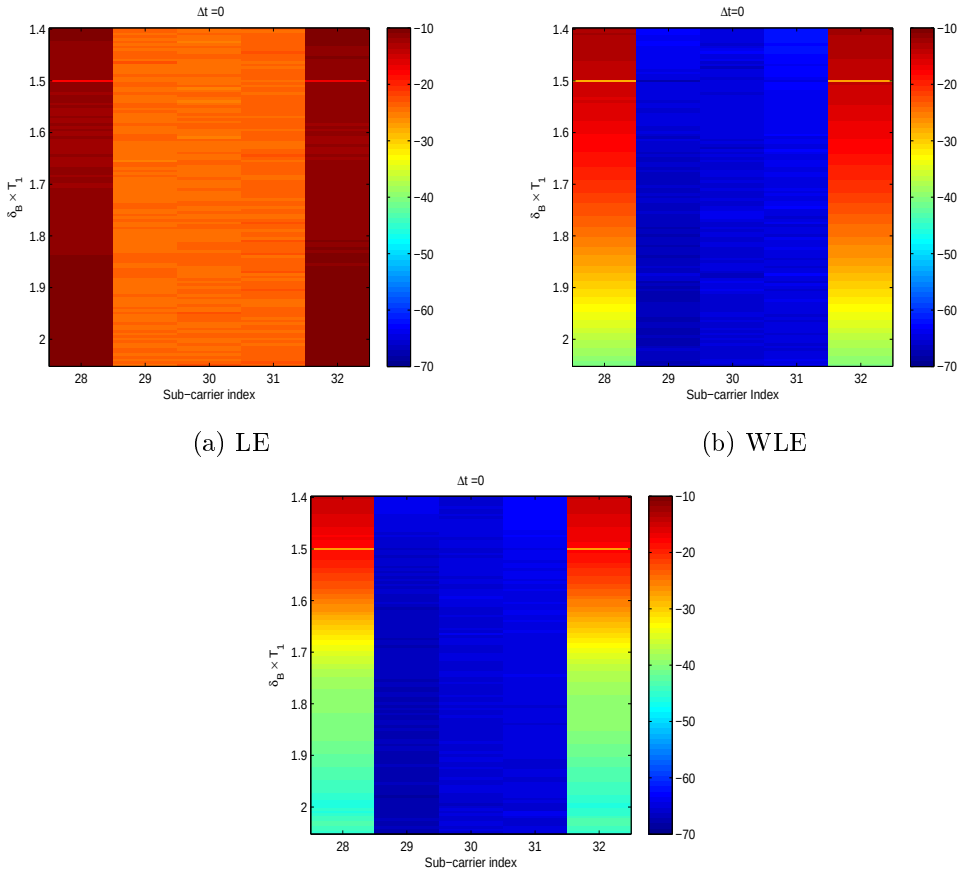

(a) LE

(b) WLE

(c) WL Fresh

FIGURE 5.10: Equalizers performances in term of MSE when UOI and UNOI are synchronous.

$i = 3 \in \mathbb{Z}$, the conjugate cyclic frequency is null ($\beta = 0$)) and since the WLE uses the information contained in ($\beta = 0$), the WLE gives the same performance as the WL Fresh. Besides, when the guard band is out of the notch, the WL Fresh outperforms the widely linear equalizer. It is noticeable that when the guard band δ_B is large, the two users are sufficiently spaced in the frequency domain, meaning while, the UNOI does not impact the UOI any more, so, the two widely linear equalizers give the same performance. This remains valid in the two contexts (synchronous as well as for the asynchronous cases). Moreover, when the two users are transmitting asynchronously (Figure 5.11), when $\delta_B = \frac{3}{2T_1}$, the notch might not be remarkable, the WLE and the WL Fresh provide the same performance.

Since only the sub-carriers in the edge of the band are affected, we have studied the impact, in terms of BER, of one UNOI SC on one active UOI SC over a frequency selective channel. The channel is a FIR filter with 8 taps chosen arbitrarily. Two scenarios are considered : synchronous ($\Delta t = 0$) and asynchronous $\left(\Delta t = \frac{T_1}{2}\right)$, with different guard band values : $\frac{3}{2T_1}$ (Figure 5.12), $\frac{1.7}{T_1}$ (Figure 5.13) and $\frac{2}{T_1}$ (Figure 5.14). The LE, WLE and WL Fresh are evaluated in their FSE version with $P = 8$.

We can see from the BER results that the classical linear equalizer has the worst per-

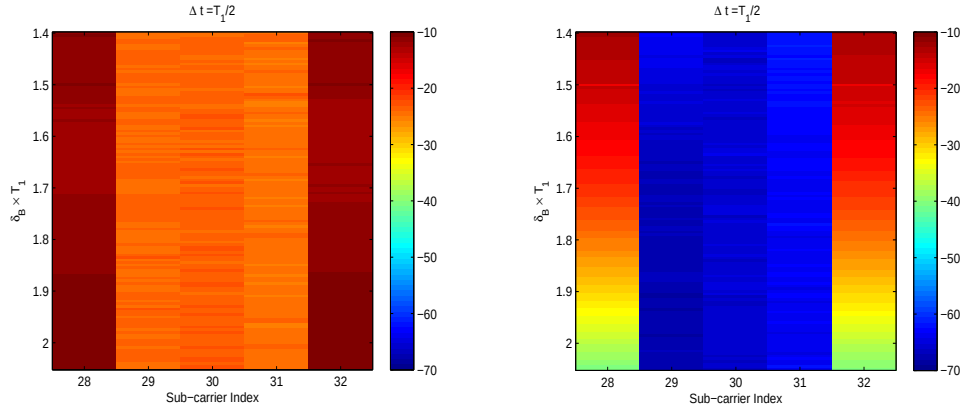

(a) LE

(b) WLE

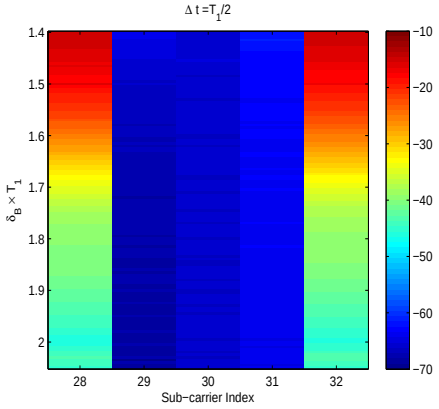

(c) WL Fresh

FIGURE 5.11: Equalizers performances in term of MSE when UNOI is asynchronous with half an UNOI symbol period.

formance. Besides, at $\delta_B = \frac{3}{2T_1}$ (Figures 5.12(a) and 5.12(b)), the widely linear and widely linear Fresh equalizers provide the same performance. A performance degradation is noted, in WLE and WL Fresh, when the two users are transmitting asynchronously.

When $\delta_B = \frac{1.7}{T_1}$ (Figure 5.13), the widely linear equalizer does not behave well and its performance is close to the classical LE, while the WL Fresh provides very good performance. We move now to the case where $\delta_B = \frac{2}{T_1}$ (Figure 5.14) where the classical WLE behaves better, but not as well as the performance of the WL Fresh equalizer. Here, it is possible to see that the WL Fresh equalizer provides the best performance, $\forall\ \delta_B$, for asynchronous and mixed numerologies transmissions.

5.4 Conclusion

During this chapter, we have studied the behavior of the LE, WLE and WL Fresh processes applied to FBMC-OQAM system. We have shown that the worst performance was given by the classical linear equalizer (LE), where its performance depends on the ICI.

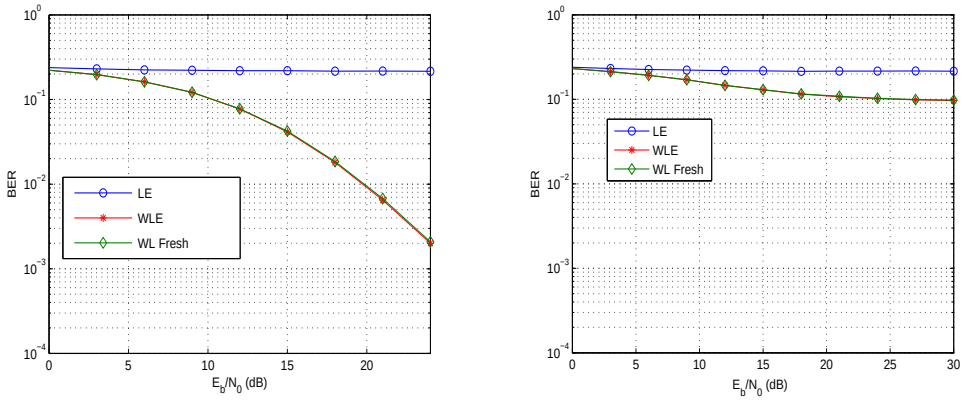

(a) Synchronous users (b) Asynchronous users

FIGURE 5.12: Equalizers performances in term of BER when $\delta_B = \dfrac{3}{2T_1}$

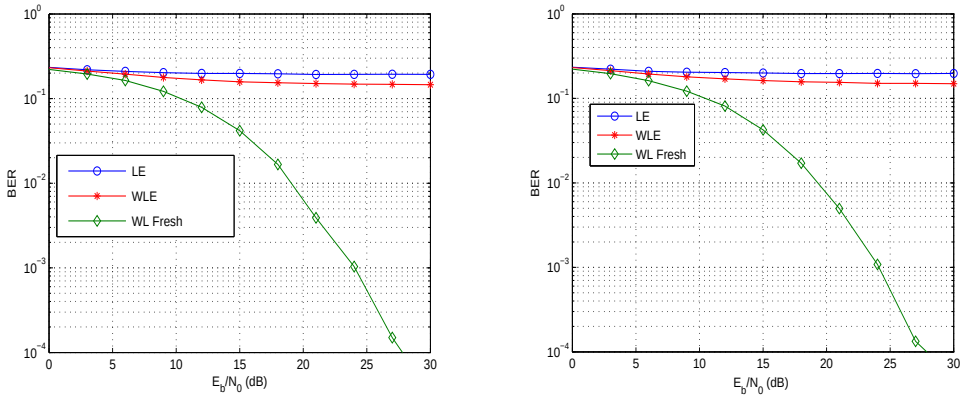

(a) Synchronous users (b) Asynchronous users

FIGURE 5.13: Equalizers performances in term of BER when $\delta_B = \dfrac{1.7}{T_1}$

Besides, since the used modulation is a NSOC one, we have shown that the widely linear processing outperforms the linear one. Furthermore, since the WL Fresh equalizer exploits the cyclo-stationarity concept of the transmitted signal, we have shown that it provides the best performance when compared to the classical ones. Moreover, with a FBMC-OQAM system using different numerologies where the UOI is corrupted by an interferer having different parameter settings, we have tested the performance of the different equalizers, in up-link and down-link scenarios. It has been shown that WL Fresh equalizer provides the best performance in synchronous and asynchronous scenarios, outperforming the classical Linear and WL equalizers.

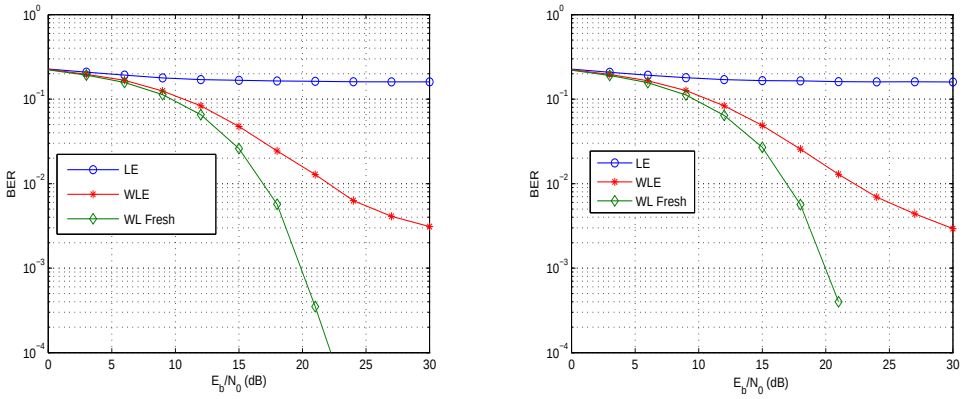

(a) Synchronous users (b) Asynchronous users

FIGURE 5.14: Equalizers performances in term of BER when $\delta_B = \frac{2}{T_1}$

Chapitre 6

Conclusions and Perspectives

6.1 Conclusions

This thesis has mainly focused on the equalization process applied over systems using non second order circular (NSOC) modulations. We have been interested in two types of the NSOC modulations. The first one is classified as the rectilinear modulation with the use of the $M-$ary pulse amplitude modulation ($M-$PAM). The second one is called quasi-rectilinear (QR) modulation representing the offset quadrature amplitude modulation (OQAM). This latter is used in filter bank multi-carrier (FBMC) system which is considered as a potential candidate for the 5G wireless communication systems. Indeed, FBMC-OQAM system, unlike the orthogonal frequency division multiplexing (OFDM) system which is widely adopted by the 4G system, owns one among the best frequency localization wave forms (WF). Besides, it has a good spectral efficiency which allows to support asynchronous and mixed numerologies transmissions. The idea behind studying the $M-$PAM modulation is the fact that the OQAM modulation can be seen as the transmission of two $M-$PAM flows modulated on the same sub-carrier (SC). On the other hand, it is known that the widely linear processing based equalizer applied for the $M-$PAM modulation outperforms the classical linear processing. Motivated by this fact, the main goal of this dissertation was to study different equalization schemes for FBMC-OQAM system.

Therefore, to do so, we first started by giving some background and concepts to be used throughout this thesis. Indeed, chapter 2 has been dedicated to describe some concepts, such as second order circularity (SOC), non second order circularity (NSOC), how to classify a modulation as SOC or NSOC, FBMC-OQAM and frequency selective channel model, which are useful for our study. Then, in chapter 3, we gave the definition of the stationarity concept where the signals can be classified according to this concept into stationary signals or non stationary ones. In case of non stationary transmitted signal, this latter can be cyclostationary. These signal second order (SO) properties have been studied in order to show how we can identify the most adequate equalization scheme. Indeed, the required equalization

process can be classified into either linear or widely linear process according to whether the transmitted signal is SOC or NSOC. It can be also classified into either FRESH process or not based on whether the signal is cyclo-stationary or stationary one. Besides, the linear (LE) and the widely linear equalizers (WLE) used in the FRESH version or the classical one can be applied in the symbol spaced mode (SSE) as well as the fractionally spaced one (FSE).

Chapter 4 and 5 have devoted for the contribution part. The equalization study has been done over rectilinear modulation in chapter 4 as well as over quasi-rectilinear one in chapter 5. Indeed, in chapter 4, we have studied the different described equalization processes over system using $M-$PAM modulation having K external interferences. In the first part, we have neglected the channel effect and have focused on the impact of the external interferences on the system performance. Results have showed that the widely linear equalizer can provide better performance compared to the linear equalizer and when the number of interferences increases, the equalizer's performance decreased and the widely linear equalizer still behave better. This out-performance of the WLE in the SSE mode has been also checked in presence of inter-symbol interferences (ISI) caused by the frequency selective channels. In the second part, we have tested, in addition to the classical equalizers, the Fresh ones used in both SSE and FSE modes. Indeed, we have analyzed the behavior of the aforementioned equalizers in a down-link (DL) transmission : for a system having two users (a primer user (PU) and a secondary user (SU)) transmitting rectilinear signals. We have shown the outperformance of the Fresh equalizers when compared to the classical ones in both studied modes (SSE and FSE) since the Fresh equalizer exploits the cyclo-stationarity properties of the transmitted signal. We have also tested the impact of the SSE/FSE processing and the impact of the guard band between the PU and the SU. We have presented new and original results elaborated in the form of existence of notches where the MSE performances of the widely linear equalizers, for both classical and Fresh processing, increases noticeably for particular guard band values. This is related to the fact that for these particular guard band values, the conjugate second order cyclic frequencies are equal to zeros, in which the maximum spectral energy exists. Besides, regarding the performance of the SSE and FSE processing, we have evaluated the impact of the number of samples per symbol on the equalization process where we have shown that the performance is enhanced by increasing the number of samples per symbol, i.e., the FSE outperforms the SSE processing.

Chapter 5 concerns the study of the different aforementioned equalization processes (linear, widely linear and Fresh equalizers) applied over the multi-carrier based filter bank (FBMC) system using the quasi-rectilinear modulation OQAM with mixed numerologies transmission. First, we have studied the performance of the classical linear and widely linear equalizers applied in the SSE mode in the presence of only ICI and/ or ISI. We have derived an equivalent system model used $M-$PAM modulation for one numerology transmission, i.e., for one single user. We have shown the dependence of the linear processing on the number of the adjacent active sub-carriers, where the widely linear equalizer behaves better than the linear one. Then, for one PU corrupted by a SU having a different numerology, we have tested the performance of LE, WLE and WL-Fresh equalizers, eventually in both SSE and FSE processing. The studied equalization processes have been tested in both up-link (UL) and down-link (DL) scenarios with synchronous transmission and also asynchronous UL transmission case. Thus, for all scenario cases, we have shown that the classical linear

equalizer has the worst performance whereas the best one is given by the Fresh equalizer and that is related to the exploitation of the cyclo-stationarity properties of the FBMC-OQAM signal. In addition, we have confirmed the outperformance of the widely linear process when compared to the linear one when using a quasi-rectilinear modulation. Besides, as done for the rectilinear case in chapter 4, we have done a comparison of the SSE and FSE process and have shown that the fractionally spaced equalization behaves better than the symbol spaced equalization process. Besides, as function of the guard band between the PU also called user of interest (UOI) and the SU also called user of non interest (UNOI), we have evaluated the performance provided by the different equalization processes : the LE, WLE and WL-Fresh, where we have shown the existence of notches in some particular guard band values indicating a better behavior of the widely linear process based equalizers (WLE and WL Fresh).

6.2 Perspectives

This PhD thesis has dealt with equalization applied to non second order circular signals of type, respectively, rectilinear (using the $M-$PAM) and quasi-rectilinear (with the use of the OQAM modulation).

Most of the equalization filters, proposed in this dissertation, are based on the minimization of the mean squared error (MSE) criterion between the transmitted symbols and the equalized ones and are thus of discrete time type. The performance achieved by the MSE based equalizers, could be compared to that achieved by the quasi-optimal continuous time-domain filters, derived in [24], which are based on the Maximum Likelihood (ML) criterion. Particularly, it would be interesting to compare the performance of the MMSE WL Fresh receivers, proposed in chapter 5, to that achieved by the pseudo-ML receivers, proposed in [24], when varying the sampling frequency and/or the equalizers lengths. This comparison should consider the complexity gain achieved thanks to the MMSE approach.

Furthermore, we have focused on the study of the capability of WL and WL Fresh equalizers to handle signal antenna interference cancellation of one/multiple rectilinear or quasi-rectilinear co-channel interferences. Despite the good performance provided by these studied equalizers, they still require enhancements, especially for quasi-rectilinear signals. In this regard, a new approach has been recently proposed, called third-order complex Volterra (CV) filtering [25, 26], that exploits both the non-circularity and the Gaussianity of the signals up to the sixth order [27]. Therefore, it would be of paramount importance to study the performance of FBMC-OQAM systems where the receiver is based on the third-order CV filtering instead of WL/WL Fresh one.

In Chapter 4, we have developed analytical expressions for both linear and widely linear equalizers performance, in a system using $M-$PAM modulation with the presence of K external interferers. The equalization process was elaborated in the SSE/FSE modes with assumption of perfect channel state information (CSI). However, the CSI may be hard to obtain in wireless systems. Therefore, as a future work, it would be important to study the performance of the studied WL/WL Fresh equalizers when imperfect CSI is occurred.

All the equalization schemes, proposed for FBMC-OQAM system, assume no mismatch between the OQAM transmitted symbols. This is equivalent to saying that the radio fre-

quency (RF) part of the FBMC-OQAM transceiver shows no I/Q imbalance. In practice and in order to develop inexpensive multi-carrier transceivers, zero-IF (intermediate Frequency) receivers could be very appealing, because they avoid costly IF filters [28]. However, these receivers could imply IQ demodulation at RF, which therefore cannot be done digitally and thus introduces IQ mismatch. Thus, it could be interesting to extend the study of the performance of the different equalizers (linear, widely linear and widely linear Fresh), proposed for the FBMC-OQAM system, to a scenario including I/Q imbalance.

In this dissertation, only single input single output (SISO) system has been considered. It will be of paramount of importance to study the performance of the studied equalizers in FBMC-OQAM based multiple input multiple output (MIMO) systems.

Recently, we can notice an increasing interest towards UAV (Unmanned Autonomous Vehicles) for services like remote sensing for earth observation (border surveillance, buildings and bridges inspections...), remote sensing for communications (in case of natural disasters for instance), as well as goods delivery, etc. For the communication link, between the UAV and the ground (or the satellite in case of areas with no terrestrial radio communication network), modulations with Continuous Phase Modulation (CPM) have been standardized for the terrestrial link [29]. Using the same modulation for the satellite link is also planned because CPM are known to be robust to the non-linear impairments due to High Power Amplifiers. CPM can be seen, thanks to the Laurent approximation [30], as the sum of several $M-$PAM signals. In case of a selective fading channel, widely linear equalization could be applied in this context.

Bibliographie

[1] "Number of smartphone users in the united states from 2010 to 2023 (in millions), statista 2019.," .

[2] "5g and beyond waveforms," in *2017 24th International Conference on Telecommunications (ICT)*, May 2017, pp. 1–42.

[3] Zekeriyya Esat Ankarali, Berker Peköz, and Hüseyin Arslan, "Flexible radio access beyond 5g : a future projection on waveform, numerology, and frame design principles," *IEEE Access*, vol. 5, pp. 18295–18309, 2017.

[4] Hmaied Shaiek, Rafik Zayani, Yahia Medjahdi, and Daniel Roviras, "Analytical analysis of ser for beyond 5g post-ofdm waveforms in presence of high power amplifiers," *IEEE Access*, vol. 7, pp. 29441–29452, 2019.

[5] Ali Fatih Demir, Mohamed Elkourdi, Mostafa Ibrahim, and Huseyin Arslan, "Waveform design for 5g and beyond," *arXiv preprint arXiv :1902.05999*, 2019.

[6] Rafik Zayani, Hmaied Shaiek, Xinying Cheng, Xiaotian Fu, Christophe Alexandre, and Daniel Roviras, "Experimental testbed of post-ofdm waveforms toward future wireless networks," *IEEE Access*, vol. 6, pp. 67665–67680, 2018.

[7] Mohamed Elkourdi, Berker Peköz, Ertuğrul Güvenkaya, and Hüseyin Arslan, "Waveform design principles for 5g and beyond," in *2016 IEEE 17th Annual Wireless and Microwave Technology Conference (WAMICON)*. IEEE, 2016, pp. 1–6.

[8] Qualcomm Technologies, "5g waveform & multiple access techniques," 2015.

[9] Xiaoying Zhang, Lei Zhang, Pei Xiao, Dongtang Ma, Jibo Wei, and Yu Xin, "Mixed numerologies interference analysis and inter-numerology interference cancellation for windowed ofdm systems," *IEEE Transactions on Vehicular Technology*, vol. 67, no. 8, pp. 7047–7061, 2018.

[10] M. Bellanger, "Physical layer for future broadband radio systems," in *2010 IEEE Radio and Wireless Symposium (RWS)*, Jan 2010, pp. 436–439.

[11] Y. Medjahdi, M. Terre, D. Le Ruyet, D. Roviras, J. A. Nossek, and L. Baltar, "Inter-cell interference analysis for ofdm/fbmc systems," in *2009 IEEE 10th Workshop on Signal Processing Advances in Wireless Communications*, June 2009, pp. 598–602.

[12] Jean Pierre Delmas and Habti Abeida, "Asymptotic distribution of circularity coefficients estimate of complex random variables," *Signal Processing*, vol. 89, no. 12, pp. 2670–2675, 2009.

[13] Jan Eriksson and Visa Koivunen, "Complex random vectors and ica models : Identifiability, uniqueness, and separability," *IEEE Transactions on Information theory*, vol. 52, no. 3, pp. 1017–1029, 2006.

[14] Pascal Chevalier and François Pipon, "New insights into optimal widely linear array receivers for the demodulation of bpsk, msk, and gmsk signals corrupted by noncircular interferences-application to saic," *IEEE Transactions on Signal Processing*, vol. 54, no. 3, pp. 870–883, 2006.

[15] Richard van Nee and Ramjee Prasad, *OFDM for wireless multimedia communications*, Artech House, Inc., 2000.

[16] Mérouane Debbah, "Short introduction to ofdm," *White Paper, Mobile Communications Group, Institut Eurecom*, pp. 0–1, 2004.

[17] Ari Viholainen, Maurice Bellanger, and Mathieu Huchard, "of deliverable prototype filter and structure optimization," *Criterion*, vol. 1, pp. C2, 2009.

[18] Maurice G Bellanger, "Specification and design of a prototype filter for filter bank based multicarrier transmission," in *icassp*. Citeseer, 2001, vol. 1, pp. 2417–2420.

[19] Thomas W Parks and C Sidney Burrus, *Digital filter design*, Wiley-Interscience, 1987.

[20] Theodore Rappaport, *Wireless Communications : Principles and Practice*, Prentice Hall PTR, Upper Saddle River, NJ, USA, 2nd edition, 2001.

[21] Hamid Jafarkhani, *Space-time coding : theory and practice*, Cambridge university press, 2005.

[22] William A Gardner, "Cyclic wiener filtering : theory and method," *IEEE Transactions on communications*, vol. 41, no. 1, pp. 151–163, 1993.

[23] Aissa Ikhlef and Jérôme Louveaux, "An enhanced mmse per subchannel equalizer for highly frequency selective channels for fbmc/oqam systems," in *2009 IEEE 10th Workshop on Signal Processing Advances in Wireless Communications*. IEEE, 2009, pp. 186–190.

[24] Rémi Chauvat, *Etude de liaisons SISO, SIMO, MISO et MIMO à base de formes d'ondes FBMC-OQAM et de récepteurs Widely Linear*, Ph.D. thesis, Paris, CNAM, 2017.

[25] P. Chevalier, J. Delmas, and M. Sadok, "Third-order volterra mvdr beamforming for non-gaussian and potentially non-circular interference cancellation," *IEEE Transactions on Signal Processing*, vol. 66, no. 18, pp. 4766–4781, Sep. 2018.

[26] P. Chevalier, J. P. Delmas, and M. Sadok, "Performance of a third-order volterramvdr-beamformer in the presence of non-gaussian and/or non-circular interference," in *2018 26th European Signal Processing Conference (EUSIPCO)*, Sep. 2018, pp. 807–811.

[27] B. Picinbono, "On circularity," *IEEE Transactions on Signal Processing*, vol. 42, no. 12, pp. 3473–3482, Dec 1994.

[28] Jan Tubbax, Boris Côme, Liesbet Van der Perre, Luc Deneire, Stéphane Donnay, and Marc Engels, "Compensation of iq imbalance in ofdm systems," in *IEEE International Conference on Communications, 2003. ICC'03.* IEEE, 2003, vol. 5, pp. 3403–3407.

[29] RTCA (Firm). SC-228, *Command and Control (C2) Data Link Minimum Operational Performance Standards (MOPS)(terrestrial)*, RTCA, Incorporated, 2016.

[30] Pierre Laurent, "Exact and approximate construction of digital phase modulations by superposition of amplitude modulated pulses (amp)," *IEEE transactions on communications*, vol. 34, no. 2, pp. 150–160, 1986.

[31] A. A. Zaidi, R. Baldemair, H. Tullberg, H. Bjorkegren, L. Sundstrom, J. Medbo, C. Kilinc, and I. Da Silva, "Waveform and numerology to support 5g services and requirements," *IEEE Communications Magazine*, vol. 54, no. 11, pp. 90–98, November 2016.

[32] Qualcomm Inc., "Waveform requirements," in *3GPP Standard Contribution (R1-162198)*, April 2016.

[33] Xi Zhang, Lei Chen, Jing Qiu, and Javad Abdoli, "On the waveform for 5g," *IEEE Communications Magazine*, vol. 54, no. 11, pp. 74–80, 2016.

[34] Huawei, HiSilicon, "5g waveform : requirements and design principles," in *3GPP Standard Contribution (R1-162151)*, April 2016.

[35] H. Chen, J. Hua, F. Li, F. Chen, and D. Wang, "Interference analysis in the asynchronous f-ofdm systems," *IEEE Transactions on Communications*, pp. 1–1, 2019.

[36] Ahmad Nimr, Marwa Chafii, Maximilian Matthé, and Gerhard Fettweis, "Extended gfdm framework : Otfs and gfdm comparison," in *2018 IEEE Global Communications Conference (GLOBECOM)*. IEEE, 2018, pp. 1–6.

[37] M. Towliat and S. M. J. Asgari Tabatabaee, "Gfdm interference mitigation without noise enhancement," *IEEE Communications Letters*, vol. 22, no. 5, pp. 1042–1045, May 2018.

[38] R. Zayani, Y. Medjahdi, H. Shaiek, and D. Roviras, "Wola-ofdm : A potential candidate for asynchronous 5g," in *2016 IEEE Globecom Workshops (GC Wkshps)*, Dec 2016, pp. 1–5.

[39] Bernard Picinbono, "On circularity," *IEEE Transactions on signal processing*, vol. 42, no. 12, pp. 3473–3482, 1994.

[40] Pierre Comon, "Circularité et signaux aléatoires à temps discret," 1994.

[41] Jonathan F Adlard, *Frequency shift filtering for cyclostationary signals.*, Ph.D. thesis, University of York, 2000.

[42] Abdelkader Oukaci, *Beamforming et détection pour signaux non circulaires et/ou non gaussiens (algorithmes et performance)*, Ph.D. thesis, Evry, Institut national des télécommunications, 2010.

[43] Khalid El-Darymli, Cecilia Moloney, Eric Gill, Peter McGuire, and Desmond Power, "On circularity/noncircularity in single-channel synthetic aperture radar imagery," in *2014 Oceans-St. John's*. IEEE, 2014, pp. 1–4.

[44] Peter J Schreier, "Bounds on the degree of impropriety of complex random vectors," *IEEE Signal Processing Letters*, vol. 15, pp. 190–193, 2008.

[45] Bernard Picinbono and Pascal Bondon, "Second-order statistics of complex signals," *IEEE Transactions on Signal Processing*, vol. 45, no. 2, pp. 411–420, 1997.

[46] Rafael Boloix-Tortosa, F Javier Payán-Somet, Eva Arias-de Reyna, and Juan José Murillo-Fuentes, "Complex kernels for proper complex-valued signals : A review," in *2015 23rd European Signal Processing Conference (EUSIPCO)*. IEEE, 2015, pp. 2371–2375.

[47] Jitendra K Tugnait, "Multisensor detection of improper signals in improper noise," in *2017 IEEE International Conference on Acoustics, Speech and Signal Processing (ICASSP)*. IEEE, 2017, pp. 3939–3943.

[48] Peter J Schreier and Louis L Scharf, "The karhunen-loeve expansion of improper complex random signals with applications in detection," in *2003 IEEE International Conference on Acoustics, Speech, and Signal Processing, 2003. Proceedings.(ICASSP'03)*. IEEE, 2003, vol. 6, pp. VI–717.

[49] Hayfa Fhima, Hmaied Shaïek, Rafik Zayani, Daniel Roviras, Bruno Sens Chang, and Ridha Bouallegue, "Analysis of widely linear equalization over frequency selective channels with multiple interferences," in *2018 14th International Conference on Wireless and Mobile Computing, Networking and Communications (WiMob)*. IEEE, 2018, pp. 83–88.

[50] Malek Messai, *Application des signaux CPM pour la collecte de données à grande échelle provenant d'émetteurs faible cout*, Ph.D. thesis, 2015.

[51] Ridha Chaggara, Gerard Maral, Francis Castanié, Jean-François Helard, Daniel Roviras, Marie-Laure Boucheret, Caroline Bazile, and Jean-Didier Gayrard, *Les modulations à phase continue pour la conception d'une forme d'onde adaptative : applications aux futurs systèmes multimédia par satellite en bande Ka*, Ph.D. thesis, École nationale supérieure des télécommunications, 2005.

[52] Philippe Gournay and Philippe Viravau, "Corrélation spectrale théorique des modulations cpm partie i : résultat analytique pour les modulations cpfsk à 2 états (1-rec)," in *Annales des télécommunications*. Springer, 1998, vol. 53, pp. 267–278.

[53] Mustapha Sadok, *Exploitation de la non-circularité pour les transmissions et l'écoute passive*, Ph.D. thesis, Evry, Institut national des télécommunications, 2017.

[54] Yahia Medjahdi, Sylvain Traverso, Robin Gerzaguet, Hmaied Shaiek, Rafik Zayani, David Demmer, Rostom Zakaria, Jean-Baptiste Doré, Mouna Ben Mabrouk, Didier Le Ruyet, et al., "On the road to 5g : Comparative study of physical layer in mtc context," *IEEE Access*, vol. 5, pp. 26556–26581, 2017.

[55] Pierre Siohan, Cyrille Siclet, and Nicolas Lacaille, "Analysis and design of ofdm/oqam systems based on filterbank theory," *IEEE transactions on signal processing*, vol. 50, no. 5, pp. 1170–1183, 2002.

[56] Sri Satish Krishna Chaitanya Bulusu, *Performance analysis and PAPR reduction techniques for filter-bank based multi-carrier systems with non-linear power amplifiers*, Ph.D. thesis, 2016.

[57] Bernard Le Floch, Michel Alard, and Claude Berrou, "Coded orthogonal frequency division multiplex [tv broadcasting]," *Proceedings of the IEEE*, vol. 83, no. 6, pp. 982–996, 1995.

[58] "http ://www.ict-phydyas.org," .

[59] Hayfa Fhima, Bruno Sens Chang, Rafik Zayani, Hmaied Shaiek, Daniel Roviras, and Ridha Bouallegue, "Performance of linear and widely linear equalizers for fbmc/oqam modulation," in *2018 25th International Conference on Telecommunications (ICT)*. IEEE, 2018, pp. 605–609.

[60] Simon R Saunders and Alejandro Aragón-Zavala, *Antennas and propagation for wireless communication systems*, John Wiley & Sons, 2007.

[61] Sofiane Maiz, *Estimation and detection of cyclostationary signals by the mean of statistical resampling methods : applications to the analysis of biomechanical signals*, Theses, Ecole Nationale Supérieure des Mines de Saint-Etienne, Dec. 2014.

[62] Nathanaël Perraudin and Pierre Vandergheynst, "Stationary signal processing on graphs," *IEEE Transactions on Signal Processing*, vol. 65, no. 13, pp. 3462–3477, 2017.

[63] Feng Liu, Xin Zhang, Ran Tao, and Yue Wang, "Cyclo-period estimation for poly-cyclostationary signals," in *2008 4th International Conference on Wireless Communications, Networking and Mobile Computing*. IEEE, 2008, pp. 1–4.

[64] Jiandong Wang, Tongwen Chen, and Biao Huang, "Cyclo-period estimation for discrete-time cyclo-stationary signals," *IEEE transactions on signal processing*, vol. 54, no. 1, pp. 83–94, 2005.

[65] Esha D Nerurkar, Stergios I Roumeliotis, and Agostino Martinelli, "Distributed maximum a posteriori estimation for multi-robot cooperative localization," in *2009 IEEE International Conference on Robotics and Automation*. IEEE, 2009, pp. 1402–1409.

[66] Wenze Xi and Tulay Adali, "Integrated maximum a posteriori (map) and turbo product coding for optical communications systems," Dec. 21 2006, US Patent App. 11/471,717.

[67] Yvon Sosthène Yameogo, *Etudes de nouvelles techniques d'estimation et d'égalisation de canal adaptées au systéme SC-FDMA*, Ph.D. thesis, 2011.

[68] Rabindra Nath Bhattacharya and Edward C Waymire, *A basic course in probability theory*, vol. 69, Springer, 2007.

[69] Monisha Ghosh and Charles L Weber, "Maximum-likelihood blind equalization," *Optical Engineering*, vol. 31, no. 6, pp. 1224–1229, 1992.

[70] Abdessalem Trimeche, Nesrine Boukid, Anis Sakly, and Abdellatif Mtibaa, "Performance analysis of zf and mmse equalizers for mimo systems," in *7th International Conference on Design & Technology of Integrated Systems in Nanoscale Era*. IEEE, 2012, pp. 1–6.

[71] Yanwu Ding, Timothy N Davidson, Zhi-Quan Luo, and Kon Max Wong, "Minimum ber block precoders for zero-forcing equalization," *IEEE Transactions on Signal Processing*, vol. 51, no. 9, pp. 2410–2423, 2003.

[72] Peter Kabal, "The stability of adaptive minimum mean square error equalizers using delayed adjustment," *IEEE transactions on Communications*, vol. 31, no. 3, pp. 430–432, 1983.

[73] N Sathish Kumar and KR Shankar Kumar, "Performance analysis of m* n equalizer based minimum mean square error (mmse) receiver for mimo wireless channel," *International Journal of Computer Applications*, vol. 16, no. 7, pp. 47–50, 2011.

[74] W. Suleiman, P. Parvazi, M. Pesavento, and A. M. Zoubir, "Non-coherent direction-of-arrival estimation using partly calibrated arrays," *IEEE Transactions on Signal Processing*, vol. 66, no. 21, pp. 5776–5788, Nov 2018.

[75] A. Wielgus, W. Magiera, and P. Smagowski, "Efficiency of the multidimensional schur-type estimation algorithms for higher-order stochastic processes," in *2018 IEEE 23rd International Conference on Digital Signal Processing (DSP)*, Nov 2018, pp. 1–5.

[76] A. Wielgus, W. Magiera, and P. Smagowski, "Efficiency of the nonlinear schur-type estimation algorithms for higher-order stochastic processes," in *2018 International Conference on Signals and Electronic Systems (ICSES)*, Sep. 2018, pp. 172–176.

[77] John G Proakis and Masoud Salehi, *Digital communications*, vol. 4, McGraw-hill New York, 2001.

[78] John R Treichler, I Fijalkow, and CR Johnson, "Fractionally spaced equalizers," *IEEE signal processing magazine*, vol. 13, no. 3, pp. 65–81, 1996.

[79] Zijing Zhang, Linrang Zhang, and Penglang Shui, "Fractionally spaced equalizer based on multichannel linear prediction," in *Proceedings of the IEEE 6th Circuits and Systems Symposium on Emerging Technologies : Frontiers of Mobile and Wireless Communication (IEEE Cat. No. 04EX710)*. IEEE, 2004, vol. 2, pp. 393–396.

[80] Mohammad Reza Heidarpour, Murat Uysal, and Mohamed Oussama Damen, "Design and analysis of broadband amplify-and-forward cooperative systems : A fractionally-spaced sampling approach," *IEEE Transactions on Signal Processing*, vol. 64, no. 19, pp. 4936–4951, 2016.

[81] Sarvraj Singh Ranhotra and Amit Mishra, "On the performance of fractionally spaced and constant modulus equalizer," in *2015 IEEE International Conference on Computational Intelligence & Communication Technology*. IEEE, 2015, pp. 627–631.

[82] H. Fhima, R. Zayani, H. Shaiek, D. Roviras, B. S. Chang, and R. Bouallegue, "Widely linear equalizer performance with multiple independent interferences," in *2017 IEEE Symposium on Computers and Communications (ISCC)*, July 2017, pp. 912–917.

[83] Bernard Picinbono and Pascal Chevalier, "Widely linear estimation with complex data," *IEEE transactions on Signal Processing*, vol. 43, no. 8, pp. 2030–2033, 1995.

[84] Pascal Chevalier, Jean-Pierre Delmas, and Rémi Chauvat, "Reception filter impact on widely linear fresh receiver performance for saic/maic with frequency offsets," in *2016 IEEE Sensor Array and Multichannel Signal Processing Workshop (SAM)*. IEEE, 2016, pp. 1–5.

[85] Rémi Chauvat, Pascal Chevalier, and Jean-Pierre Delmas, "Widely linear fresh receiver for saic/maic with frequency offsets," in *2015 International Symposium on Wireless Communication Systems (ISWCS)*. IEEE, 2015, pp. 536–540.

[86] R. Dayana and R. Kumar, "Co-operative cyclo-stationary feature detection with universal filtered multi-carrier spectrum sensing for cognitive radio network," in *2016 IEEE International Conference on Recent Trends in Electronics, Information Communication Technology (RTEICT)*, May 2016, pp. 1647–1650.

[87] V. Lazov and G. Vandersteen, "Cyclo-stationary process analysis within telecom applications," in *2016 IEEE International Instrumentation and Measurement Technology Conference Proceedings*, May 2016, pp. 1–6.

[88] Daiming Qu, Shixian Lu, and Tao Jiang, "Multi-block joint optimization for the peak-to-average power ratio reduction of fbmc-oqam signals," *IEEE transactions on signal processing*, vol. 61, no. 7, pp. 1605–1613, 2013.

[89] Hanen Bouhadda, *Impacts des non-linéarités dans les systèmes multi-porteuses de type FBMC-OQAM*, Ph.D. thesis, 2016.

[90] Yao Cheng and Martin Haardt, "Widely linear processing in mimo fbmc/oqam systems," in *ISWCS 2013; The Tenth International Symposium on Wireless Communication Systems*. VDE, 2013, pp. 1–5.

[91] Dirk S Waldhauser, Leonardo G Baltar, and Josef A Nossek, "Mmse subcarrier equalization for filter bank based multicarrier systems," in *2008 IEEE 9th Workshop on Signal Processing Advances in Wireless Communications*. IEEE, 2008, pp. 525–529.

[92] Leonardo G Baltar, Dirk S Waldhauser, and Josef A Nossek, "Mmse subchannel decision feedback equalization for filter bank based multicarrier systems," in *2009 IEEE International Symposium on Circuits and Systems*. IEEE, 2009, pp. 2802–2805.

[93] Leonardo G Baltar, Amine Mezghani, and Josef A Nossek, "Mlse and mmse subchannel equalization for filter bank based multicarrier systems : Coded and uncoded results," in *2010 18th European Signal Processing Conference*. IEEE, 2010, pp. 2186–2190.

[94] Tero Ihalainen, Tobias Hidalgo Stitz, Mika Rinne, and Markku Renfors, "Channel equalization in filter bank based multicarrier modulation for wireless communications," *EURASIP Journal on Advances in Signal Processing*, vol. 2007, no. 1, pp. 049389, 2006.

[95] Bruno S Chang, Carlos Af Da Rocha, Didier Le Ruyet, and Daniel Roviras, "Widely linear mmse precoding and equalization techniques for sc-fde systems," *EURASIP Journal on Advances in Signal Processing*, vol. 2014, no. 1, pp. 124, 2014.

[96] H Gerstacker, Robert Schober, and Alexander Lampe, "Receivers with widely linear processing for frequency-selective channels," *IEEE Transactions on Communications*, vol. 51, no. 9, pp. 1512–1523, 2003.

[97] Paul A Voois, Inkyu Lee, and John M Cioffi, "The effect of decision delay in finite-length decision feedback equalization," *IEEE transactions on Information Theory*, vol. 42, no. 2, pp. 618–621, 1996.

[98] KE Baddour and PJ McLane, "Analysis of optimum diversity combining and decision feedback equalization in dispersive rayleigh fading," in *1999 IEEE Communications Theory Mini-Conference (Cat. No. 99EX352)*. IEEE, 1999, pp. 21–26.

Hayfa FHIMA

Study and implementation of Widely Linear (WL) Receiver for Filter Bank based Multicarrier (FBMC-OQAM) modulations over Frequency Selective Channels .

Résumé : La forte demande des besoins, des services et des exigences des utilisateurs est le moteur du développement des systèmes de communication sans fils modernes. Ainsi, depuis les systèmes de deuxième génération (2G), de nombreux changements ont eu lieu, principalement, le passage des modulations mono-porteuses aux modulations multi-porteuses (MC) introduites pour la transmission de la 4G en sens descendant. En effet, l'idée d'introduire les formes d'ondes (WF) MC est de combattre les effets du canal de propagation, en relâchant le processus d'égalisation par la transmission des symboles de données sur des sous-canaux ou des sous-porteuses à évanouissements plats. En outre, la modulation MC la plus répandue est l'orthogonal frequency division multiplexing (OFDM), qui est devenue très dominante et largement utilisée dans de nombreuses normes sans fil, telles que long term evolution (LTE)- Advanced (LTE-A) et le Wi-Fi. Le succès de l'OFDM est principalement du à ses avantages présentés dans la simple implémentation par le biais de l'utilisation d'une transformée de Fourrier rapide inverse (IFFT) à la transmission et d'une FFT à la réception. De plus, avec l'utilisation du préfixe cyclique (CP), la transmission est sans interférences inter-symboles (ISI) avec une égalisation simple.

Malgré la dominante utilisation de l'OFDM, cette modulation présente des inconvénients. En effet, cette technique souffre de la perte de l'efficacité spectrale à cause de l'utilisation du CP, sans oublier la mauvaise localisation fréquentielle à cause de la mise en forme rectangulaire du filtre prototype utilisé dans OFDM. Ces inconvénients ont été une source de motivation pour les chercheurs pour la conception de nouvelles MC WF, ayant une meilleure localisation fréquentielle, une meilleure robustesse au synchronisme des utilisateurs, tout en conservant une complexité de mise en oeuvre modérée. Dans ce contexte, un nombre élevé de MC WF post-OFDM ont été proposés et mises en oeuvre pour répondre aux scénarios et aux exigences de la 5G d'une manière flexible. Ainsi, la modulation multi-porteuse à base des bancs de filtres (FBMC-OQAM) a été proposée en tant que solution alternative à la WF OFDM et ce pour surmonter ses inconvénients. En effet, la modulation FBMC-OQAM utilise un filtre prototype (Phydyas) qui lui permet d'avoir une excellente localisation fréquentielle ce que lui permet de fournir une meilleure performance en supportant les phénomènes d'asynchronisme entre les utilisateurs ainsi que la transmission avec différentes numérologies. En outre, l'efficacité spectrale est améliorée grâce à la suppression du CP et de large bandes de garde. De plus, l'orthogonalité dans le domaine réel est garantie grâce à l'utilisation de la modulation OQAM. Cependant, cette orthogonalité est perdue dans les canaux sélectifs en fréquence, ce qui nécessite des techniques d'égalisation avancées.

Dans ce contexte, l'objectif de cette thèse est d'étudier plusieurs types d'égalisation appliqués aux systèmes FBMC-OQAM. Vu que la modulation utilisée en FBMC-OQAM peut être considérée comme la transmission de deux flux de modulation $M-$PAM sur la même sous porteuse et comme le traitement largement linéaire (widely linéaire) est plus performant par rapport au traitement classique pour la modulatyion $M-$PAM, on va se concentrer sur les avantages de ce traitement largement linéaire utilisé pour le système FBMC-OQAM. En outre, en se basant sur le caractère cyclo-stationnaire du signal FBMC-OQAM, nous avons proposés une structure d'égalisation avancée basée sur le traitement FRESH (FREquency SHift) qui a été appliqué sur un système FBMC-OQAM utilisant différentes numérologies.

Mots clés : OFDM, FBMC-OQAM, PAM, ISI, ICI, égalisation, traitement widely linear, numérologie, canal sélectif en fréquence.

Abstract : The increasing demand of user's requirements is one of the main reasons in technical progress and development of modern wireless communication systems. Thus, since 2G and beyond, there have been many changes, especially, the switch from the mono carrier to the multi-carrier (MC), introduced for the Down-Link (DL) 4G transmission. Indeed, the predominant idea behind introducing MC waveforms (WF) is to get rid of the propagation channel effects, by relaxing the equalization process through the transmission of the data symbols over flat fading sub-channels or sub-carriers. Furthermore, the widely adopted MC WF is the orthogonal frequency division multiplexing (OFDM), which became very popular and widely used in many wireless standards like long term evolution (LTE)- Advanced (LTE-A) and Wi-Fi. The standardization of OFDM, for these applications and also for some others, is related to the advantages shown by this MC WF. One of these advantages is its simple implementation through the use of the inverse fast Fourier transform (IFFT) at the transmitter side, and a FFT at the receiver side. Also, OFDM introduces a cyclic prefix (CP), making the transmission free from inter-symbol-interference (ISI).

Despite the large success of the OFDM WF, this technique suffers from the loss of spectral efficiency due to the use of the CP. Besides, it suffers from bad frequency localization due the use of a rectangular prototype filter. These OFDM drawbacks, have motivated researchers to design new MC WF, with better frequency domain localization, better robustness to user's synchronism, while keeping moderate implementation complexity. In this context, high number of post-OFDM MC WF have been proposed and implemented to meet 5G scenarios and requirements in a flexible manner.

Therefore, the offset-quadrature amplitude modulation-based filter-bank multi-carrier (FBMC-OQAM) has been proposed as an alternative to overcome some drawbacks of the OFDM WF. Indeed, FBMC-OQAM is characterized by owning one of the best frequency localization among all the post-OFDM WFs, thanks to its prototype filter (Phydyas), providing then the best performance in supporting asynchronous and mixed numerologies transmissions. Besides, it offers high spectrum efficiency since it avoids the use of CP and large guard bands. Furthermore, the orthogonality in real domain is guaranteed thanks to the use of the OQAM modulation. However, this orthogonality is lost under frequency selective channels which requires advanced equalization techniques.

In this context, the main objective of this thesis is to study different types of equalization applied on FBMC-OQAM system. Since the modulation used in the FBMC-OQAM system can be seen as the transmission of two $M-$PAM modulations over one single carrier and since the widely linear processing outperforms the classical one for $M-$PAM modulation, we will focus on the advantages of using the widely linear processing over FBMC-OQAM system. Additionally, and based on the cyclo-stationarity of the FBMC-OQAM signal, we have proposed an advanced equalization structure based on FRESH processing that have been applied in to a FBMC-OQAM system using different numerologies.

Keywords : OFDM, FBMC-OQAM, PAM, ISI, ICI, equalization, widely linear processing, numerology, frequency selective channel